Supporting Information

Modulating the Dynamics of Förster Resonance Energy Transfer and Singlet Fission by Variable Molecular Spacers

Johannes Zirzlmeier,‡[a] Giulia Lavarda,‡[b] Henrik Gotfredsen,‡[c] Ilias Papadopoulos,‡[a] Lan Chen,[d] Timothy Clark,[e] Rik R. Tykwinski,*[d] Tomás Torres,*[b,f,g] and Dirk M. Guldi*[a]

[a]*Department of Chemistry and Pharmacy & Interdisciplinary Center for Molecular Materials (ICMM), Friedrich-Alexander-University Erlangen-Nuremberg, Egerlandstraße 3, 91058 Erlangen, Germany. E-mail: dirk.guldi@fau.de*

[b]*Departamento de Química Orgánica, Universidad Autónoma de Madrid, 28049 Madrid, Spain. E-mail: tomas.torres@uam.es*

[c]*Department of Chemistry, University of Copenhagen, Universitetsparken 5, DK-2100 Copenhagen, Denmark.*

[d]*Department of Chemistry, University of Alberta, Edmonton, Alberta, T6G 2G2, Canada. E-mail: rik.tykwinski@ualberta.ca*

[e]*Department of Chemistry and Pharmacy & Computer-Chemie-Center (CCC), Friedrich-Alexander-University Erlangen-Nuremberg, Nägelsbachstr. 25, 91052 Erlangen, Germany*

[f]*Institute for Advanced Research in Chemical Sciences (IAdChem), Universidad Autónoma de Madrid , Cantoblanco, 28049 Madrid, Spain.*

[g]*IMDEA-Nanociencia. c/ Faraday 9, Cantoblanco, 28049 Madrid, Spain.*

Electronic Supplementary Information (ESI) available: [details of any supplementary information available should be included here]. See DOI: 10.1039/x0xx00000x

‡ These authors contributed equally to this work.

General Procedures, Materials, and Methods

Synthesis and characterization

Synthesis and characterization of Pnc_2 derivatives 2a-d. All reagents and solvents were obtained from commercial suppliers and used as received unless otherwise stated. Anhydrous solvents were obtained from a solvent purification system. Purification by column chromatography was carried out on silica gel (SiO_2, 60 Å, 40–63 μm). Thin-layer chromatography (TLC) was carried out using commercially available aluminum sheets precoated with silica gel and a fluorescence indicator with visualization under UV light at 254 or 360 nm. Brine refers to a saturated, aqueous solution of NaCl. ^{1}H and ^{13}C-NMR spectra were recorded on a Varian/Agilent instrument equipped with a cryoprobe at 500 MHz and 126 MHz, respectively. Chemical shift values are quoted in ppm and coupling constants (*J*) in Hz. ^{1}H and ^{13}C-NMR spectra, respectively) are referenced against the residual solvent peak ($CDCl_3$ 7.26 ppm, 77.16 ppm; CD_2Cl_2 5.32 ppm, 53.84 ppm; THF-d_8 1.72 ppm, 25.31 ppm). UV-Vis spectroscopic measurements were done on a Cary 400 scan spectrophotometer using a 1 cm path-length quartz cuvette, and the neat solvent was used as baseline; sh = shoulder absorption. IR spectra were recorded on a Thermo Nicolet 8700 FTIR spectrometer and samples were measured as solids or cast films. High-resolution mass spectrometry (HRMS) spectra were recorded on a Bruker 9.4T Apex-Qe FTICR instrument (MALDI), an Agilent Technologies 6220 oaTOF instrument (APPI) or a Kratos MS50G instrument (EI). Differential scanning calorimetry (DSC) measurements were made on a Perkin Elmer Pyris 1 DSC or a Mettler Toledo Polymer DSC. Thermogravimetric analyses (TGA) were made on a Perkin Elmer Pyris 1 TGA or a Mettler Toledo TGA/DSC 1. Thermal analyses were carried out under a flow of nitrogen with a heating rate of 10 °C/min. Thermal decomposition temperature as measured by TGA (as sample weight loss) is reported as T_d in which the temperature listed corresponds to the intersection of the baseline and the tangent lines of the edge of the peak corresponding to the first significant weight loss, typically >5%. Melting points from DSC analysis are reported as the peak maxima, except in cases when the sample decomposed, in which case the onset temperature of the decomposition exothermic peak is reported, as well as the exothermic maxima corresponding to the decomposition. Melting points were measured on a Thomas Hoover capillary melting point apparatus.

Synthesis and characterization of SubPc-Pnc_2 derivatives 1a-d. All reagents and solvents were purchased from commercial suppliers and used without further purification unless otherwise stated. The synthesis and characterization of SubPcCl **9** has been reported elsewhere.[1] Anhydrous solvents were obtained from a solvent purification system. Celite plugs were performed using Celite® 545. Size exclusion chromatography was carried out on Bio-Beads™ S-X1 Support (200–400 mesh). NMR spectra were

recorded with a BRUKER Avance-300 (300 MHz) and a BRUKER DRX-500 (500 MHz) spectrometer. Chemical shifts (δ) are measured in ppm and coupling constants (J) in Hz. ^{1}H-NMR and ^{13}C-NMR spectra, respectively, are referenced against the residual solvent peak ($CDCl_3$ 7.26 ppm, 77.16 ppm; THF-d_8 1.73 ppm, 67.57 ppm). All the ^{13}C-NMR spectra were acquired during 18 hours. High-resolution mass spectrometry (HRMS) spectra were recorded employing Matrix Assisted Laser Desorption/Ionization-Time of Flight (MALDI-TOF) using a BRUKER ULTRAFLEX III instrument equipped with a Nd-YAG laser. A convenient matrix for these measurements is indicated for each compound.

Photophysical Studies

Steady-State Absorption and Emission. A Lambda 2 spectrometer from Perkin Elmer was utilized for all the steady-state UV-Vis absorption spectra at room temperature (rt). A FluoroMax3 emission spectrometer from Horiba was used for the steady-state fluorescence measurements in the visible detection range, again at rt. Fluorescence quantum yields were determined by means of gradient analyses using (1) for the SubPc fluorescence: F_{12}SubPc in toluene (axially substituted with a phenoxy-ligand, $\Phi_F = 0.17$)[2] as well as Rhodamine 6G in ethanol ($\Phi_F = 0.95$)[3] and (2) for the Pnc_2 fluorescence: Zinc phthalocyanine in toluene ($\Phi_F = 0.30$)[4] as reference compounds. All measurements were performed at rt in 10 × 10 mm quartz cuvettes.

Time-Correlated Single Photon Counting (TCSPC). Fluorescence lifetimes were determined by the time-correlated single photon counting technique using a FluoroLog3 emission spectrometer (Horiba) equipped with an R3809U-58 MCP (Hamamatsu) and a SuperK Extreme high-power supercontinuum fiber laser EXB-6 (NKT) exciting at 532 and 632 nm (~150 ps pulse width).

Femtosecond (fsTA) and Nanosecond Transient Absorption (nsTA). Femtosecond (0 to 5500 ps) and nanosecond (1 ns to 400 μs) transient absorption (fsTA and nsTA) experiments were carried out using transient absorption pump/probe detection systems (HELIOS and EOS, Ultrafast Systems). A 1050 Hz Ti:sapphire output (Clark-MXR, CPA-2101, 775 nm fundamental, ~150 fs pulse width) was applied, from which a fraction is focused onto a sapphire disk (fsTA, 2 mm), generating the white light of the probe beam (~420-800 nm). For nsTA, the white light (~370-900 nm) was generated instead by a photonic crystal fiber supercontinuum laser source (1064 nm fundamental, 2100 kHz, ~1 ns pulse width). Measurements were performed in 2 × 10 mm cuvettes and argon-purged solutions (~10 minutes) at rt. The pump pulses at 530 and 632 nm were generated with a non-collinear optical parametric amplifier (NOPA; Clark-MXR). The

repetition rate of the pump pulses was set to 525 Hz for fsTA (by means of a chopper) and to 1050 Hz for nsTA. Bandpass filters were used to ensure low spectral width of the pump pulses. The spot diameter of the pump beam was always kept larger than that of the probe beam in order to homogeneously excite the complete probed area. The delay of the probe pulses with respect to the pump pulses was reached with a controlled delay stage (fsTA) or electronically (nsTA). A beam splitter was used to split the probe pulses into two (signal and reference beam) before passing the sample. The probe and reference beam were detected independently to correct for fluctuations in the probe beam intensity. The transient spectra were acquired shot-by-shot and averaged at each delay until a reasonable signal-to-noise ratio was reached (~1500 times).

Data Analysis. Data evaluation of the fsTA and nsTA data has been conducted by means of global analysis and fitting of the transient absorption data were performed with the help of the open-source software package GloTarAn.[5] The latter is a Java-based graphical user interface to the R-package TIMP.[6,7] The latter was developed for global and target analysis of time-resolved spectroscopy data. The dispersion (chirp of the white-light pulse) of the instrument response function (IRF) was modeled during the fitting procedure.

FRET Rate Constant Determination. For the calculations, the following **Equations S1**-**S5** were used:

$$R = R_0\left(\frac{1-E}{E}\right)^{\frac{1}{6}} \qquad \textbf{Equation S1}$$

R = FRET distance; R_0 = critical energy donor-acceptor distance; E = FRET efficiency.

$$E = 1 - \frac{\tau_{DA}}{\tau_D} \qquad \textbf{Equation S2}$$

E = FRET efficiency; τ_{DA} = experimental lifetime (TA) of energy donor-acceptor conjugate; τ_D = experimental fluorescence lifetime of energy donor (TCSPC).

$$R_0 = 0.2108\left(\kappa^2 \Phi_F n^{-4} J\right)^{\frac{1}{6}} \qquad \textbf{Equation S3}$$

R_0 = critical energy donor-acceptor distance; κ^2 = orientation factor; Φ_F = fluorescence quantum yield; n = refractive index of the solvent; J = degree of spectral overlap.

$$J = \int_0^\infty F_D(\lambda)\varepsilon_A(\lambda)\lambda^4 d\lambda \qquad \textbf{Equation S4}$$

J = degree of spectral overlap; F_D = fluorescence intensity of the donor at wavelength λ. The fluorescence spectra must be normalized to fulfill **Equation S5**; ε_A = extinction coefficient of the acceptor at wavelength λ.

$$\int_0^\infty F_D(\lambda) d\lambda = 1 \qquad \textbf{Equation S5}$$

The detailed procedure (including a description of a software-based algorithm to calculate the spectral overlap integral J is described by Hink et al.[8] For κ^2 we used the values obtained from our computational studies (**Table S3**). The refractive index n was taken as 1.496 for toluene.[9] We calculated the FRET distances R for conjugates **1a**-**d**, that is, the distances between SubPc and the Pnc_2 in **1a**-**d** by means of **Equation S1** through **Equation S5** based on the experimental lifetimes obtained for τ_{DA} (fsTA) and τ_D (TCSPC).[10] See also **Table 2** for a summary of the parameters used for the FRET distance calculation as well as for an overview of the obtained values for R.[11]

Synthesis and Characterization

Synthesis and characterization of Pnc_2 derivatives 2a-d.

Compounds **8**,[12] **7**,[13] **6b**,[14] and **5a**[15] were synthesized as reported.

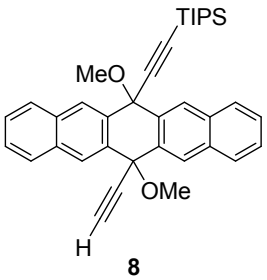

8

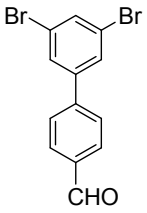

7

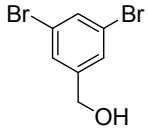

6b

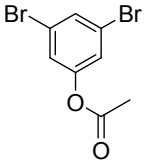

5a

Scheme S1. Synthesis of aryl precursors **5a-d**.dibromide

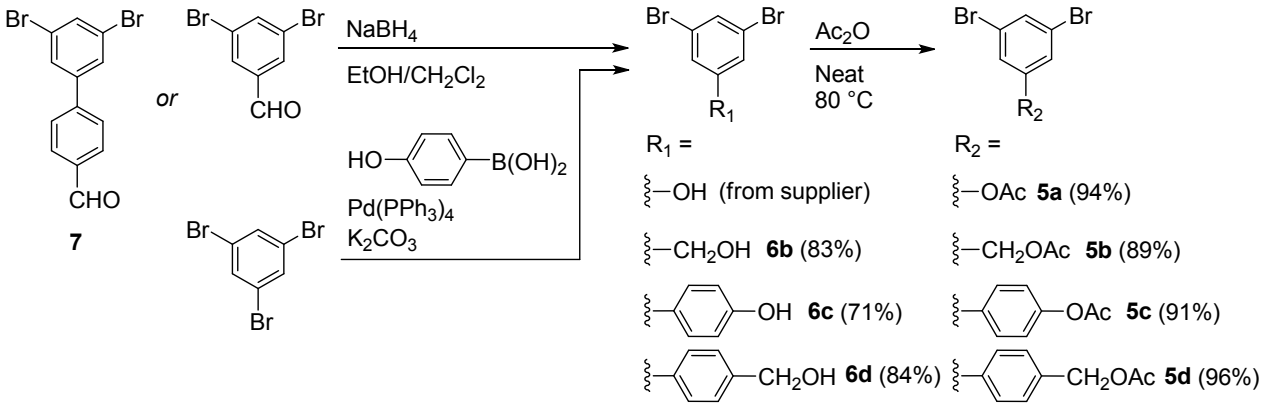

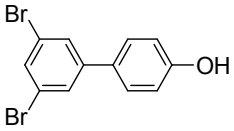

Compound 6c. To a N_2-purged solution of 1,3,5-tribromobenzene (11.41 g, 36.25 mmol), 4-hydroxylphenylboronic acid (2.00 g, 14.5 mmol) and K_2CO_3 (3.01 g, 21.8 mmol) in toluene (120 mL) and EtOH (40 mL) was added $Pd(PPh_3)_4$ (168 mg, 0.145 mmol). The reaction mixture was heated to reflux and stirred for 12 h. After cooling to room temperature, the reaction mixture was poured into sat. aq. NH_4Cl (150 mL), the phases were separated, and the aqueous phase extracted with CH_2Cl_2 (2 x 50 mL). The combined organic phases were washed with H_2O (200 mL) and brine (150 mL), dried over $MgSO_4$, filtered, and concentrated *in vacuo*. Purification by flash column chromatography (SiO_2, CH_2Cl_2/hexanes 4:1) afforded **6c** (3.40 g, 71%) as an off-white crystalline solid. $\boldsymbol{R_f}$ = 0.20 (EtOAc/CH_2Cl_2 1:19). **Mp** = 150–152 °C. **IR** (cast film CH_2Cl_2): 3315 (br s), 3106 (w), 3067 (w), 3026 (w), 1882 (w), 1756 (w), 1692 (w), 1610 (m), 1595 (m), 1584 (s), 1544 (m), 1520 (s) cm^{-1}. **^{1}H-NMR** (500 MHz, $CDCl_3$) δ 7.60 (d, J = 1.6 Hz, 2H), 7.59 (t, J = 1.6 Hz, 1H), 7.42 (d, J = 8.6 Hz, 2H), 6.91 (d, J = 8.6 Hz, 2H), 4.79 (s, 1H). **^{13}C-NMR** (126 MHz, $CDCl_3$) δ 156.1, 144.5, 132.1, 131.3, 128.7, 128.6, 123.4, 116.1. **EI MS** m/z 327.9 (M^+, 100), 168.1 ([M – $^{79}Br^{81}Br$]$^+$, 49). **EI HRMS** m/z calcd for $C_{12}H_8O^{79}Br^{81}Br$ (M^+) 327.8922, found 327.8928.

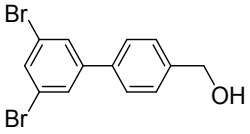

Compound 6d. To a solution of **7**[13] (1.00 g, 2.94 mmol) in CH_2Cl_2 (15 mL) and ethanol (15 mL) at rt was added $NaBH_4$ (111 mg, 2.94 mmol) in several portions. After stirring for 2 h, the reaction mixture was poured into sat. aq. NH_4Cl (100 mL) and extracted twice with CH_2Cl_2 (100 and 50 mL). The combined organic phases were washed with H_2O (100 mL) and brine (100 mL), dried over $MgSO_4$, filtered, and concentrated under reduced pressure. The remaining solid was suspended in hexane and collected by vacuum filtration, washed with hexanes (3 x 5 mL), and dried *in vacuo* to afford **6d** (851 mg, 84%) as a white solid. $\boldsymbol{R_f}$ = 0.13 (CH_2Cl_2). **Mp** = 128–130 °C. **IR** (solid): 3257 (br, s), 3064 (m), 3027 (m), 2922 (m), 2889 (m), 2869 (m), 1909 (w), 1770 (w), 1586 (s), 1545 (s), 1516 (m) cm^{-1}. **^{1}H-NMR** (500 MHz, $CDCl_3$) δ 7.65 (d, J = 1.7 Hz, 2H), 7.64 (t, J = 1.7 Hz, 1H), 7.53 (d, J = 8.3 Hz, 2H), 7.45 (d, J = 8.3 Hz, 2H), 4.76 (d, J = 5.7 Hz, 2H), 1.69 (t, J = 5.7 Hz, 1H). **^{13}C-NMR** (126 MHz, $CDCl_3$) δ 144.6, 141.4, 137.8, 132.8, 129.1, 127.7, 127.4, 123.5, 65.0. **APPI HRMS** m/z calcd for $C_{13}H_{10}{}^{79}Br_2O^+$ (M^+) 339.9093, found 341.9077.

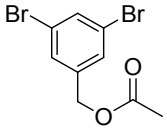

Compound 5b. A solution of **6b**[14] (2.00 g, 7.52 mmol) in acetic anhydride (15 mL) was heated to 80 °C. After stirring for 3 h, the reaction mixture was cooled to rt, poured onto ice (ca. 150 mL), and neutralized by addition of K_2CO_3 until the effervescences ceased. The aqueous suspension was extracted twice with CH_2Cl_2 (100 and 50 mL), and the combined organic phases were washed with H_2O (150 mL) and brine (100 mL), dried over $MgSO_4$, filtered, and concentrated under reduced pressure. Purification by flash column chromatography (SiO_2, CH_2Cl_2/hexanes 4:1) afforded **5b** (2.07 g, 89%) as a colorless oil. R_f = 0.84 (CH_2Cl_2/hexanes 7:3). **IR** (neat): 3073 (w), 2955 (w), 2895 (w), 1745 (s), 1590 (m), 1559 (s) cm^{-1}. **^{1}H-NMR** (500 MHz, $CDCl_3$) δ 7.62 (t, J = 1.7 Hz, 1H), 7.43 (d, J = 1.7 Hz, 2H), 5.03 (s, 2H), 2.13 (s, 3H). **^{13}C-NMR** (126 MHz, $CDCl_3$) δ 170.6, 140.0, 134.0, 129.8, 123.2, 64.6, 21.0. **EI MS** m/z 307.9 (M^+, 29), 265.9 ([M – C_2H_2O]$^+$, 100), 248.9 ([M – AcO]$^+$, 19). **EI HRMS** m/z calcd for $C_9H_8O_2{}^{79}Br^{81}Br$ (M^+) 307.8871, found 307.8871.

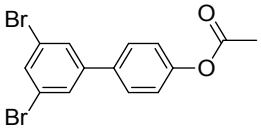

Compound 5c. A solution of **6c** (3.18 g, 9.70 mmol) in acetic anhydride (15 mL) was heated to 80 °C. After stirring for 3 h, the reaction mixture was cooled to rt, poured onto ice (ca. 150 mL), and neutralized by addition of K_2CO_3 until the effervescences ceased. The aqueous suspension was extracted twice with CH_2Cl_2 (150 and 50 mL), and the combined organic phases were washed with H_2O (150 mL) and brine (100 mL), dried over $MgSO_4$, filtered, and concentrated under reduced pressure. Purification by flash column chromatography (SiO_2, CH_2Cl_2/hexanes 3:2) afforded **5c** (3.27 g, 91%) as a white solid. R_f = 0.84 (CH_2Cl_2/hexanes 7:3). **Mp** = 98 °C. **IR** (cast film CH_2Cl_2): 3070 (w), 1760 (s), 1606 (w), 1584 (s), 1547 (s), 1511 (s) cm^{-1}. **^{1}H-NMR** (500 MHz, $CDCl_3$) δ 7.64 (t, J = 1.7 Hz, 1H), 7.62 (d, J = 1.7 Hz, 2H), 7.53 (d, J = 8.7 Hz, 2H), 7.18 (d, J = 8.7 Hz, 2H), 2.33 (s, 3H). **^{13}C-NMR** (126 MHz, $CDCl_3$) δ 169.5, 151.1, 144.0, 136.2, 132.9, 129.1, 128.4, 123.5, 122.4, 21.3. **EI MS** m/z 369.9 (M^+, 7), 327.9 ([M – C_2H_2O]$^+$, 100). **EI HRMS** m/z calcd for $C_{14}H_{10}O_2{}^{79}Br^{81}Br$ (M^+) 369.9029, found 369.9027.

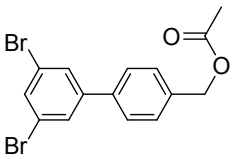

Compound 5d. A solution of **6d** (820 mg, 2.40 mmol) in acetic anhydride (10 mL) was heated to 80 °C. After stirring for 4 h, the reaction mixture was cooled to rt, poured onto ice (ca. 150 mL), and neutralized by addition of K_2CO_3 until the effervescences ceased. The aqueous suspension was extracted twice with CH_2Cl_2 (100 and 50 mL), and the combined organic phases were washed with H_2O (150 mL) and brine (100 mL), dried over $MgSO_4$, filtered, and concentrated under reduced pressure. Purification by flash column chromatography (SiO_2, CH_2Cl_2/hexanes 4:1) afforded **5d** (885 mg, 96%) as a white solid. R_f = 0.51 (CH_2Cl_2/hexanes 4:1). **Mp** = 52 °C. **IR** (solid): 3088 (m), 3070 (m), 3033 (w), 2963 (m), 2874 (w), 1743 (s), 1613 (m), 1585 (s), 1551 (m), 1522 (m) cm^{-1}. **^{1}H-NMR** (500 MHz, $CDCl_3$) δ 7.64 (s, 3H), 7.52 (d, J = 8.2 Hz, 2H), 7.44 (d, J = 8.2 Hz, 2H), 5.15 (s, 2H), 2.13 (s, 3H). **^{13}C-NMR** (126 MHz, $CDCl_3$) δ 171.0, 144.4, 138.4, 136.5, 132.9, 129.1, 129.0, 127.5, 123.5, 65.9, 21.2. **EI MS** m/z 383.9 (M^+, 52), 341.9 ([M – C_2H_2O]$^+$, 100), 324.9 ([M – AcO]$^+$, 64). **EI HRMS** m/z calcd for $C_{15}H_{12}O_2{}^{79}Br^{81}Br$ (M^+) 383.9184, found 383.9184.

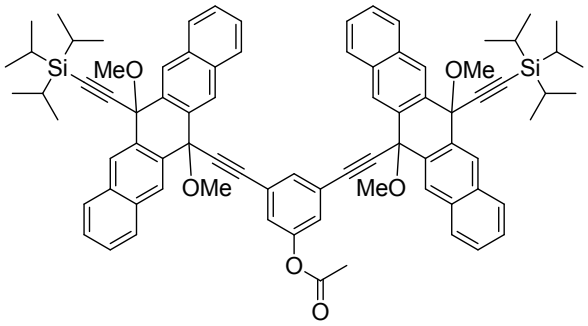

Compound 4a. To a N_2-purged solution of **5a**[15] (294 mg, 1.00 mmol) and **8**[12] (1.20 g, 2.20 mmol) in THF (50 mL) and Et_3N (20 mL) was added $Pd(PPh_3)_4$ (173 mg, 0.150 mmol) and CuI (19 mg, 0.10 mmol). The reaction mixture was heated to reflux and stirred for 18 h. After cooling to room temperature, the reaction mixture was poured into sat. aq. NH_4Cl (50 mL), H_2O (50 mL) was added, and the phases were separated. The aqueous phase was extracted with CH_2Cl_2 (50 mL) and the combined organic phases were washed with H_2O (100 mL) and brine (100 mL), dried over $MgSO_4$, filtered, and concentrated *in vacuo*. Purification by flash column chromatography (SiO_2, CH_2Cl_2/hexanes 85:15) afforded **4a** (856 mg, 70%) as a white solid. R_f = 0.20 (CH_2Cl_2/hexanes 85:15). **Mp**: decomposition, 218 °C (turns into dark green liquid accompanied by evolution of gas). **IR** (solid): 3055 (w), 2942 (s), 2891 (m), 2865 (s),

2817 (w), 2164 (w), 1772 (s), 1598 (m), 1578 (m) cm^{-1}. **^{1}H-NMR** (500 MHz, CD_2Cl_2) δ 8.68 (s, 4H), 8.41 (s, 4H), 8.01–7.96 (m, 4H), 7.96–7.90 (m, 4H), 7.61–7.52 (m, 8H), 7.20 (t, J = 1.4 Hz, 1H), 6.96 (d, J = 1.4 Hz, 2H), 3.08 (s, 6H), 2.99 (s, 6H), 2.15 (s, 3H), 1.40–1.13 (m, 42H). **^{13}C-NMR** (126 MHz, CD_2Cl_2) δ 169.2, 150.8, 134.5, 134.0, 133.9, 133.4, 132.3, 128.8, 128.72, 128.68, 127.5, 127.4, 127.3, 125.3, 124.6, 106.1, 93.3, 92.4, 84.8, 76.5, 74.1, 52.7, 52.3, 21.2, 19.2, 12.0. **MALDI HRMS** (DCTB): m/z calcd for $C_{82}H_{84}O_6Si_2^+$ (M^+) 1220.5801, found 1220.5794.

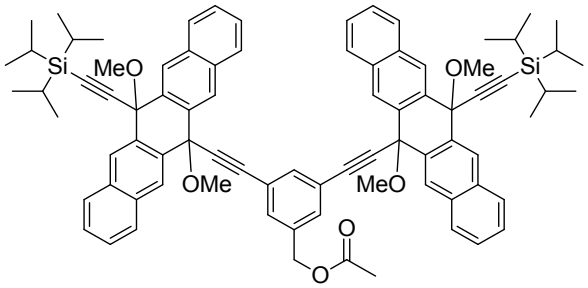

Compound 4b. To a N_2-purged solution of **5b** (262 mg, 0.850 mmol) and **8**[12] (1.00 g, 1.84 mmol) in THF (40 mL) and Et_3N (15 mL) was added $Pd(PPh_3)_4$ (145 mg, 0.125 mmol) and CuI (16 mg, 0.083 mmol). The reaction mixture was heated to reflux and stirred for 10 h. After cooling to room temperature, the reaction mixture was poured into sat. aq. NH_4Cl (50 mL), H_2O (50 mL) was added and the phases were separated. The aqueous phase was extracted with CH_2Cl_2 (50 mL) and the combined organic phases were washed with H_2O (100 mL) and brine (100 mL), dried over $MgSO_4$, filtered, and concentrated *in vacuo*. Purification by flash column chromatography (SiO_2, CH_2Cl_2) afforded **4b** (565 mg, 70%) as an off-white solid. R_f = 0.25 (CH_2Cl_2). **Mp** = 190–194 °C. **IR** (cast film CH_2Cl_2): 3055 (m), 2942 (s), 2891 (m), 2865 (s), 2817 (w), 2167 (w), 1745 (s), 1593 (m) cm^{-1}. **^{1}H-NMR** (500 MHz, CD_2Cl_2) δ 8.69 (s, 4H), 8.41 (s, 4H), 8.01–7.96 (m, 4H), 7.96–7.91 (m, 4H), 7.62–7.51 (m, 8H), 7.28 (s, 1H), 7.22 (s, 2H), 4.87 (s, 2H), 3.07 (s, 6H), 3.00 (s, 6H), 1.97 (s, 3H), 1.44–1.05 (m, 42H). **^{13}C-NMR** (126 MHz, CD_2Cl_2) δ 170.9, 137.3, 134.6, 134.4, 134.0, 133.9, 133.4, 131.3, 128.8, 128.7, 128.7, 127.5, 127.4, 127.3, 123.7, 106.1, 92.9, 92.4, 85.3, 76.5, 74.1, 65.4, 52.6, 52.3, 21.2, 19.2, 12.0. **MALDI HRMS** (DCTB) m/z calcd for $C_{83}H_{86}O_6Si_2$ (M^+) 1234.5957, found 1234.5943.

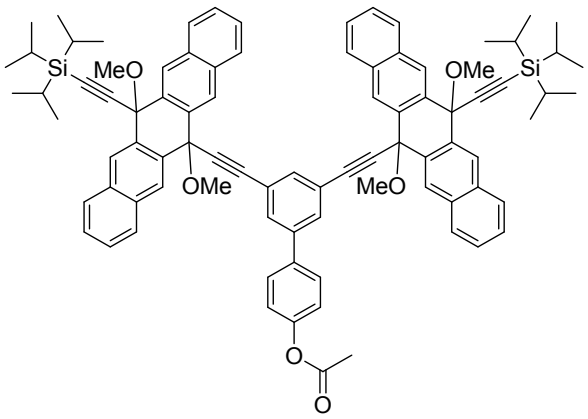

Compound 4c. To a N_2-purged solution of **5c** (340 mg, 0.918 mmol) and **8**[12] (1.10 g, 2.02 mmol) in THF (50 mL) and Et_3N (20 mL) was added $Pd(PPh_3)_4$ (159 mg, 0.138 mmol) and CuI (17 mg, 0.092 mmol). The reaction mixture was heated to reflux and stirred for 12 h. After cooling to room temperature, the reaction mixture was poured into sat. aq. NH_4Cl (50 mL), H_2O (50 mL) was added, and the phases were separated. The aqueous phase was extracted with CH_2Cl_2 (50 mL), and the combined organic phases were washed with H_2O (100 mL) and brine (100 mL), dried over $MgSO_4$, filtered, and concentrated *in vacuo*. Purification by flash column chromatography (SiO_2, CH_2Cl_2/hexanes 9:1) afforded **4c** (474 mg, 40%) as a pale green solid. $\boldsymbol{R_f}$ = 0.35 (CH_2Cl_2/hexanes 9:1). **Mp**: decomposition, 230 °C (color change to green). **IR** (cast film CH_2Cl_2): 3054 (m), 2945 (s), 2893 (m), 2867 (s), 2818 (w), 2162 (w), 1771 (s), 1595 (m), 1504 (m) cm^{-1}. **^{1}H-NMR** (500 MHz, CD_2Cl_2) δ 8.69 (s, 4H), 8.44 (s, 4H), 8.02–7.97 (m, 4H), 7.97–7.92 (m, 4H), 7.60–7.53 (m, 8H), 7.46 (d, J = 1.5 Hz, 2H), 7.44 (d, J = 8.6 Hz, 2H), 7.32 (t, J = 1.5 Hz, 1H), 7.07 (d, J = 8.6 Hz, 2H), 3.09 (s, 6H), 3.01 (s, 6H), 2.25 (s, 3H), 1.41–1.06 (m, 42H). **^{13}C-NMR** (126 MHz, CD_2Cl_2) δ 169.8, 151.3, 141.1, 137.5, 134.7, 134.1, 133.9, 133.7, 133.4, 130.5, 128.8, 128.72, 128.68, 128.5, 127.5, 127.4, 127.3, 124.0, 122.6, 106.2, 92.7, 92.3, 85.6, 76.5, 74.2, 52.6, 52.3, 21.5, 19.2, 12.0. **MALDI HRMS** (DCTB): m/z calcd for $C_{88}H_{88}O_6Si_2^+$ (M^+) 1296.6114, found 1296.6106.

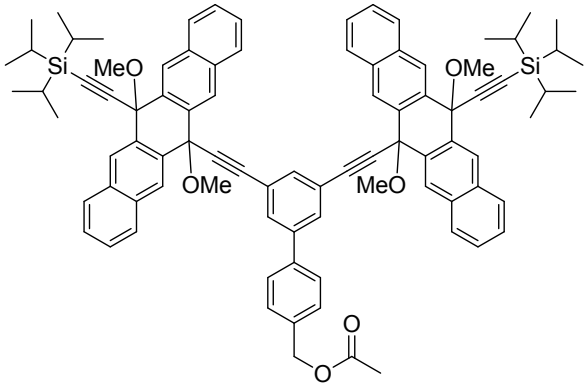

Compound 4d. To a N_2-purged solution of **5d** (352 mg, 0.918 mmol) and **8**[12] (1.10 g, 2.02 mmol) in THF (50 mL) and Et_3N (20 mL) was added $Pd(PPh_3)_4$ (159 mg, 0.138 mmol) and CuI (17 mg, 0.092 mmol). The reaction mixture was heated to reflux and stirred for 12 h. After cooling to room temperature, the reaction mixture was poured into sat. aq. NH_4Cl (50 mL), H_2O (50 mL) was added and the phases were separated. The aqueous phase was extracted with CH_2Cl_2 (50 mL) and the combined organic phases were washed with H_2O (100 mL) and brine (100 mL), dried over $MgSO_4$, filtered, and concentrated *in vacuo*. Purification by flash column chromatography (SiO_2, CH_2Cl_2/hexanes 9:1) afforded **4d** (567 mg, 47%) as a pale green solid. $\boldsymbol{R_f}$ = 0.19 (CH_2Cl_2/hexanes 9:1). **Mp** = decomposition, 230 °C (color change to green), 245 °C (melts into dark green liquid). **IR** (cast film CH_2Cl_2): 3055 (m), 2943 (s), 2892 (m), 2865 (s), 2816 (w), 2167 (w), 1741 (s), 1589 (m) cm^{-1}. **^{1}H-NMR** (500 MHz, CD_2Cl_2) δ 8.69 (s, 4H), 8.44 (s, 4H), 8.02–7.97 (m, 4H), 7.97–7.92 (m, 4H), 7.60–7.53 (m, 8H), 7.47 (d, J = 1.4 Hz, 2H), 7.44 (d, J = 8.2 Hz, 2H), 7.34 (d, J = 8.2 Hz, 2H), 7.32 (t, J = 1.4 Hz, 1H), 5.06 (s, 2H), 3.09 (s, 6H), 3.01 (s, 6H), 2.06 (s, 3H), 1.38–1.11 (m, 42H). **^{13}C-NMR** (126 MHz, CD_2Cl_2) δ 171.1, 141.4, 139.6, 136.6, 134.7, 134.1, 133.9, 133.7, 133.4, 130.5, 129.1, 128.8, 128.73, 128.67, 127.6, 127.5, 127.4, 127.3, 124.0, 106.2, 92.7, 92.4, 85.6, 76.5, 74.2, 66.2, 52.6, 52.3, 21.3, 19.2, 12.0. **MALDI HRMS** (DCTB) m/z calcd for $C_{89}H_{90}O_6Si_2$ (M^+) 1310.6271, found 1310.6265.

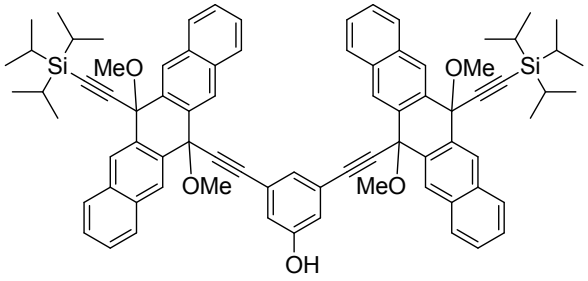

Compound 3a. To a solution of **4a** (829 mg, 0.679 mmol) in THF (30 mL) and H_2O (15 mL) was added $LiOH \cdot H_2O$ (142 mg, 3.39 mmol) and the reaction mixture was stirred at room temperature for 17 h. The clear solution was poured into sat. aq. NH_4Cl (50 mL) and extracted with CH_2Cl_2 (100 mL). The organic phase was washed with sat. $NaHCO_3$ (2 x 50 mL), H_2O (100 mL) and brine (100 mL), dried over $MgSO_4$, filtered, and concentrated *in vacuo*. The remaining solid was suspended in hexanes (50 mL), collected on a glass frit and washed with additional hexanes (3 x 10 mL) to obtain **3a** (744 mg, 93%) as a white solid. $\boldsymbol{R_f}$ = 0.40 (EtOAc/CH_2Cl_2 1:49). **Mp**: decomposition, 160 °C (color change to grey). **IR** (solid): 3374 (w, broad), 3056 (w), 2943 (s), 2892 (m), 2865 (s), 2824 (w), 2166 (w), 1600 (m), 1584 (s) cm^{-1}. **^{1}H-NMR** (500 MHz, CD_2Cl_2) δ 8.67 (s, 4H), 8.45 (s, 4H), 8.04–7.96 (m, 4H), 7.96–7.89 (m, 4H), 7.60–7.51 (m, 8H), 6.77–6.73 (m, 1H), 6.55 (s, 2H), 5.41 (s, 1H), 3.08 (s, 6H), 2.98 (s, 6H), 1.45–1.12 (m, 42H). **^{13}C-NMR** (126 MHz, CD_2Cl_2) δ 155.7, 134.4, 133.9, 133.5, 133.1, 128.6, 128.50, 128.47, 127.3, 127.2, 127.1, 124.1, 118.7, 105.9, 92.2, 92.0, 85.4, 76.4, 73.9, 52.4, 52.1, 18.9, 11.8 (one signal coincident or not observed). **MALDI HRMS** (DCTB): *m*/*z* calcd for $C_{80}H_{82}O_5Si_2^+$ (M^+) 1178.5695, found 1178.5697.

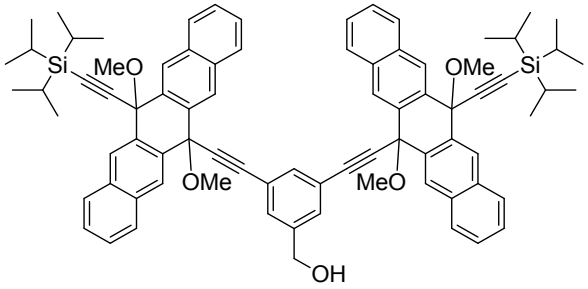

Compound 3b. To a solution of **4b** (550 mg, 0.449 mmol) in THF (15 mL) and H_2O (7.5 mL) was added $LiOH·H_2O$ (113 mg, 2.69 mmol) and the reaction mixture was stirred at room temperature for 18 h. The clear solution was poured into sat. aq. NH_4Cl (50 mL) and extracted with CH_2Cl_2 (100 mL). The organic phase was washed with sat. aq. $NaHCO_3$ (2 x 50 mL), H_2O (100 mL) and brine (100 mL), dried over $MgSO_4$, filtered, and concentrated *in vacuo*. Purification by flash column chromatography (SiO_2, EtOAc/CH_2Cl_2 1:49) afforded **3b** (481 mg, 90%) as a white solid. $\boldsymbol{R_f}$ = 0.42 (EtOAc/CH_2Cl_2 1:49). **Mp** = decomposition, 160 °C (color change to yellow), 180 °C (melt), 210 °C (turns into dark green liquid accompanied by evolution of gas). **IR** (cast film CH_2Cl_2): 3468 (br, w), 3055 (m), 2943 (s), 2891 (m), 2865 (s), 2818 (w), 2226 (w), 2167 (w), 1738 (w), 1591 (m) cm^{-1}. **^{1}H-NMR** (500 MHz, CD_2Cl_2) δ 8.68 (s, 4H), 8.42 (s, 4H), 8.00–7.96 (m, 4H), 7.96–7.92 (m, 4H), 7.60–7.52 (m, 8H), 7.27–7.24 (m, 1H), 7.24–7.22 (m, 2H), 4.48 (d, *J* = 5.8 Hz, 2H), 3.08 (s, 6H), 3.00 (s, 6H), 1.66 (t, *J* = 5.8 Hz, 1H), 1.33–1.18 (m, 42H). **^{13}C-NMR** (126 MHz, CD_2Cl_2) δ 142.3, 134.7, 134.0, 133.9, 133.7, 133.4, 130.1, 128.8, 128.72, 128.66, 127.44, 127.38, 127.3, 123.6, 106.2, 92.5, 92.3, 85.7, 76.5, 74.2, 64.5, 52.6, 52.3, 19.2, 12.0. **MALDI HRMS** (DCTB) *m*/*z* calcd for $C_{81}H_{84}O_5Si_2$ (M^+) 1192.5852, found 1192.5863.

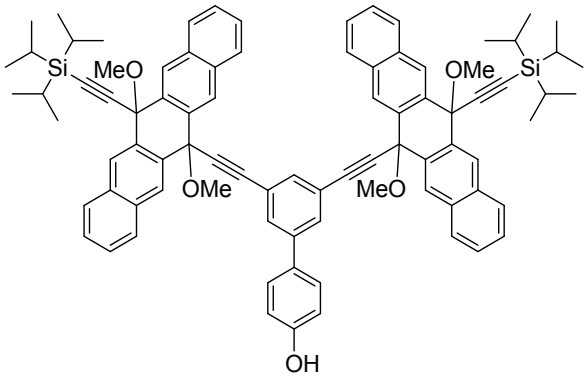

Compound 3c. To a solution of **4c** (462 mg, 0.356 mmol) in THF (15 mL) and H_2O (7.5 mL) was added $LiOH·H_2O$ (90 mg, 2.1 mmol) and the reaction mixture was stirred at room temperature for 20 h. The clear solution was poured into sat. aq. NH_4Cl (50 mL)

and extracted with CH_2Cl_2 (100 mL). The organic phase was washed with sat. aq. $NaHCO_3$ (2 x 50 mL), H_2O (100 mL) and brine (100 mL), dried over $MgSO_4$, filtered, and concentrated *in vacuo*. Purification by flash column chromatography (SiO_2, CH_2Cl_2) afforded **3c** (400 mg, 89%) as a white solid. R_f = 0.29 (CH_2Cl_2). **Mp** = decomposition, 160 °C (color change to dark green). **IR** (cast film CH_2Cl_2): 3372 (br, m), 3055 (m), 2942 (s), 2892 (m), 2865 (m), 2827 (w), 2229 (w), 2166 (w), 1612 (m), 1586 (m), 1516 (m) cm^{-1}. **^{1}H-NMR** (500 MHz, CD_2Cl_2) δ 8.69 (s, 4H), 8.44 (s, 4H), 8.01–7.96 (m, 4H), 7.96–7.92 (m, 4H), 7.59–7.53 (m, 8H), 7.38 (d, *J* = 1.5 Hz, 2H), 7.29–7.24 (m, 3H), 6.75 (d, *J* = 8.7 Hz, 2H), 5.12 (s, 1H), 3.08 (s, 6H), 3.01 (s, 6H), 1.44–1.11 (m, 42H). **^{13}C-NMR** (126 MHz, CD_2Cl_2) δ 156.4, 141.5, 134.7, 134.1, 133.9, 133.4, 133.0, 132.3, 130.1, 128.8, 128.73, 128.72, 128.67, 127.5, 127.4, 127.3, 123.8, 116.2, 106.2, 92.42, 92.35, 85.8, 76.5, 74.2, 52.6, 52.3, 19.2, 12.0. **MALDI HRMS** (DCTB): *m*/*z* calcd for $C_{86}H_{86}O_5Si_2^+$ (M^+) 1254.6008, found 1254.6015.

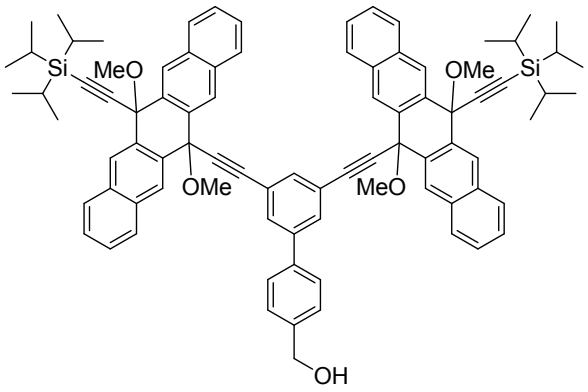

Compound 3d. To a solution of **4d** (552 mg, 0.421 mmol) in THF (15 mL) and H_2O (7.5 mL) was added $LiOH·H_2O$ (106 mg, 2.52 mmol) and the reaction mixture was stirred at room temperature for 20 h. The clear solution was poured into sat. aq. NH_4Cl (50 mL) and extracted with CH_2Cl_2 (100 mL). The organic phase was washed with sat. aq. $NaHCO_3$ (2 x 50 mL), H_2O (100 mL) and brine (100 mL), dried over $MgSO_4$, filtered, and concentrated *in vacuo*. Purification by flash column chromatography (SiO_2, EtOAc/CH_2Cl_2 1:99) afforded **3d** (430 mg, 81%) as a white solid. R_f = 0.26 (EtOAc/CH_2Cl_2 1:99). **Mp** = decomposition, 230 °C (color change to pale green); 250 °C (melts into dark green liquid with evolution of gas). **IR** (cast film CH_2Cl_2): 3499 (br, w), 3055 (m), 2943 (s), 2891 (m), 2865 (s), 2815 (w), 2163 (w), 1591 (m) cm^{-1}. **^{1}H-NMR** (500 MHz, CD_2Cl_2) δ 8.69 (s, 4H), 8.44 (s, 4H), 8.01–7.96 (m, 4H), 7.96–7.92 (m, 4H), 7.60–7.52 (m, 8H), 7.48 (d, *J* = 1.5 Hz, 2H), 7.43 (d, *J* = 8.4 Hz, 2H), 7.34 (d, *J* = 8.4 Hz, 2H), 7.31 (t, *J* = 1.5 Hz, 1H), 4.65 (d, *J* = 6.0 Hz, 2H), 3.08 (s, 6H), 3.01 (s, 6H), 1.73 (t, *J* = 6.0 Hz, 1H), 1.39–1.13 (m, 42H). **^{13}C-NMR** (126 MHz, CD_2Cl_2) δ 141.64, 141.58, 138.9, 134.7, 134.1, 133.9, 133.6, 133.4, 130.5, 128.8, 128.72, 128.67, 127.8, 127.54,

127.45, 127.4, 127.3, 124.0, 106.2, 92.6, 92.4, 85.7, 76.5, 74.2, 65.2, 52.6, 52.3, 19.2, 12.0. **MALDI HRMS** (DCTB) *m*/*z* calcd for $C_{87}H_{88}O_5Si_2$ (M^+) 1268.6165, found 1268.6156.

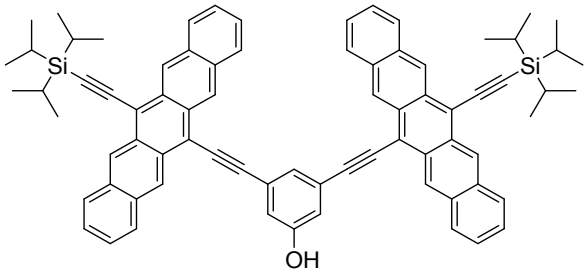

Compound 2a. A solution of **3a** (704 mg, 0.60 mmol) in THF (60 mL) was purged with N_2 for 2 min. To this solution was added $SnCl_2{\cdot}2H_2O$ (539 mg, 2.39 mmol) and 10% H_2SO_4 (0.65 mL) in that order, and the reaction mixture was further purged with N_2 for 2 min. To limit light exposure, the reaction flask was covered in aluminum foil. After stirring for 5 h, the reaction mixture was poured into H_2O/MeOH (1:1, 300 mL), and the precipitate was collected on a glass frit, washed with H_2O/MeOH (1:1, 100 mL) and MeOH (50 mL). The remaining solid was dissolved in THF (20 mL) and stirred for 30 minutes before being poured into hexanes (100 mL). The precipitate was collected on a glass frit and washed with hexanes (100 mL). The solid was dissolved in THF (20 mL) and filtered through a glass frit. The filtrate was concentrated *in vacuo*, and the dry solid was suspended in MeOH, collected on a glass frit and washed with additional MeOH (100 mL) to obtain **2a** (612 mg, 97%) as a green-blue solid. $\boldsymbol{R_f}$ = 0.58 (CH_2Cl_2/hexanes 4:1). **Mp**: decomposition, 200 °C (color change to pale-green). **UV-Vis** (THF): λ_{max} 310, 348, 366, 414, 439, 519, 558, 602, 656 nm. **IR** (solid): 3672-3113 (w), 3559 (w), 3049 (m), 2942 (s), 2890 (m), 2864 (s), 2127 (m), 1754 (w), 1704 (w), 1596 (m), 1581 (s) cm^{-1}. **^{1}H-NMR** (500 MHz, CD_2Cl_2) δ 9.16 (s, 4H), 9.14 (s, 4H), 8.04–7.90 (m, 9H), 7.49–7.35 (m, 10H), 5.51 (s, 1H), 1.48–1.36 (m, 42H). **^{13}C-NMR** (126 MHz, CD_2Cl_2) δ 156.5, 132.80, 132.79, 130.9, 130.6, 129.2, 129.1, 128.2, 126.9, 126.8, 126.7, 126.2, 126.0, 119.6, 119.2, 117.9, 108.2, 105.1, 104.1, 89.3, 19.4, 12.3. **MALDI HRMS** (DCTB): *m*/*z* calcd for $C_{76}H_{70}O_1Si_2^+$ (M^+) 1054.4960, found 1054.4963. **DSC**: decomposition, 121 °C (onset), 174 °C (peak). **TGA**: $T_d \approx 470$ °C.

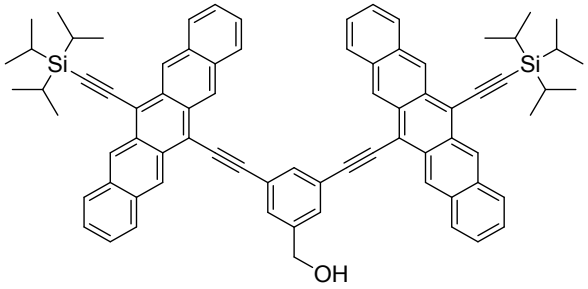

Compound 2b. A solution of **3b** (471 mg, 0.395 mmol) in THF (35 mL) was purged with N_2 for 2 min. To this solution was added $SnCl_2 \cdot 2H_2O$ (356 mg, 1.58 mmol) and 10% aq. H_2SO_4 (0.40 mL) in that order, and the reaction mixture was further purged with N_2 for 2 min. To limit light exposure, the reaction flask was covered in aluminum foil. After stirring for 5 h, the reaction mixture was poured into MeOH (600 mL) and the precipitate was collected on a glass frit, washed with MeOH (150 mL) and dried *in vacuo* to obtain **2b** (371 mg, 88%) as a dark blue solid. $\boldsymbol{R_f}$ = 0.58 (CH_2Cl_2/hexanes 4:1). **Mp** = no visible change below 250 °C. **UV-Vis** (THF): λ_{max} (ε) 310 (496 000), 350 (37 500), 368 (51 500), 415 (5 480), 440 (8 010), 512 (sh, 2 810), 557 (10 100), 602 (27 700), 657 (54 200) nm. **IR** (cast film CH_2Cl_2): 3332 (br, w), 3049 (w), 2942 (s), 2891 (m), 2865 (s), 2126 (m), 1587 (m) cm^{-1}. **^{1}H-NMR** (500 MHz, THF-d_8) δ 9.42 (s, 4H), 9.31 (s, 4H), 8.46 (s, 1H), 8.21–8.14 (m, 4H), 8.12–8.08 (m, 2H), 8.01–7.95 (m, 4H), 7.49–7.40 (m, 8H), 4.91 (d, J = 5.8 Hz, 2H), 4.67 (t, J = 5.8 Hz, 1H), 1.60–1.22 (m, 42H). **^{13}C-NMR** (126 MHz, THF-d_8) δ 145. 6, 134.1, 133.6, 133.5, 131.5, 131.1, 131.0, 129.6, 129.3, 127.3, 127.2, 127.0, 126.9, 125.0, 119.2, 118.9, 107.9, 105.9, 105.3, 89.1, 64.3, 19.5, 12.7. **MALDI HRMS (DCTB)** m/z calcd for $C_{77}H_{72}OSi_2$ (M^+) 1068.5116, found 1068.5110. **DSC**: decomposition, 141 °C (onset), 183 °C (peak); 403 °C (onset), 460 °C (peak). **TGA**: $T_d \approx$ 485 °C. Crystals suitable for X-ray crystallography were grown by vapor diffusion from MeOH/THF.

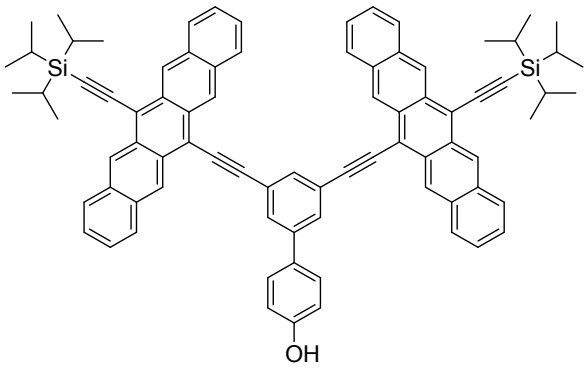

Compound 2c. A solution of **3c** (390 mg, 0.311 mmol) in THF (30 mL) was purged with N_2 for 2 min. To this solution was added $SnCl_2{\cdot}2H_2O$ (280 mg, 1.24 mmol) and 10% H_2SO_4 (0.35 mL) in that order, and the reaction mixture was further purged with N_2 for 2 min. To limit light exposure, the reaction flask was covered in aluminum foil. After stirring for 6 h, the reaction mixture was poured into MeOH (450 mL) and the precipitate was collected on a glass frit, washed with MeOH (150 mL), and dried *in vacuo* to obtain **2c** (268 mg, 76%) as a dark blue solid. $\boldsymbol{R_f}$ = 0.45 (CH_2Cl_2/hexanes 4:1). **Mp**: no visible change below 250 °C. **UV-Vis** (THF): λ_{max} 310, 351, 369, 416, 440, 515 (sh), 558, 603, 657 nm. **IR** (cast film CH_2Cl_2): 3553 (w), 3368 (br, w), 3048 (m), 2942 (s), 2890 (m), 2865 (s), 2126 (m), 1612 (m), 1582 (m), 1515 (m) cm^{-1}. **^{1}H-NMR** (500 MHz, THF-d_8) δ 9.46 (s, 4H), 9.33 (s, 4H), 8.54 (s, 1H), 8.50 (t, J = 1.3 Hz, 1H), 8.30 (d, J = 1.3 Hz, 2H), 8.22–8.16 (m, 4H), 8.01–7.96 (m, 4H), 7.83 (d, J = 8.5 Hz, 2H), 7.48–7.40 (m, 8H), 7.01 (d, J = 8.5 Hz, 2H), 1.56–1.31 (m, 42H). **^{13}C-NMR** (126 MHz, THF-d_8) δ 159.4, 143.6, 133.59, 133.55, 133.5, 131.5, 131.4, 131.2, 131.0, 129.7, 129.4, 129.3, 127.3, 127.2, 127.02, 126.98, 125.6, 119.2, 118.9, 116.8, 108.0, 105.9, 105.3, 89.2, 19.5, 12.7. **MALDI HRMS** (DCTB): m/z calcd for $C_{82}H_{74}OSi_2^+$ (M^+) 1130.5273, found 1130.5260. **DSC**: decomposition, 89 °C (onset), 148 °C (peak); 396 °C (onset), 446 °C (peak). **TGA**: $T_d \approx$ 490 °C.

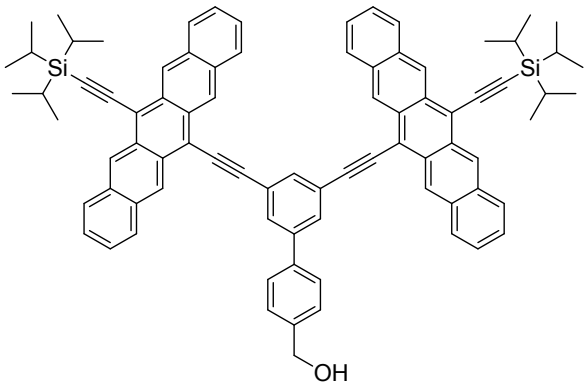

Compound 2d. A solution of **3d** (420 mg, 0.331 mmol) in THF (30 mL) was purged with N_2 for 2 min. To this solution was added $SnCl_2 \cdot 2H_2O$ (299 mg, 1.32 mmol) and 10% aq. H_2SO_4 (0.35 mL) in that order, and the reaction mixture was further purged with N_2 for 2 min. To limit light exposure, the reaction flask was covered in aluminum foil. After stirring for 6 h, the reaction mixture was poured into MeOH (450 mL) and the precipitate was collected on a glass frit, washed with MeOH (150 mL) and dried *in vacuo* to obtain **2d** (341 mg, 90%) as a dark blue solid. $\boldsymbol{R_f}$ = 0.25 (CH_2Cl_2/hexanes 4:1). **Mp** = no visible change below 250 °C. **UV-Vis** (THF): λ_{max} (ε) 310 (582 300), 351 (40 400), 371 (57 100), 416 (51 700), 440 (8 400), 510 (sh, 3 110), 557 (11 600), 602 (32 100), 357 (61 800) nm. **IR** (cast film CH_2Cl_2): 3556 (w), 3443 (w), 3048 (w), 2942 (s), 2890 (m), 2865 (s), 2123 (m), 1586 (m), 1516 (w) cm^{-1}. **^{1}H-NMR** (500 MHz, THF-d_8) δ 9.45 (s, 4H), 9.32 (s, 4H), 8.57–8.53 (m, 1H), 8.38 (s, 2H), 8.22–8.13 (m, 4H), 8.04–7.93 (m, 6H), 7.63 (d, J = 7.9 Hz, 2H), 7.52–7.36 (m, 8H), 4.76 (d, J = 5.8 Hz, 2H), 4.32 (t, J = 5.8 Hz, 1H), 1.66–1.20 (m, 42H). **^{13}C-NMR** (126 MHz, THF-d_8) δ 144.3, 143.5, 138.8, 134.2, 133.6, 133.5, 131.47, 131.46, 131.2, 129.6, 129.3, 128.0, 127.9, 127.3, 127.2, 127.0, 126.9, 125.7, 119.3, 118.8, 108.0, 105.9, 105.1, 89.4, 64.6, 19.5, 12.7. **MALDI HRMS** (DCTB) *m*/*z* calcd for $C_{83}H_{76}OSi_2$ (M^+) 1144.5429, found 1144.5418. **DSC**: decomposition, 147 °C (onset), 206 °C (peak); 236 °C (onset), 268 °C (peak); 388 °C (onset), 411 °C (peak); 413 °C (onset), 460 °C (peak). **TGA**: $T_d \approx$ 485 °C.

Table S1. Crystallographic Experimental Details of **2b**

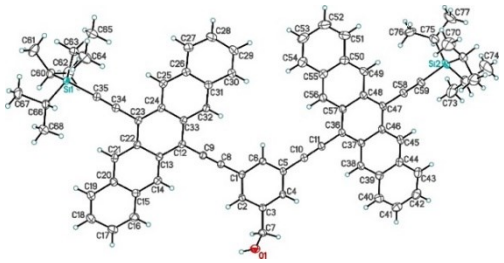

A. Crystal Data

formula $C_{81}H_{80}O_2Si_2$

formula weight 1141.63

crystal dimensions (mm) 0.27 × 0.06 × 0.05

crystal system triclinic

space group *P*-1 (No. 2)

unit cell parameters[a]

a (Å) 8.9356(3)

b (Å) 17.9940(7)

c (Å) 22.2531(9)

α (deg) 69.3269(18)

β (deg) 80.898(2)

γ (deg) 85.2585(19)

V (Å^3) 3304.1(2)

Z 2

*ρ*calcd (g cm–3) 1.147

μ (mm^{-1}) 0.840

B. Data Collection and Refinement Conditions

diffractometer Bruker D8/APEX II CCD[b]

radiation (*λ* [Å]) Cu K*α* (1.54178) (microfocus source)

temperature (°C) –100

scan type *ω* and *ϕ* scans (1.0°) (5 s exposures)

data collection 2*θ* limit (deg) 140.74

total data collected 22808 (–10 ≤ *h* ≤ 10, –21 ≤ *k* ≤ 21, –27 ≤ *l* ≤ 26)

independent reflections 12150 (*R*int = 0.0291)

number of observed reflections (*NO*) 9884 [$F_o^2 \geq 2\sigma(F_o^2)$]

structure solution method intrinsic phasing (*SHELXT-2014*[c])

refinement method full-matrix least-squares on F^2 (*SHELXL–2016*[d])

absorption correction method Gaussian integration (face-indexed)

range of transmission factors 1.0000–0.8139

data/restraints/parameters 12150 / 0 / 770

goodness-of-fit (S)[e] [all data] 1.047

final R indices[f]

R_1 [$F_o^2 \geq 2\sigma(F_o^2)$] 0.0575

wR_2 [all data] 0.1620

largest difference peak and hole 1.116 and –0.677 e Å^{-3}

[a] Obtained from least-squares refinement of 9830 reflections with 5.26° < 2θ < 140.52°.

[b] Programs for diffractometer operation, data collection, data reduction and absorption correction were supplied by Bruker.

[c] Sheldrick, G. M. *Acta Crystallogr.* **2015**, *A71*, 3–8. (*SHELXT-2014*)

[d] Sheldrick, G. M. *Acta Crystallogr.* **2015**, *C71*, 3–8. (*SHELXL-2017*)

[e] $S = [\sum w(F_o^2 - F_c^2)^2/(n-p)]^{1/2}$ (n = number of data; p = number of parameters varied; $w = [\sum^2(F_o^2) + 1.6513P]^{-1}$ where $P = [\mathrm{Max}(F_o^2, 0) + 2F_c^2]/3$).

[f] $R1 = \sum||F_o| - |F_c||/\sum|F_o|$; $wR2 = [\sum w(F_o^2 - F_c^2)^2/\sum w(F_o^4)]^{1/2}$.

Figure S1. ^{1}H-NMR spectrum (500 MHz) of **6c** recorded in $CDCl_3$. Residual solvent signal denoted by asterisk (*).

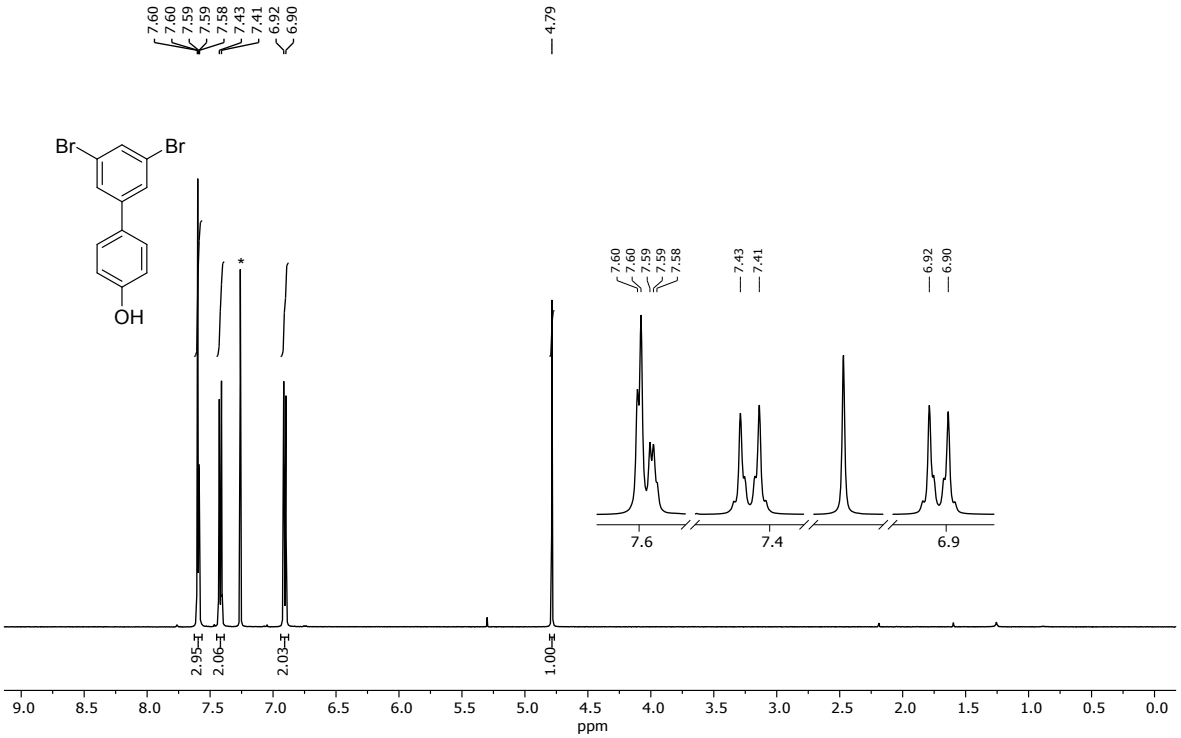

Figure S2. ^{13}C-NMR spectrum (126 MHz) of **6c** recorded in $CDCl_3$. Residual solvent signals denoted by asterisk (*).

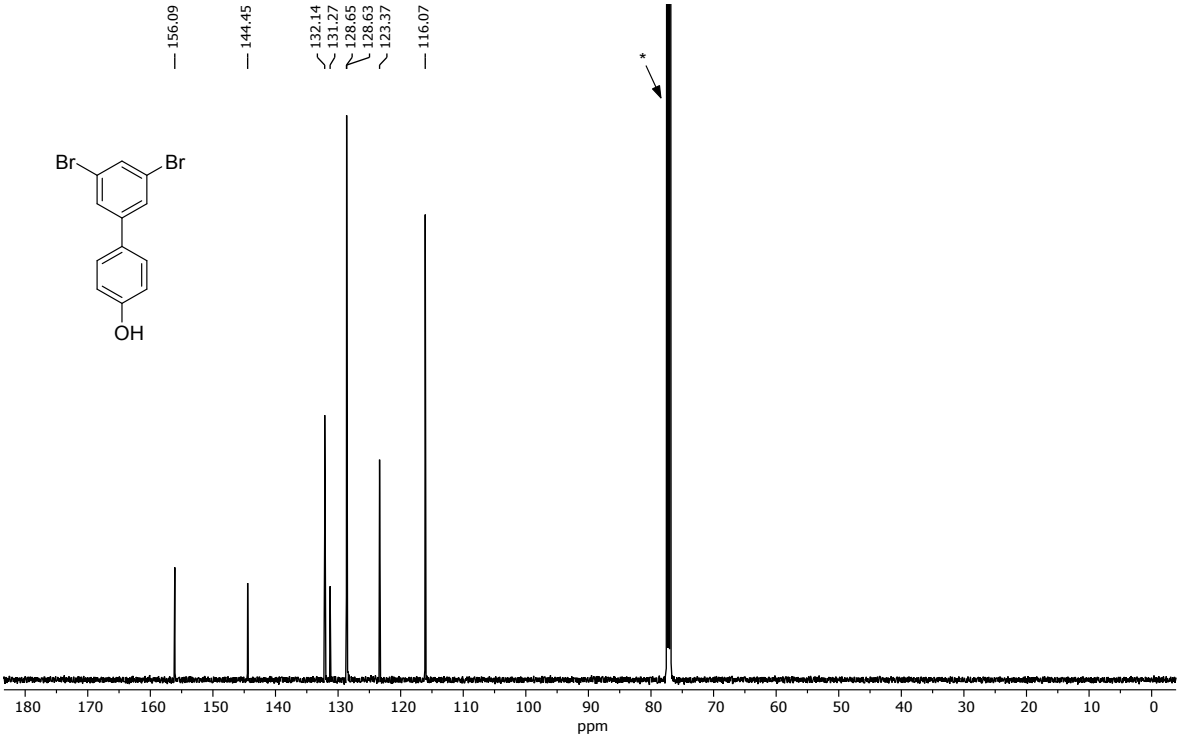

Figure S3. ^{1}H-NMR spectrum (500 MHz) of **6d** recorded in $CDCl_3$. Residual solvent signal denoted by asterisk (*).

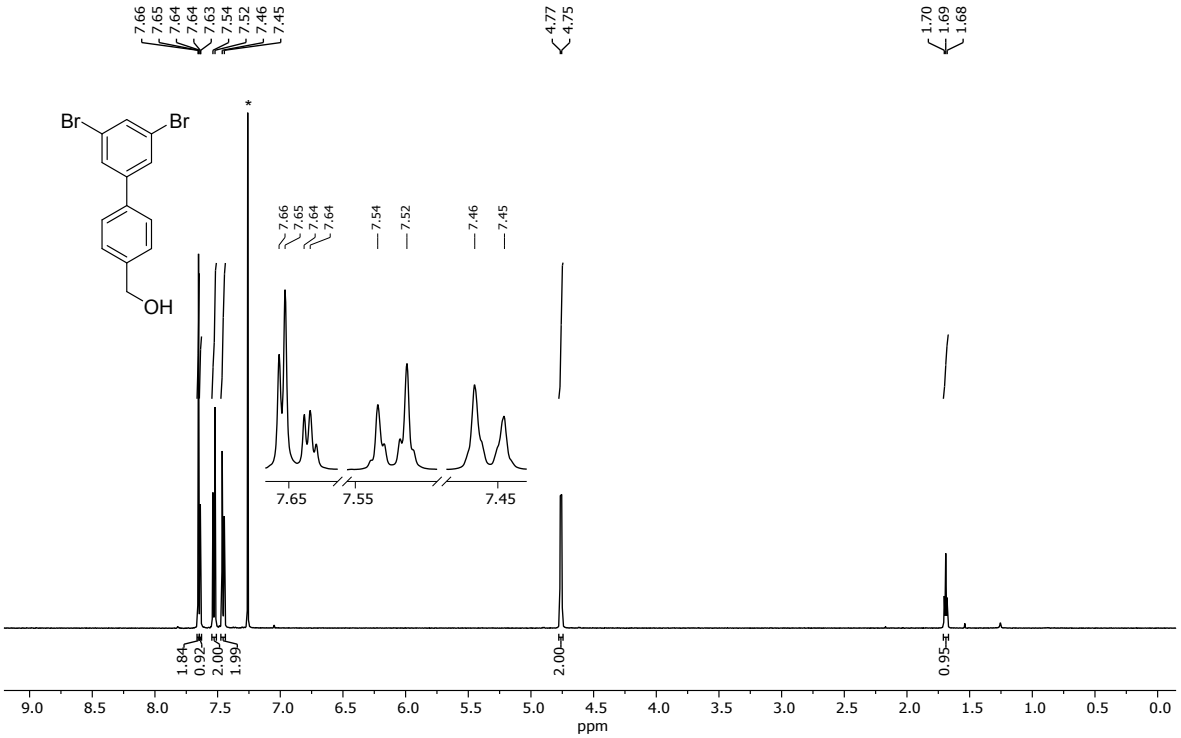

Figure S4. ^{13}C-NMR spectrum (126 MHz) of **6d** recorded in $CDCl_3$. Residual solvent signals denoted by asterisk (*).

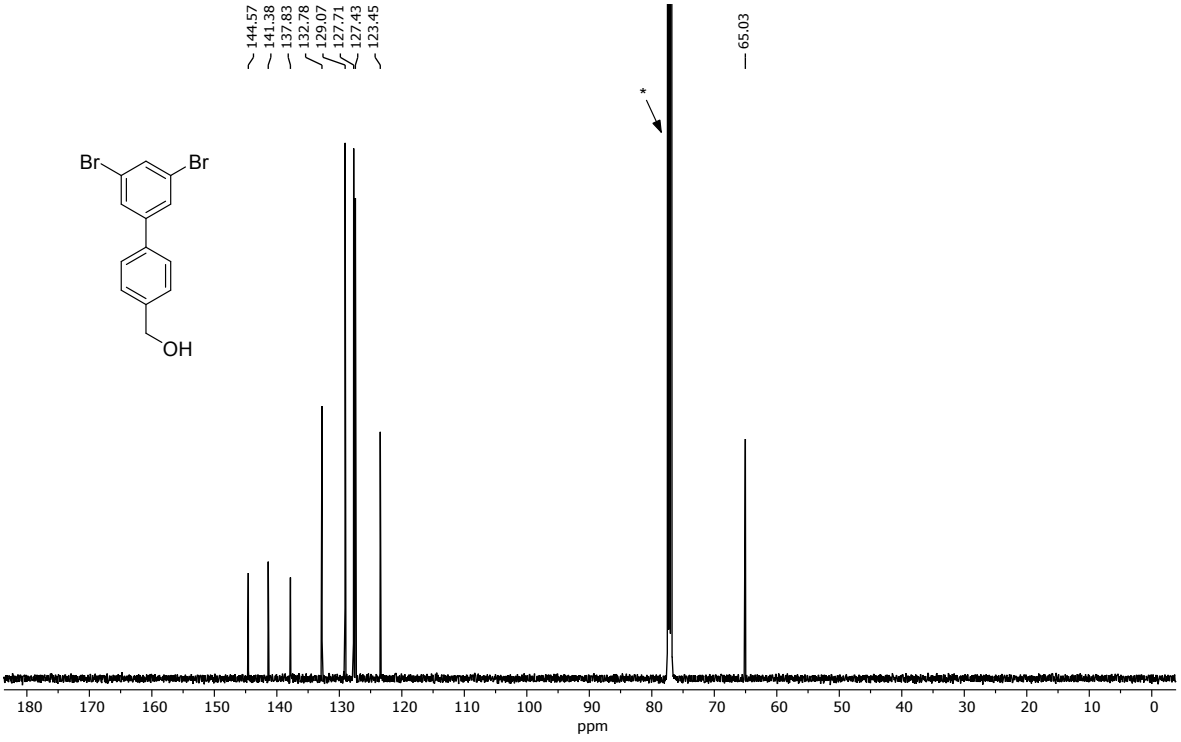

Figure S5. ^{1}H-NMR spectrum (500 MHz) of **5b** recorded in $CDCl_3$. Residual solvent signal denoted by asterisk (*).

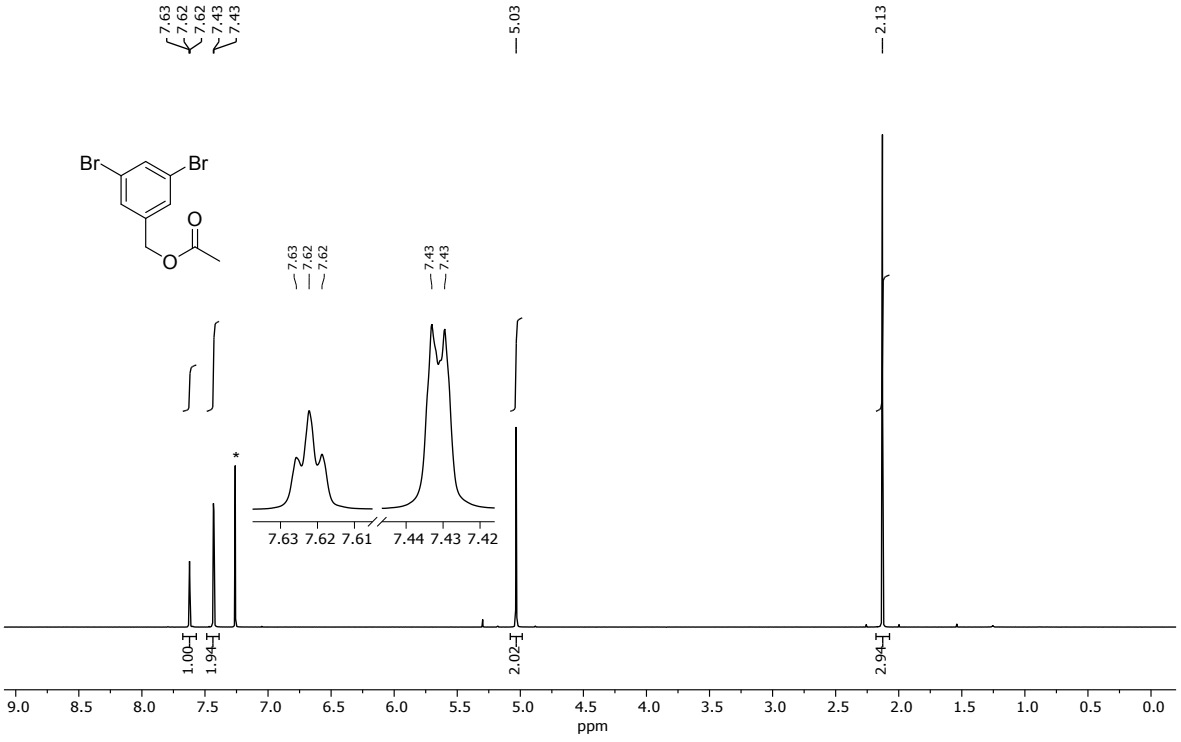

Figure S6. ^{13}C-NMR spectrum (126 MHz) of **5b** recorded in $CDCl_3$. Residual solvent signals denoted by asterisk (*).

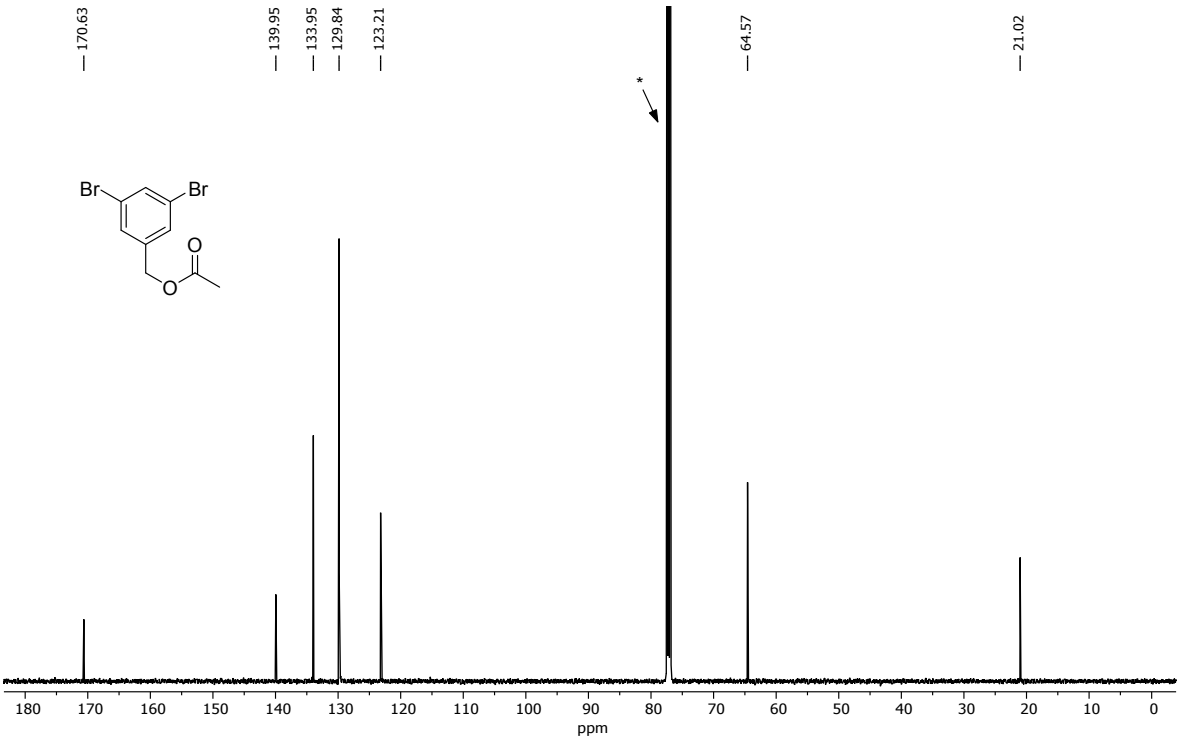

Figure S7. ^{1}H-NMR spectrum (500 MHz) of **5c** recorded in $CDCl_3$. Residual solvent signal denoted by asterisk (*).

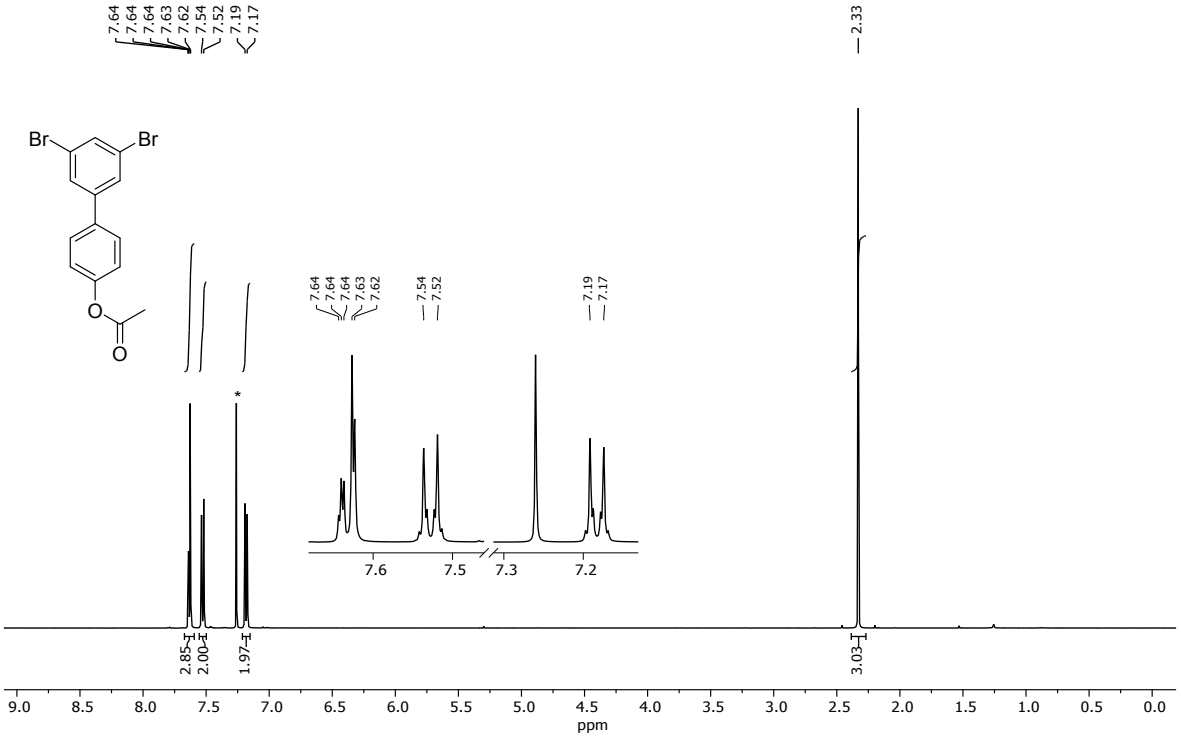

Figure S8. ^{13}C-NMR spectrum (126 MHz) of **5c** recorded in $CDCl_3$. Residual solvent signals denoted by asterisk (*).

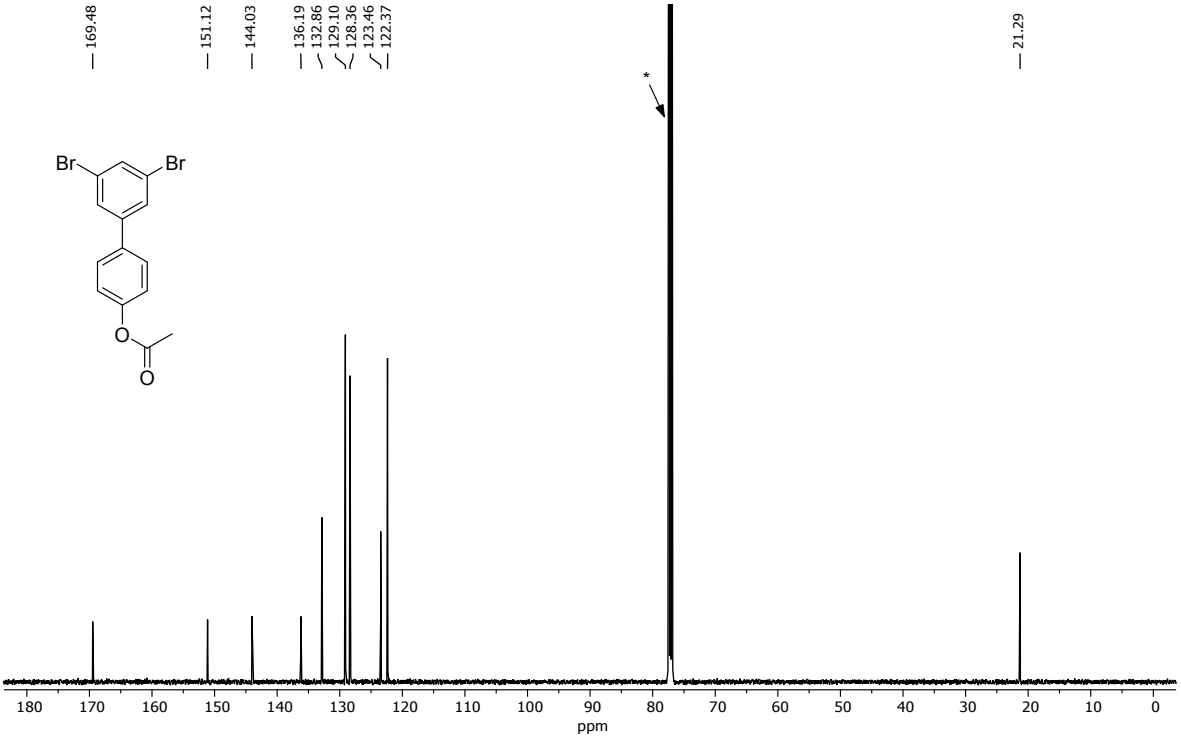

Figure S9. ^{1}H-NMR spectrum (500 MHz) of **5d** recorded in $CDCl_3$. Residual solvent signal denoted by asterisk (*).

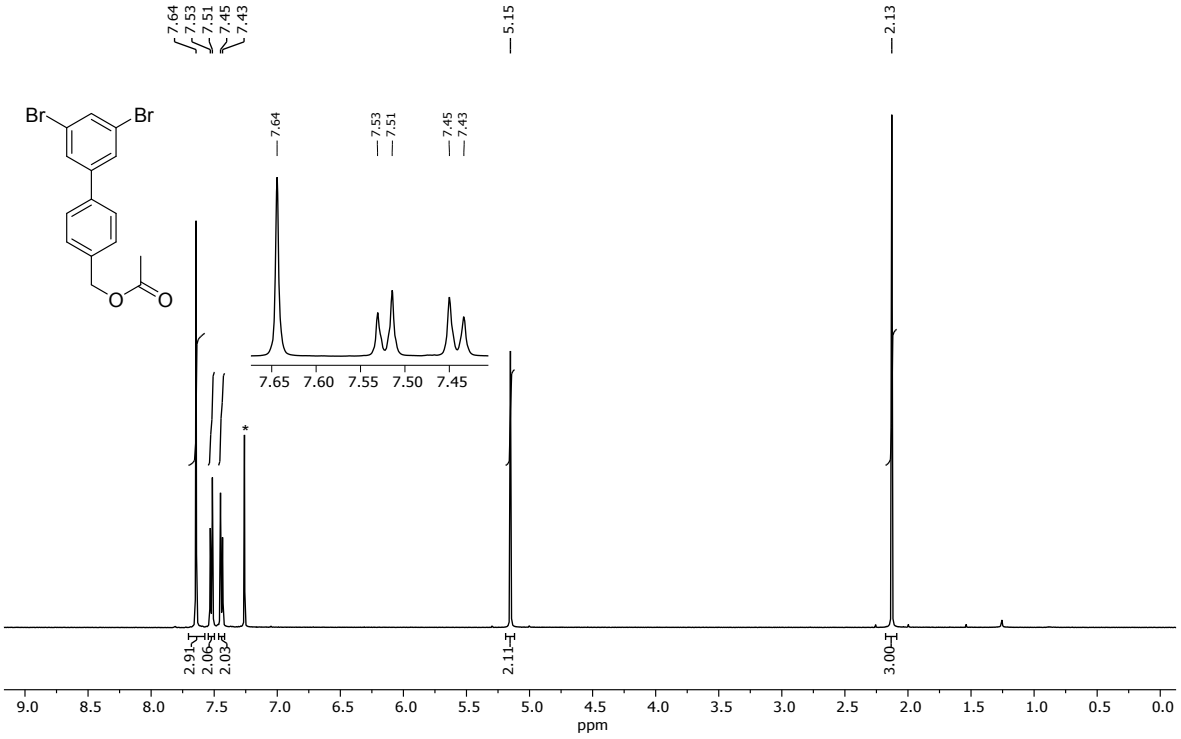

Figure S10. ^{13}C-NMR spectrum (126 MHz) of **5d** recorded in $CDCl_3$. Residual solvent signals denoted by asterisk (*).

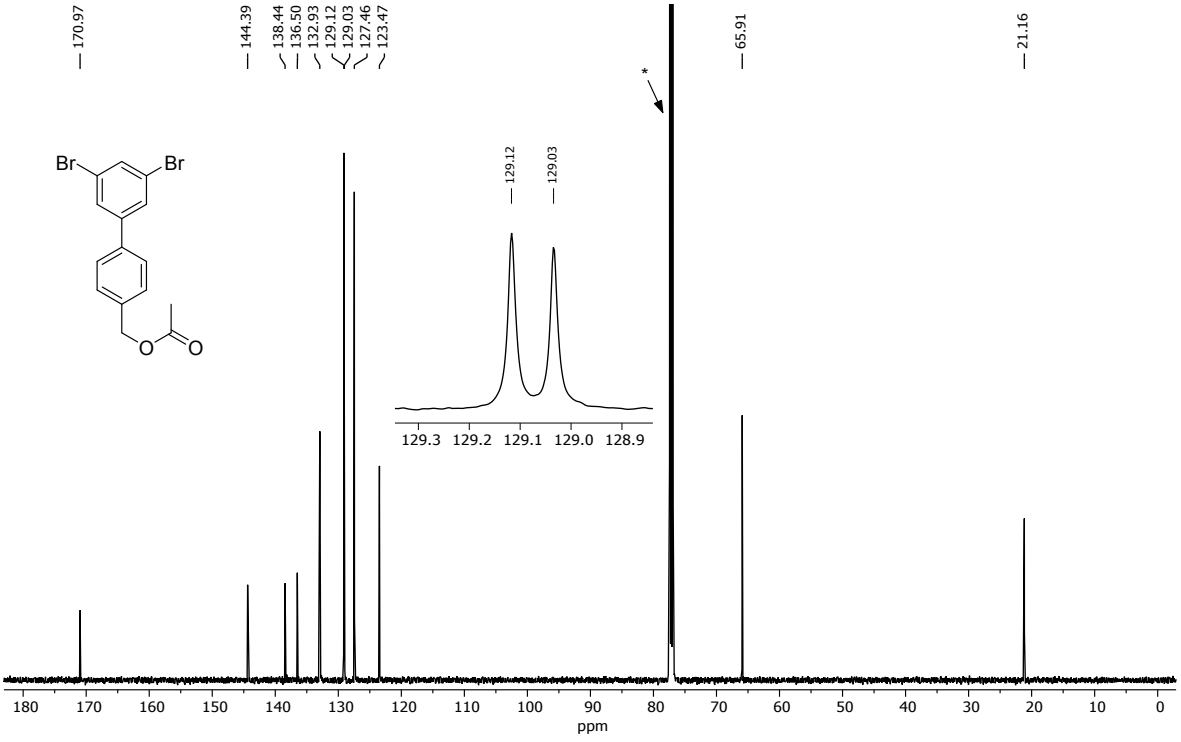

Figure S11. ^{1}H-NMR spectrum (500 MHz) of **4a** recorded in CD_2Cl_2. Residual solvent signal denoted by asterisk (*).

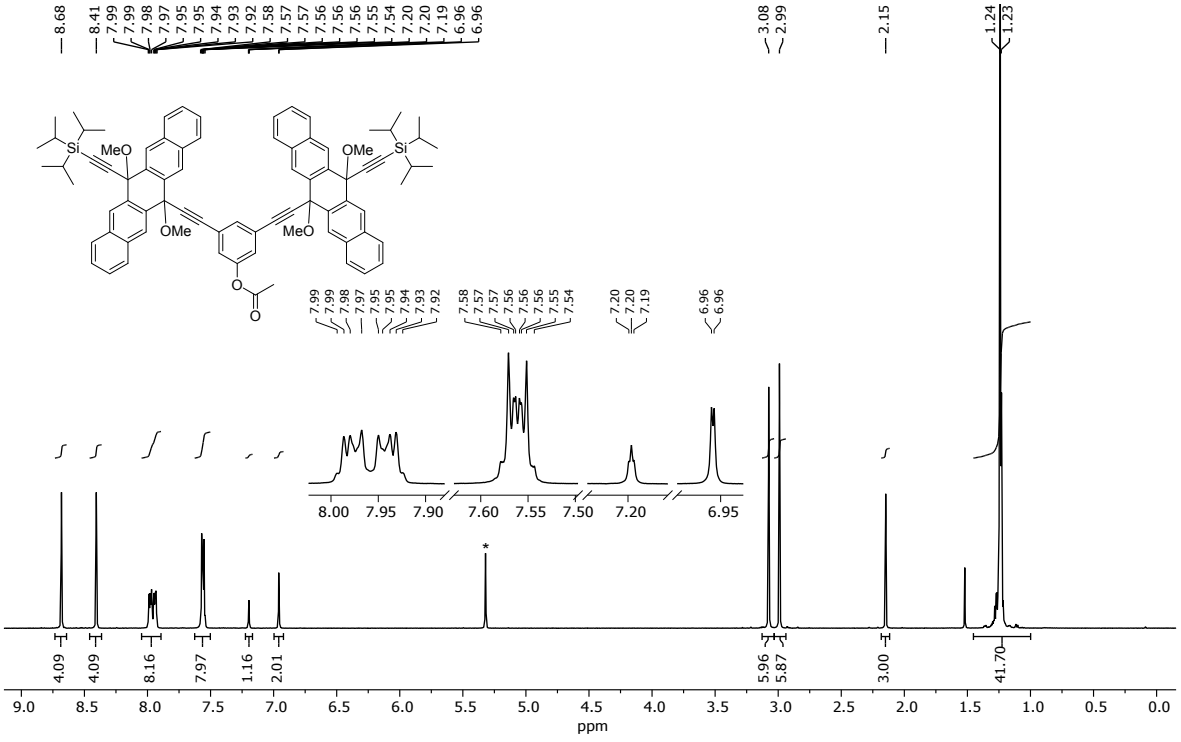

Figure S12. ^{13}C-NMR spectrum (126 MHz) of **4a** recorded in CD_2Cl_2. Residual solvent signals denoted by asterisk (*).

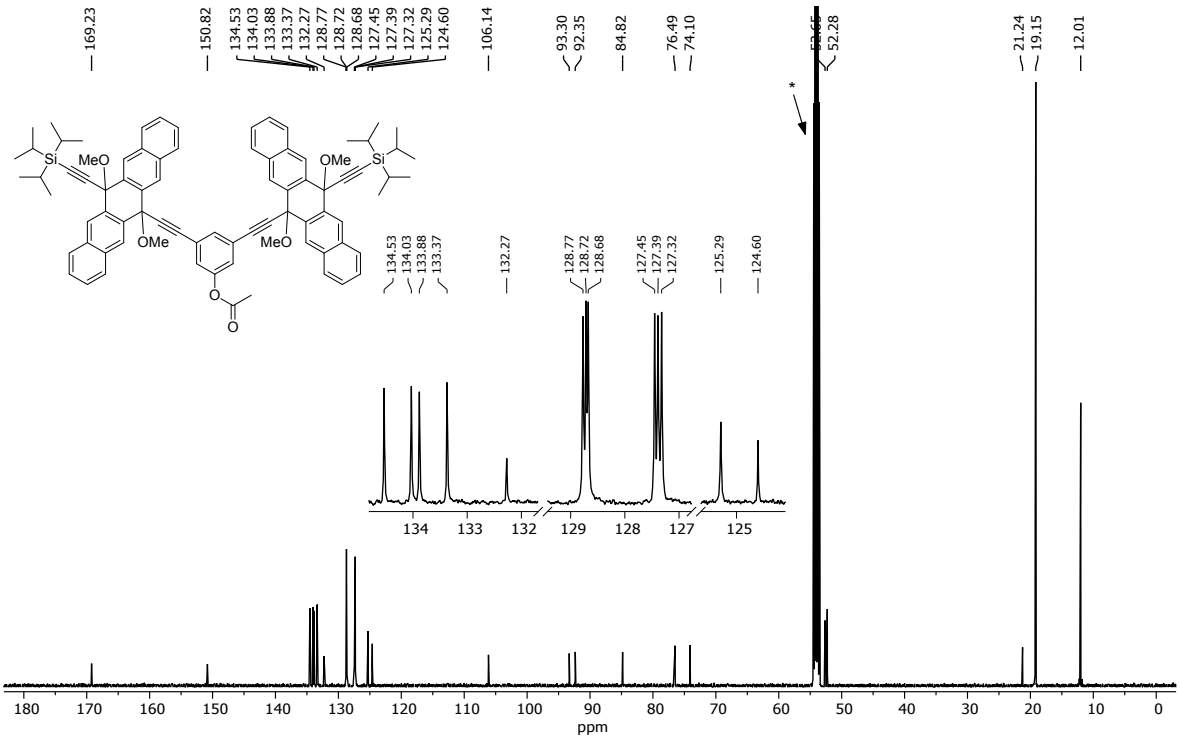

Figure S13. ^{1}H-NMR spectrum (500 MHz) of **4b** recorded in CD_2Cl_2. Residual solvent signal denoted by asterisk (*).

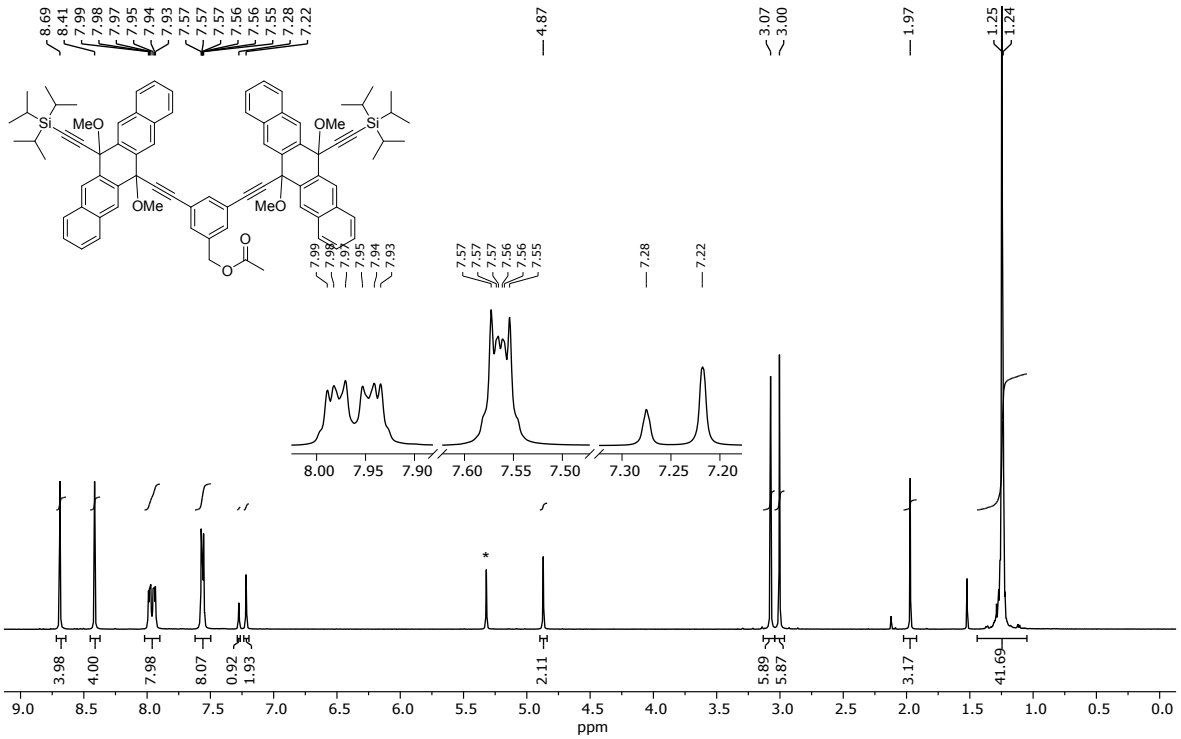

Figure S14. ^{13}C-NMR spectrum (126 MHz) of **4b** recorded in CD_2Cl_2. Residual solvent signals denoted by asterisk (*).

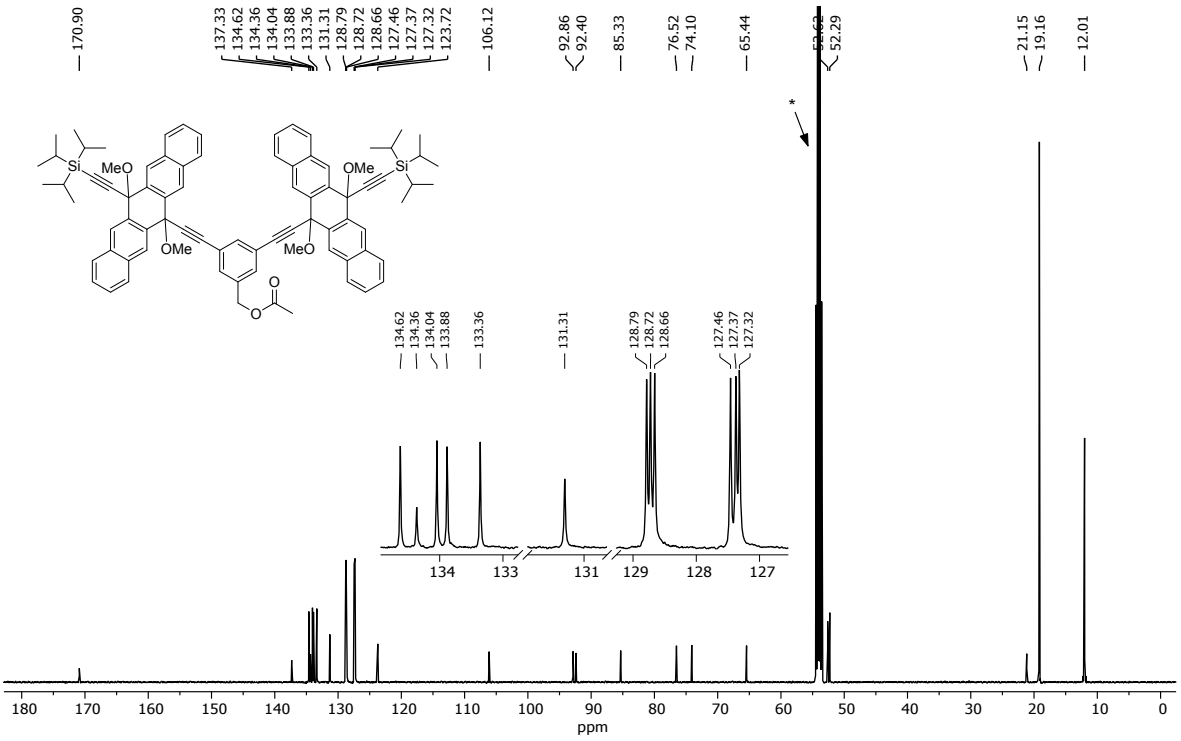

Figure S15. ^{1}H-NMR spectrum (500 MHz) of **4c** recorded in CD_2Cl_2. Residual solvent signal denoted by asterisk (*).

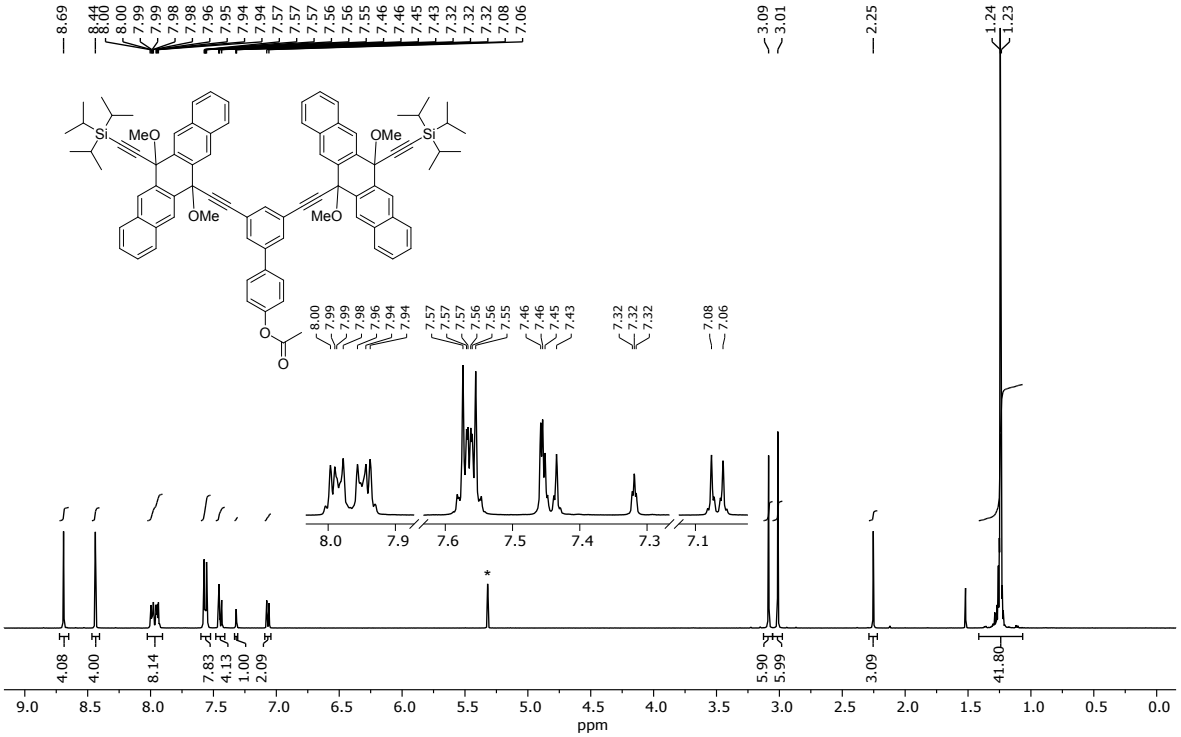

Figure S16. ^{13}C-NMR spectrum (126 MHz) of **4c** recorded in CD_2Cl_2. Residual solvent signals denoted by asterisk (*).

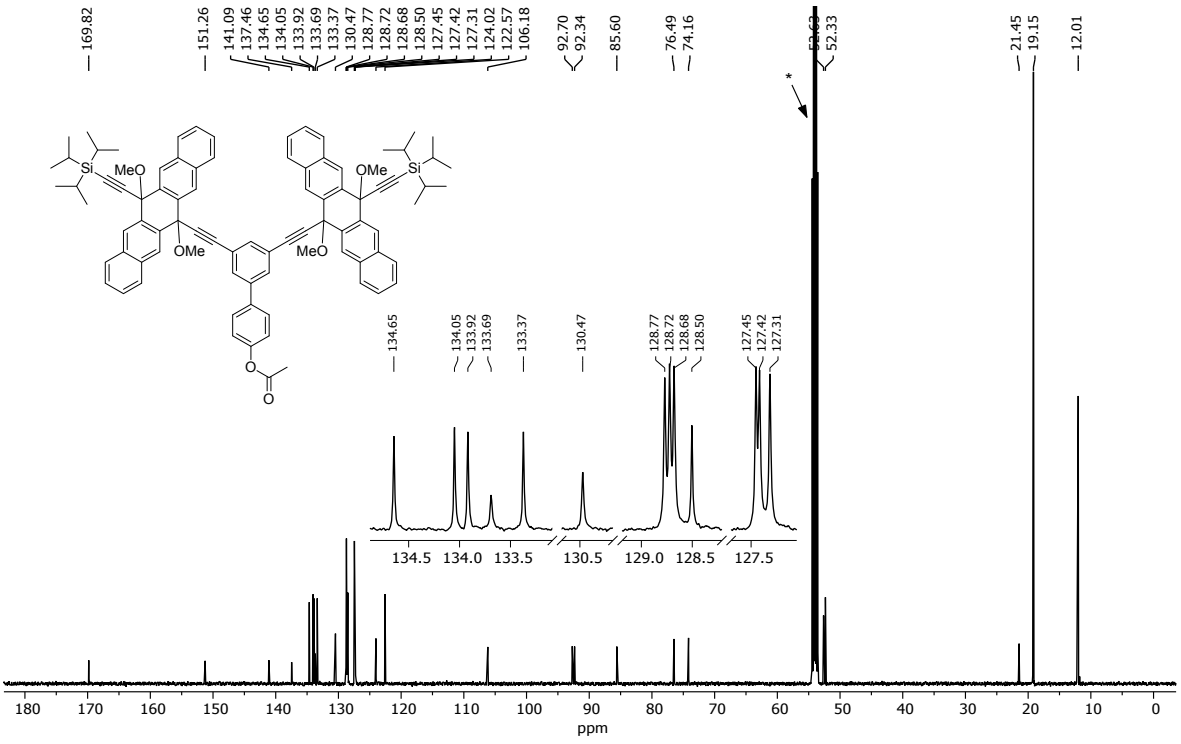

Figure S17. ^{1}H-NMR spectrum (500 MHz) of **4d** recorded in CD_2Cl_2. Residual solvent signal denoted by asterisk (*).

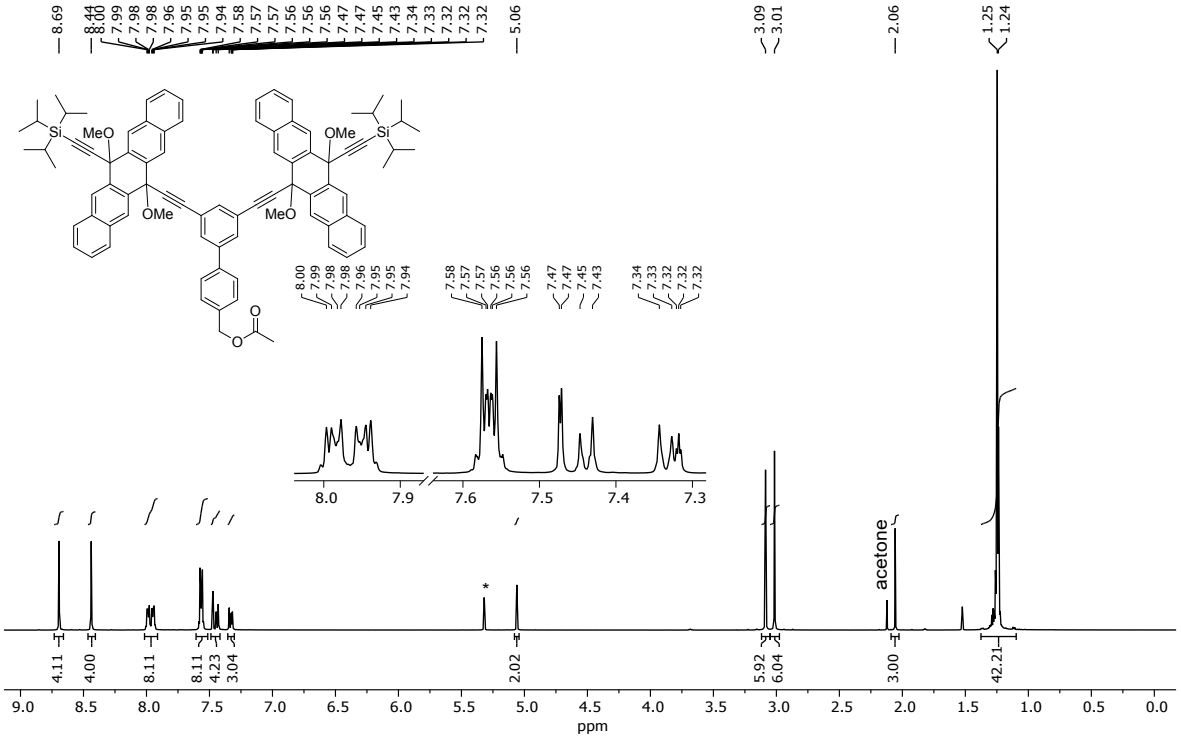

Figure S18. ^{13}C-NMR spectrum (126 MHz) of **4d** recorded in CD_2Cl_2. Residual solvent signals denoted by asterisk (*).

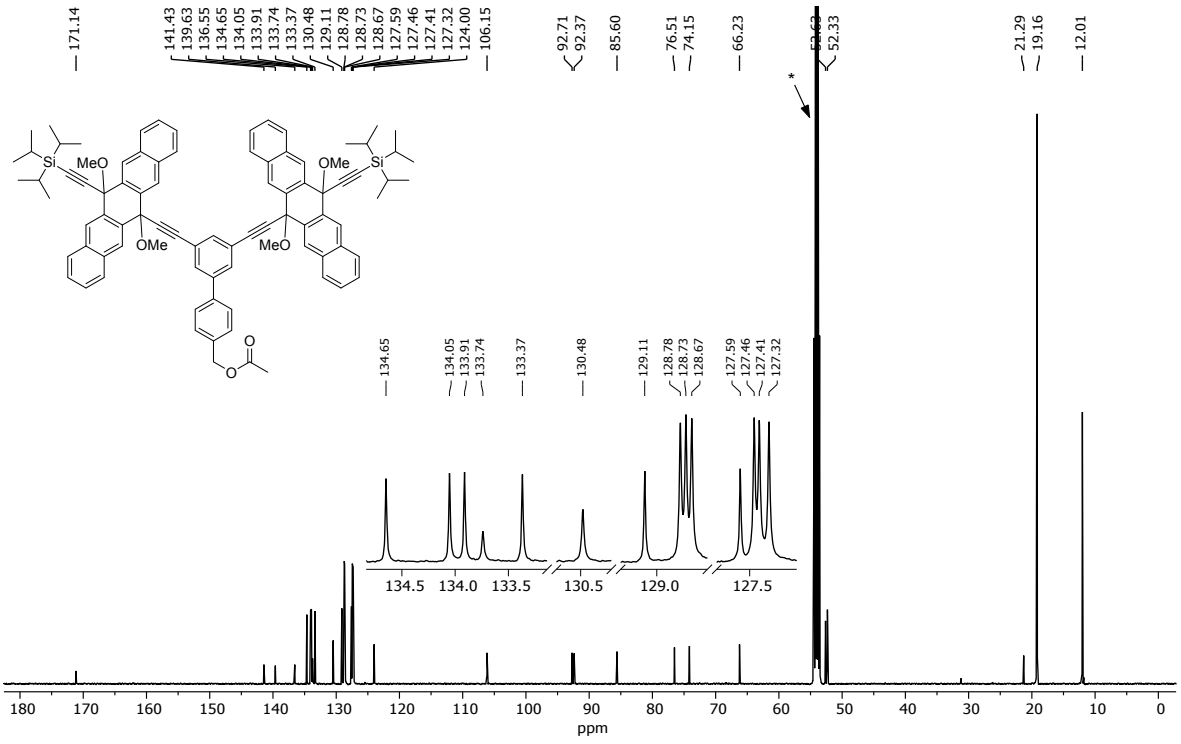

Figure S19. ^{1}H-NMR spectrum (500 MHz) of **3a** recorded in CD_2Cl_2. Residual solvent signal denoted by asterisk (*).

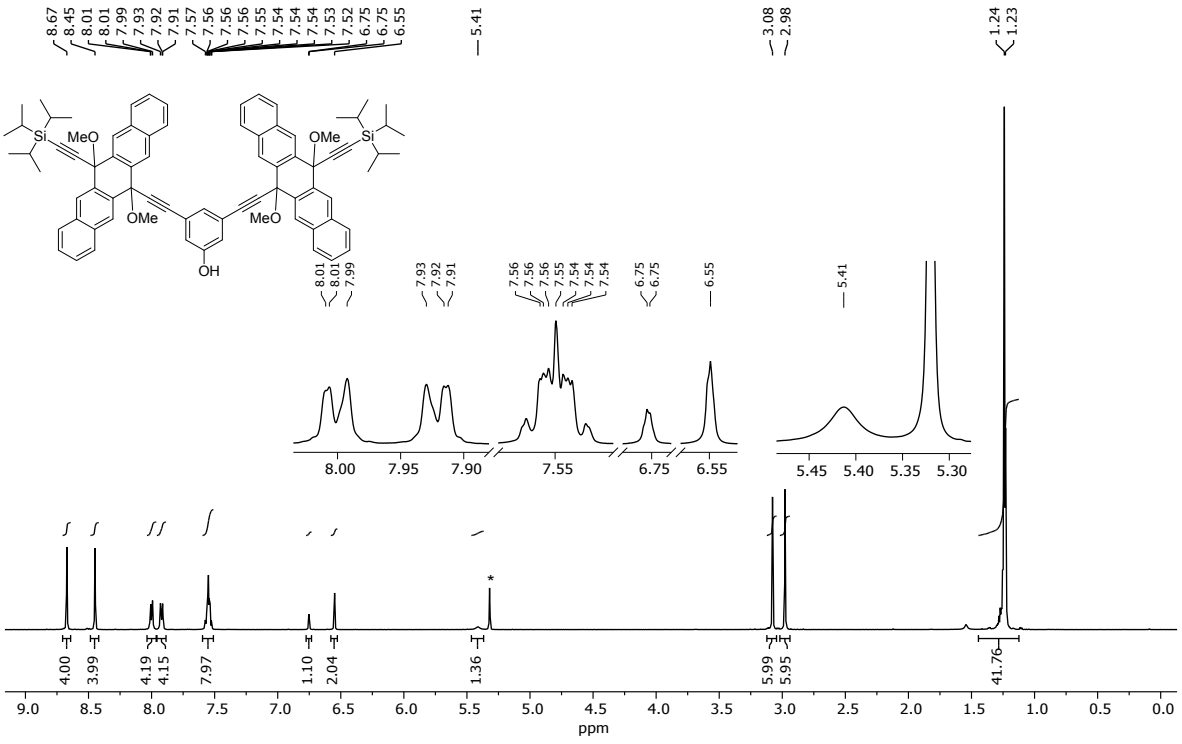

Figure S20. ^{13}C-NMR spectrum (126 MHz) of **3a** recorded in CD_2Cl_2. Residual solvent signals denoted by asterisk (*).

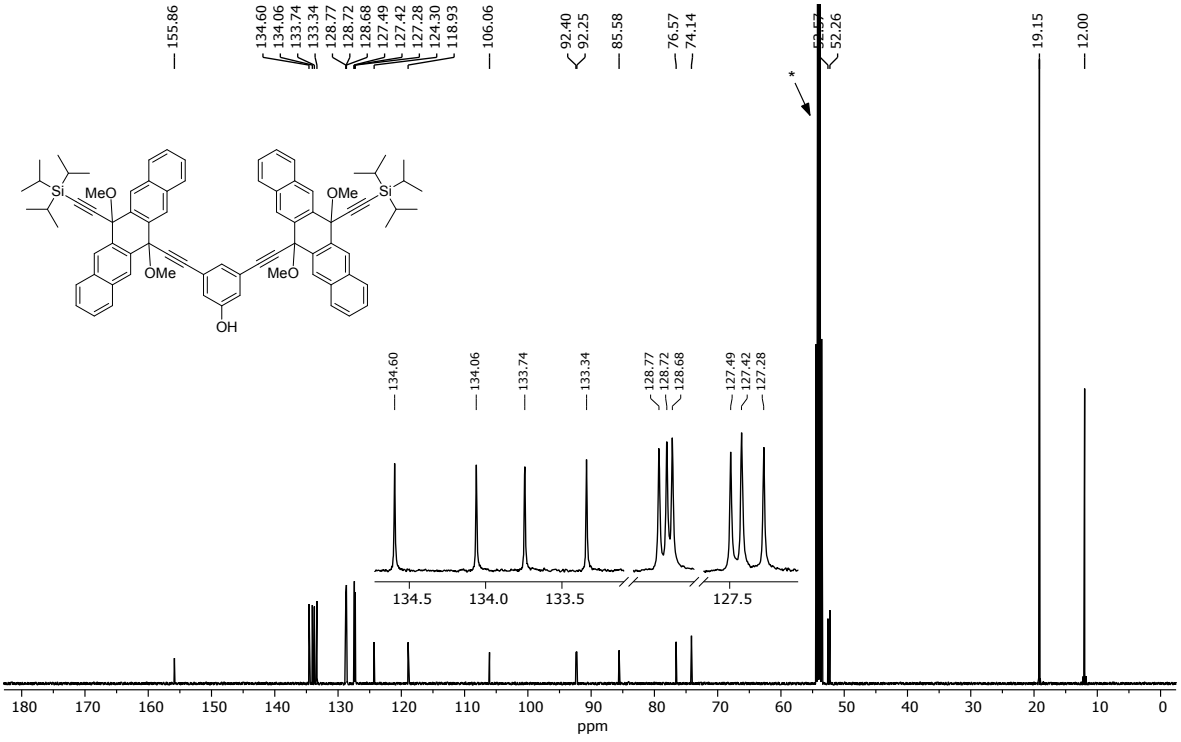

Figure S21. ^{1}H-NMR spectrum (500 MHz) of **3b** recorded in CD_2Cl_2. Residual solvent signal denoted by asterisk (*).

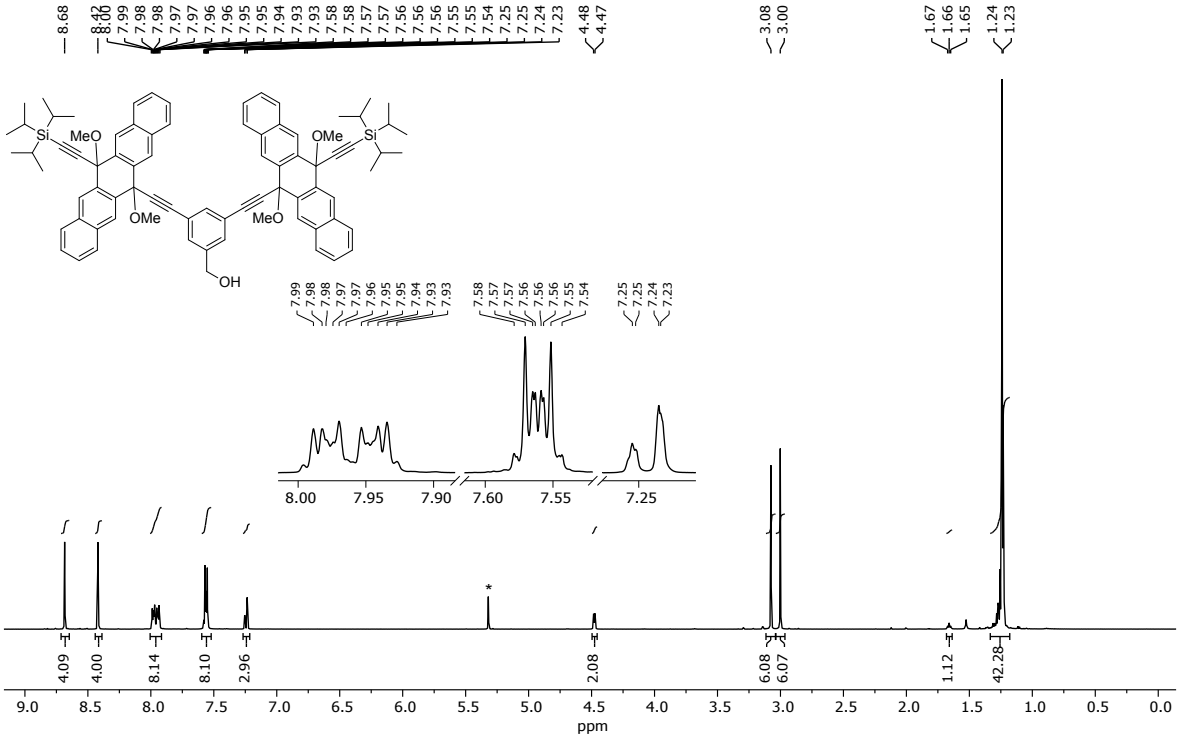

Figure S22. ^{13}C-NMR spectrum (126 MHz) of **3b** recorded in CD_2Cl_2. Residual solvent signals denoted by asterisk (*).

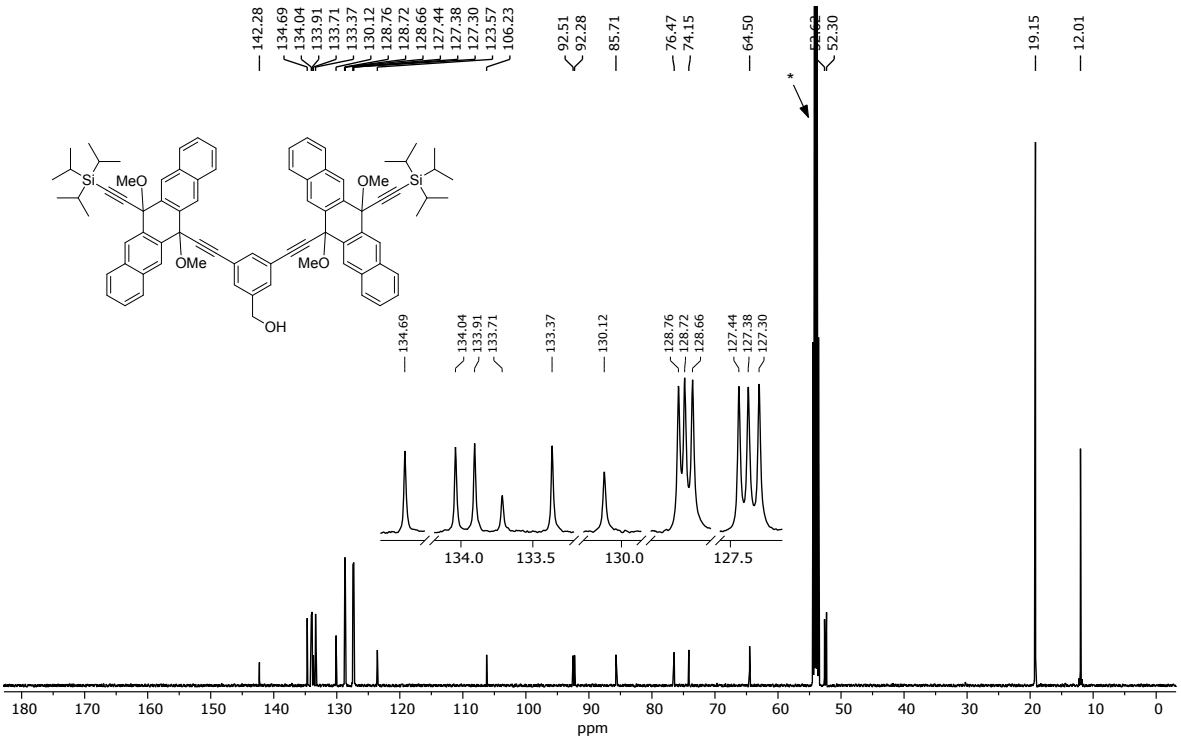

Figure S23. ^{1}H-NMR spectrum (500 MHz) of **3c** recorded in CD_2Cl_2. Residual solvent signal denoted by asterisk (*).

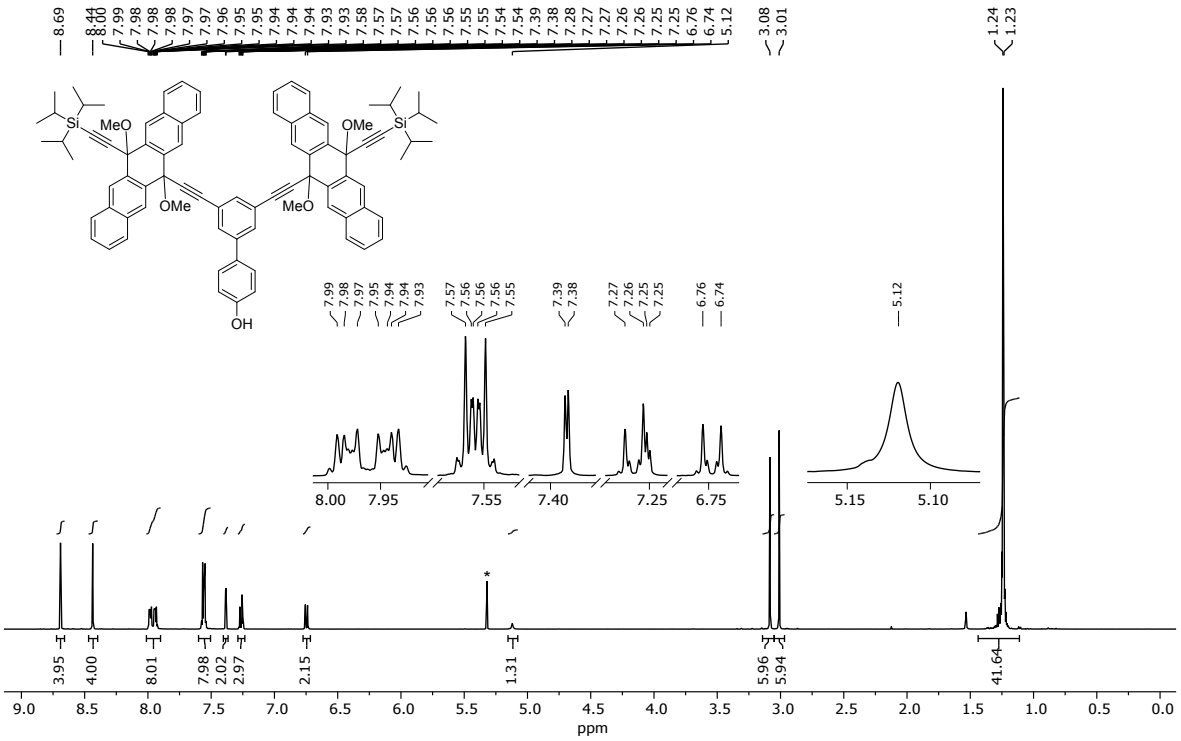

Figure S24. ^{13}C-NMR spectrum (126 MHz) of **3c** recorded in CD_2Cl_2. Residual solvent signals denoted by asterisk (*).

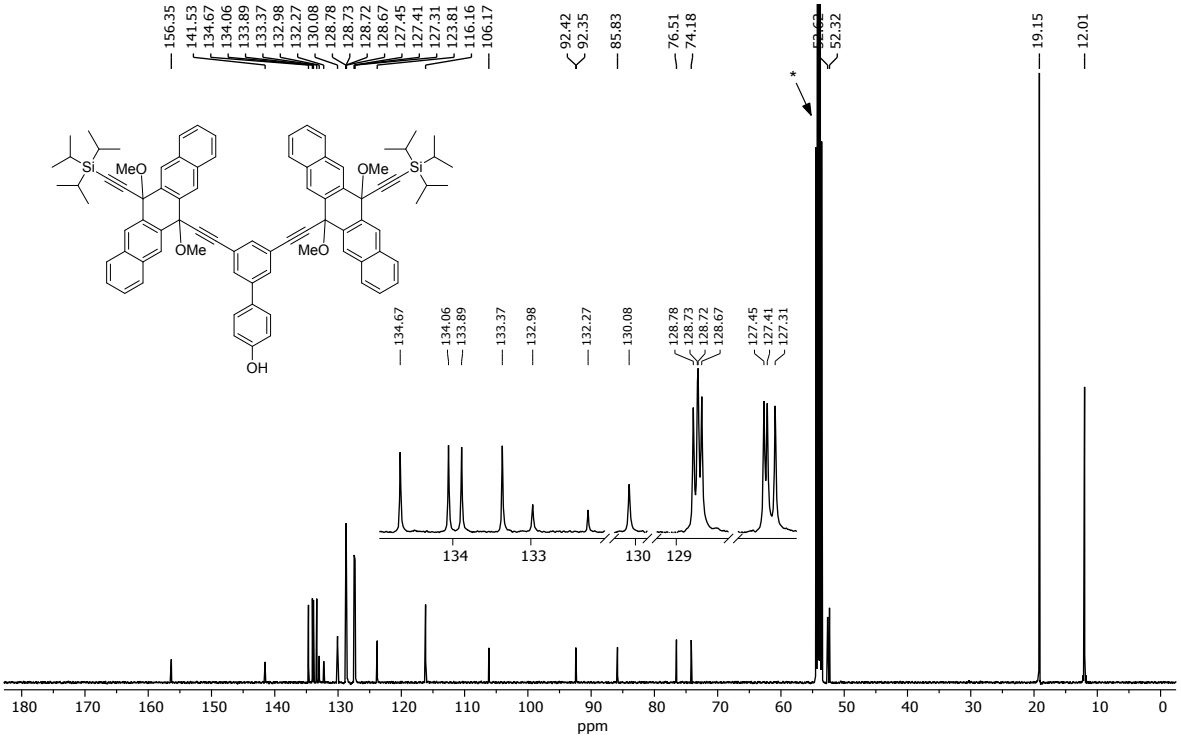

Figure S25. ^{1}H-NMR spectrum (500 MHz) of **3d** recorded in CD_2Cl_2. Residual solvent signal denoted by asterisk (*).

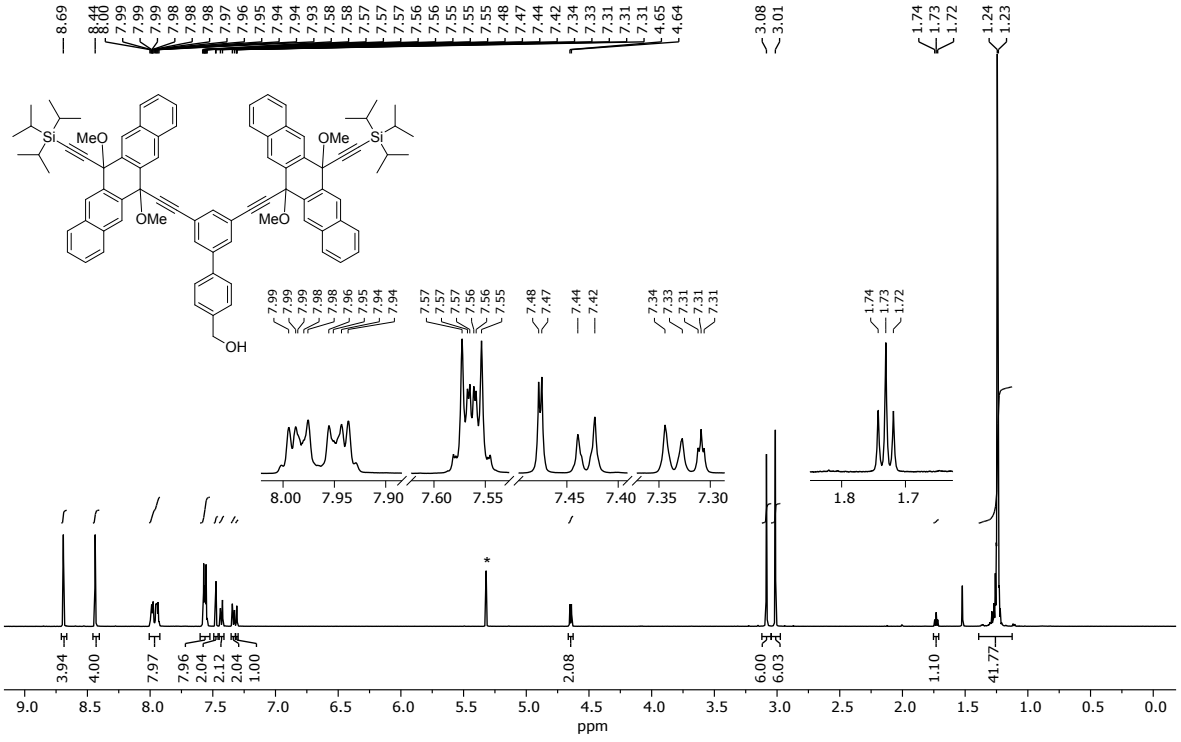

Figure S26. ^{13}C-NMR spectrum (126 MHz) of **3d** recorded in CD_2Cl_2. Residual solvent signals denoted by asterisk (*).

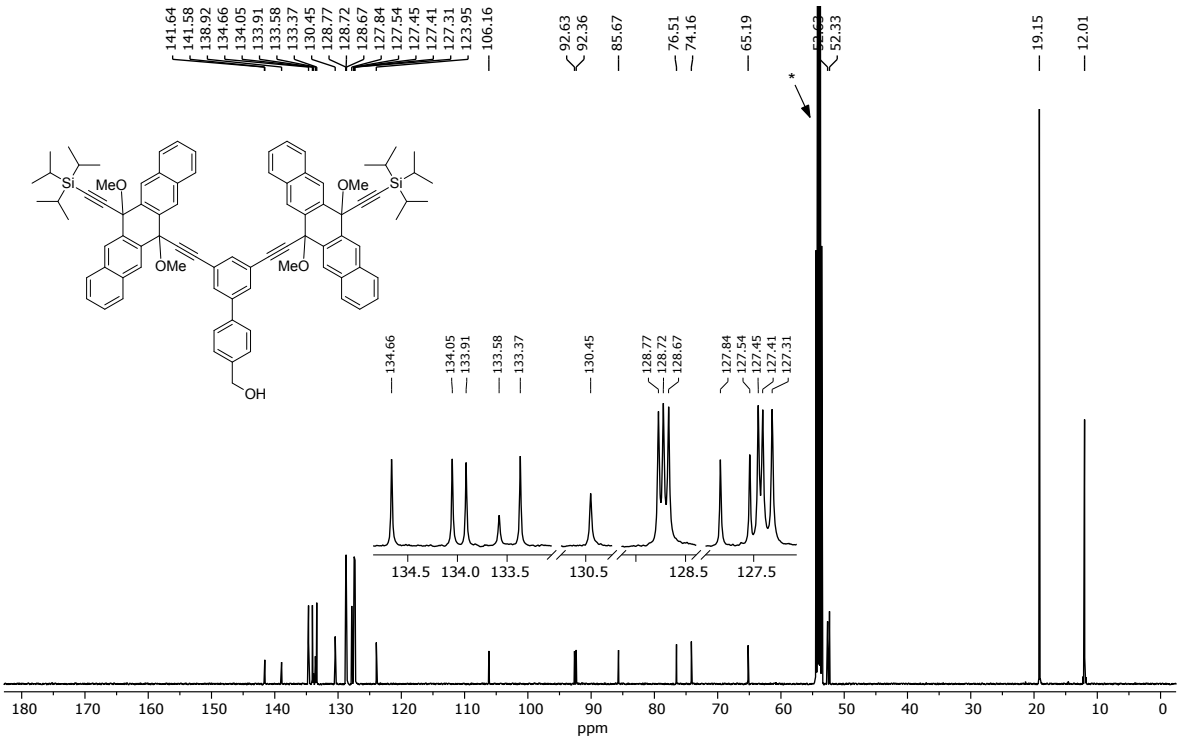

Figure S27. ^{1}H-NMR spectrum (500 MHz) of **2a** recorded in CD_2Cl_2. Residual solvent signal denoted by asterisk (*).

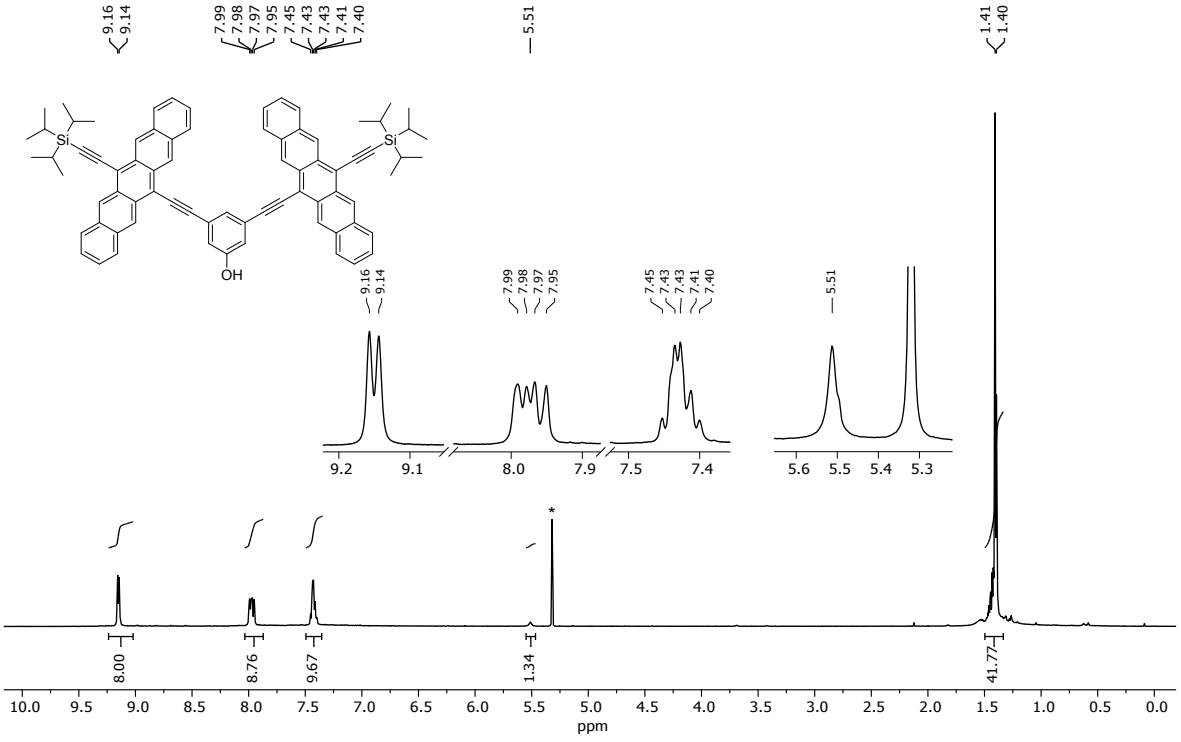

Figure S28. ^{13}C-NMR spectrum (126 MHz) of **2a** recorded in CD_2Cl_2. Residual solvent signals denoted by asterisk (*).

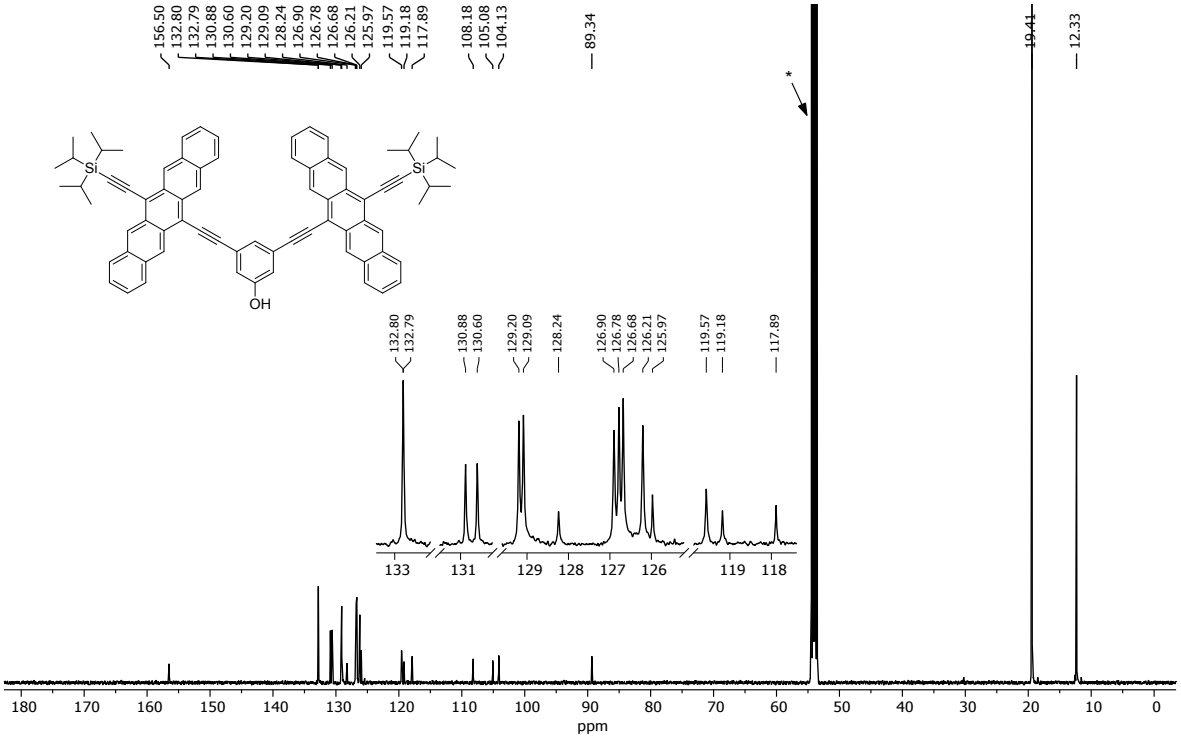

Figure S29. ^{1}H-NMR spectrum (500 MHz) of **2b** recorded in THF-d_8. Residual solvent signal denoted by asterisk (*).

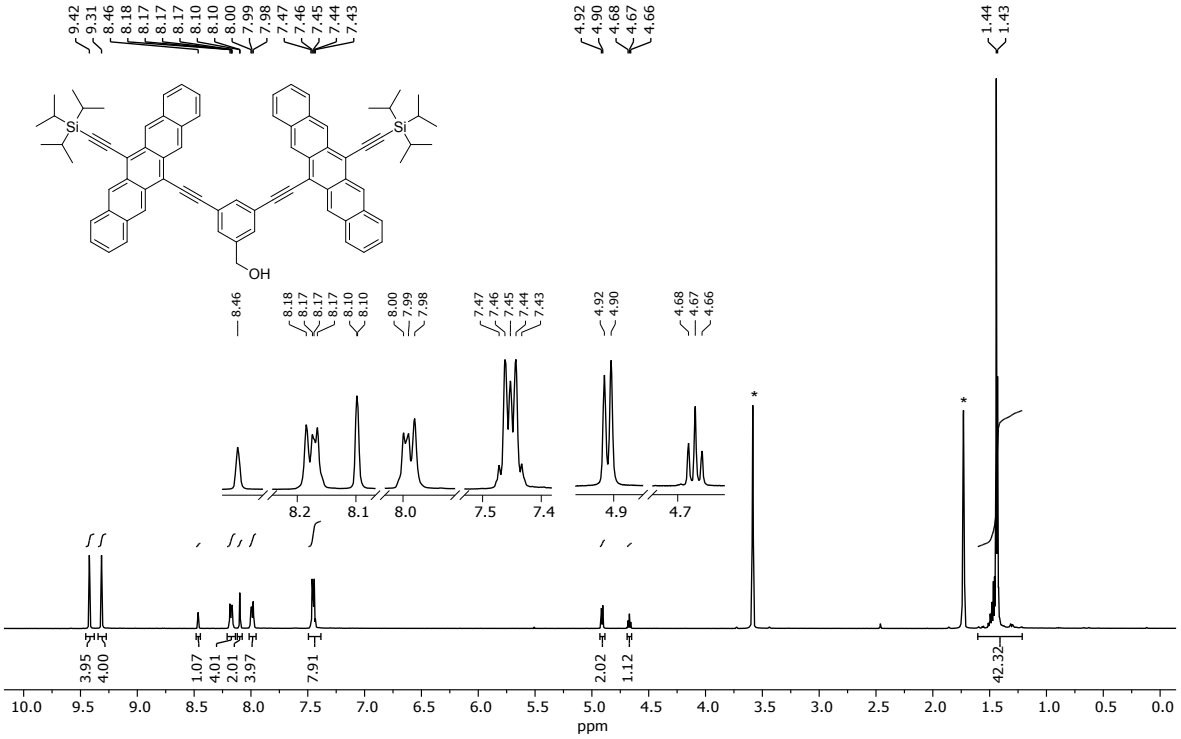

Figure S30. ^{13}C-NMR spectrum (126 MHz) of **2b** recorded in THF-d_8. Residual solvent signals denoted by asterisk (*).

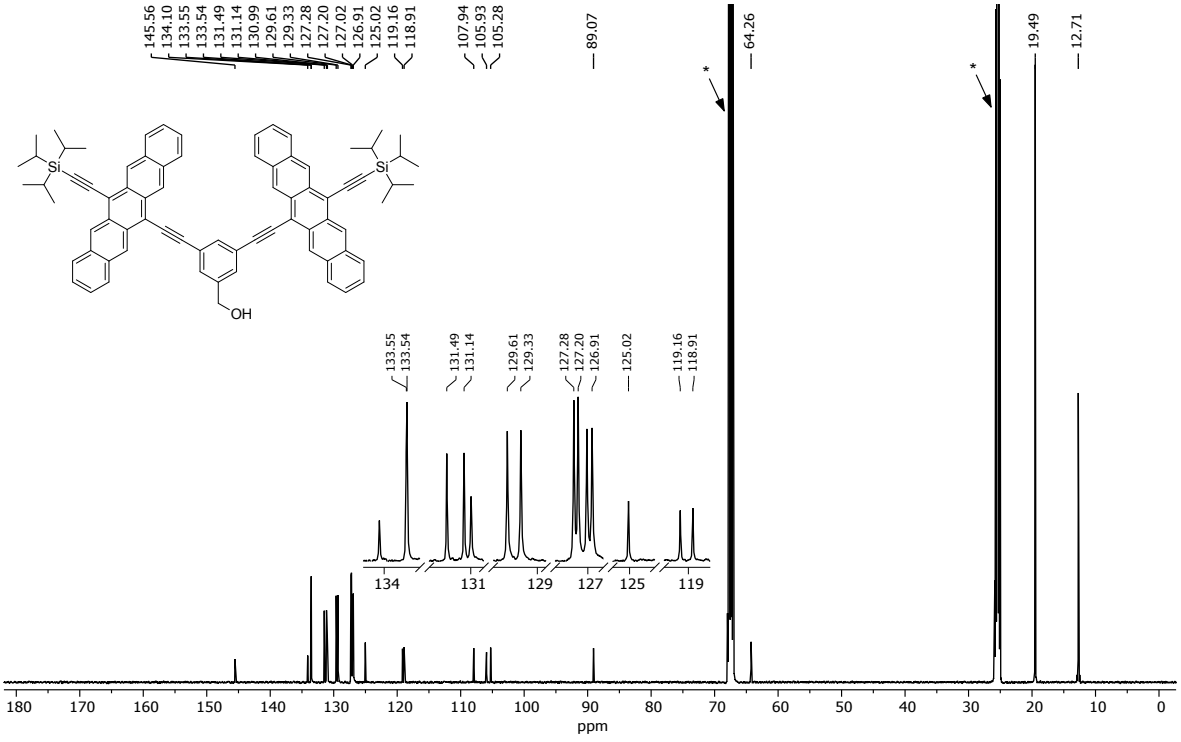

Figure S31. ^{1}H-NMR spectrum (500 MHz) of **2c** recorded in THF-d_8. Residual solvent signal denoted by asterisk (*).

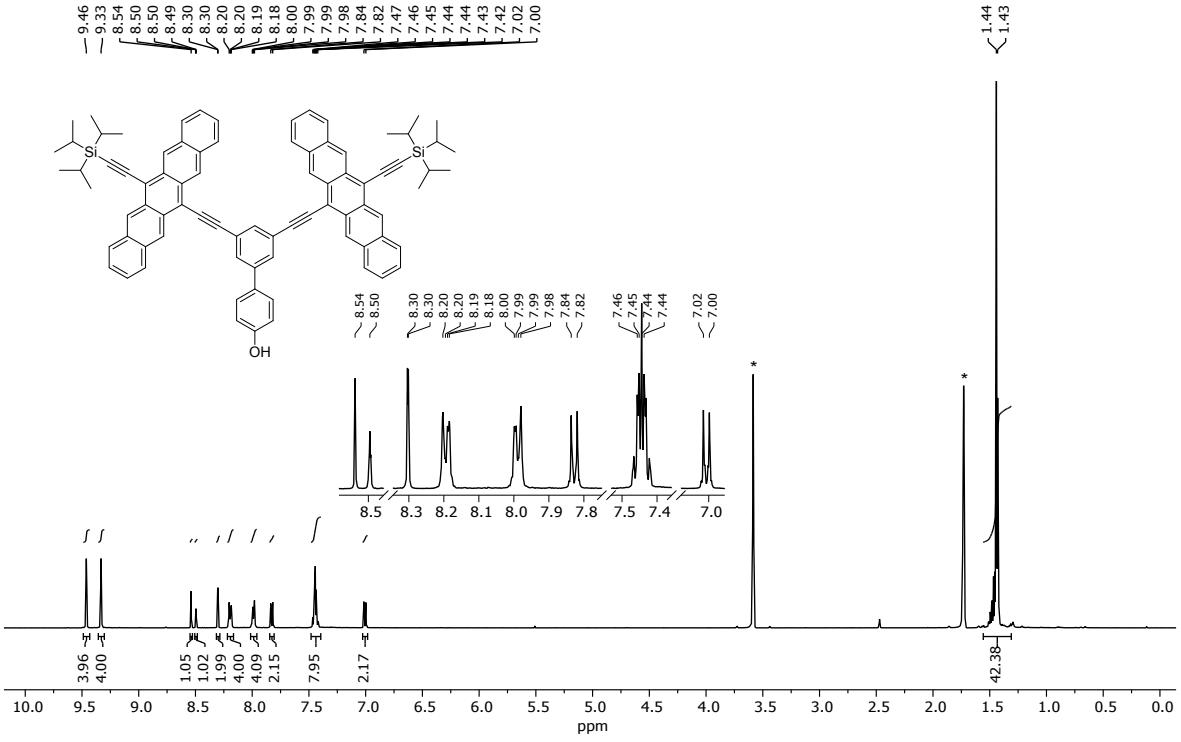

Figure S32. ^{13}C-NMR spectrum (126 MHz) of **2c** recorded in THF-d_8. Residual solvent signals denoted by asterisk (*).

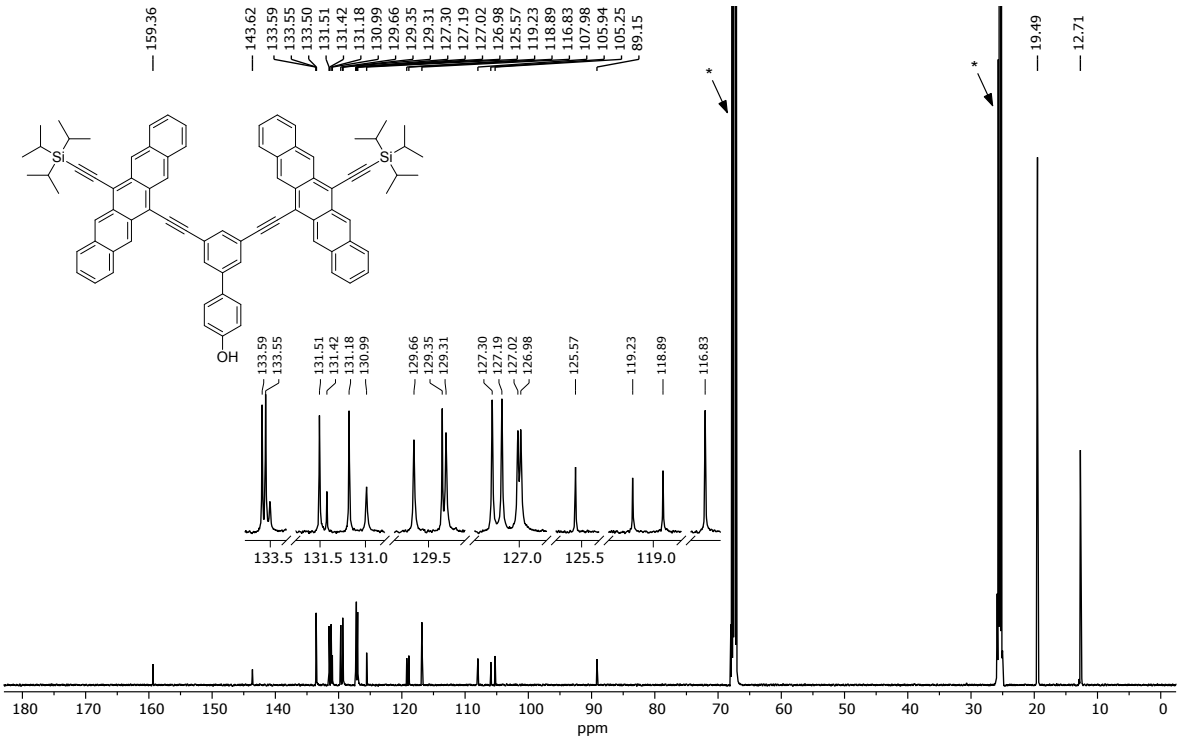

Figure S33. ^{1}H-NMR spectrum (500 MHz) of **2d** recorded in THF-d_8. Residual solvent signal denoted by asterisk (*).

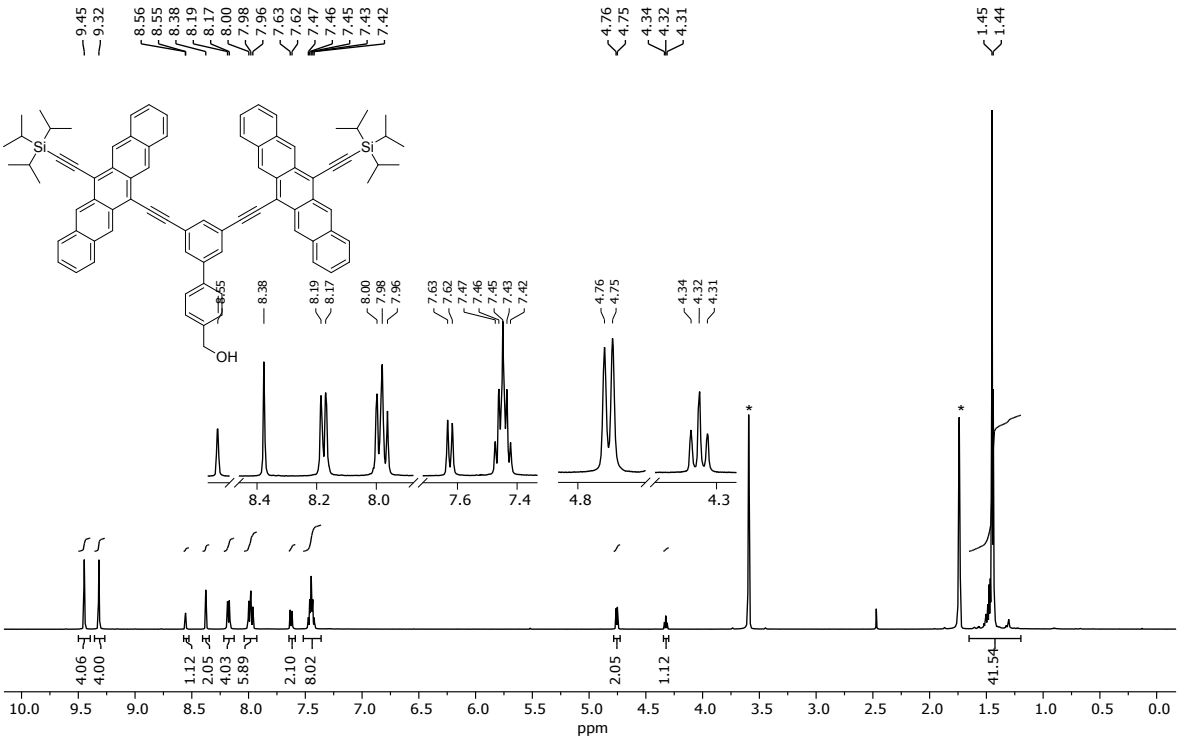

Figure S34. ^{13}C-NMR spectrum (126 MHz) of **2d** recorded in THF-d_8. Residual solvent signal denoted by asterisk (*).

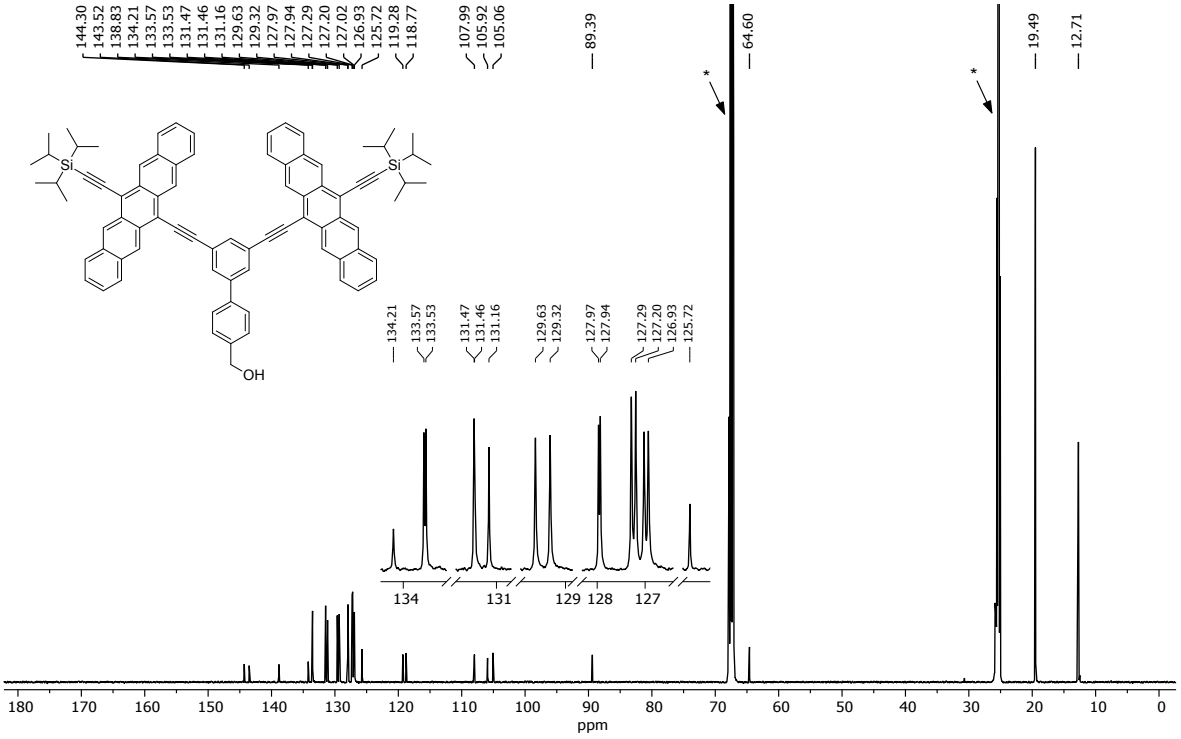

Synthesis and characterization of SubPc-Pnc$_2$ derivatives 1a-d.

*General method for the synthesis of SubPc-Pnc$_2$ derivatives **1a-d**:* In a 10 mL round-bottomed flask equipped with a magnetic stirrer and a rubber seal, SubPcCl **9** (0.025 mmol) and silver trifluoromethanesulfonate (0.031 mmol, 1.25 equiv) were placed. Anhydrous toluene (1 mL) was added and the mixture was stirred under argon atmosphere at room temperature until the disappearance of the SubPcCl starting material, which was monitored by TLC. At this point Pnc$_2$ **2a-d** (0.031 mmol, 1.25 equiv) and *N*,*N*-diisopropylethylamine (0.031 mmol, 1.25 equiv) were added, and the reaction mixture was stirred at 50 °C. To limit light exposure, the reaction flask was covered in aluminum foil. The reaction mixture was then passed through a short Celite plug. The solvent was removed by evaporation under reduced pressure and the product was directly purified by size exclusion chromatography using $CHCl_3$ as eluent. The solvent was evaporated under reduced pressure and the product was then recrystallized from a CH_2Cl_2/hexane mixture. The reaction time and the reaction yields are indicated below for each compound.

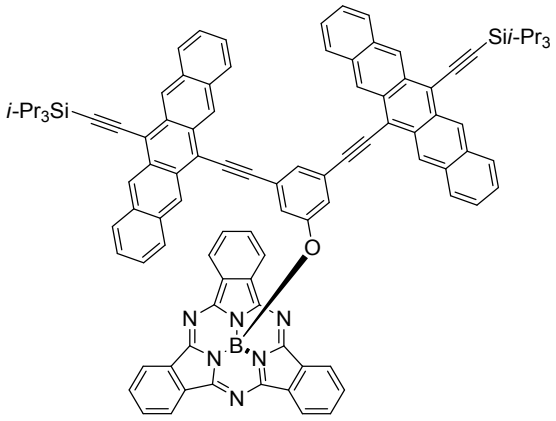

SubPc-Pnc$_2$ 1a. Reaction time: 5 h. SubPc-Pnc$_2$ **1a** was afforded as a purple solid in 19% yield. **^{1}H-NMR** (500 MHz, $CDCl_3$): δ (ppm) = 9.31 (s, 4H), 9.26 (s, 4H), 8.94–8.91 (AA'XX' system, 6H), 8.27–8.25 (m, 4H), 8.00–7.98 (m, 4H), 7.90–7.86 (AA'XX' system, 6H), 7.76 (t, *J* = 1.5 Hz, 1H), 7.45–7.43 (m, 8H), 6.00 (d, *J* = 1.5 Hz, 2H), 1.40–1.39 (m, 42H); **^{13}C-NMR** (125.7 MHz, $CDCl_3$): δ (ppm) = 151.92, 132.53, 132.49, 131.28, 131.27, 130.77, 130.42, 130.24, 129.11, 128.83, 127.85, 126.60, 126.24, 126.12, 124.73, 122.54, 122.16, 118.75, 117.85, 107.50, 104.93, 103.60, 88.49, 19.18, 11.88 (one signal coincident or not observed); **^{11}B-NMR** (160.4 MHz, $CDCl_3$): δ (ppm) = −14.51; **HRMS (MALDI-TOF)**: Calculated for $C_{100}H_{81}BN_6OSi_2$: 1449.6136; Found: 1449.6167; **UV/Vis** (toluene): λ_{max} (log ε) = 661 (4.83), 606 (4.54), 565 (4.99), 549 (sh), 525 (4.48), 442 (3.98), 417 (3.78), 374 (4.69), 353 (4.66) nm.

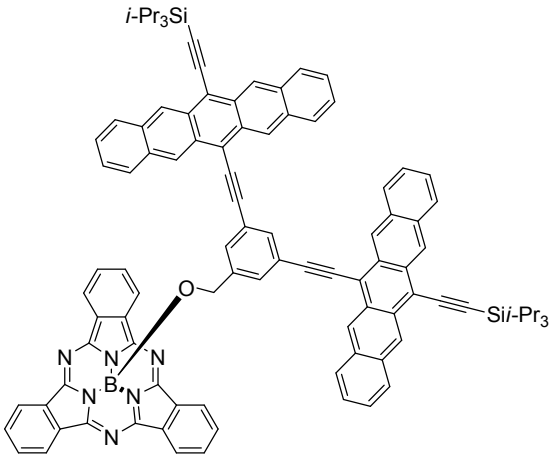

SubPc-Pnc$_2$ 1b. Reaction time: 13 h. SubPc-Pnc$_2$ **1b** was afforded as a purple solid in 26% yield. **^{1}H-NMR** (500 MHz, THF-d_8): δ (ppm) = 9.43 (s, 4H), 9.38 (s, 4H), 8.88–8.85 (AA'XX' system, 6H), 8.32–8.30 (m, 4H), 8.12 (s, 1H), 8.02–8.00 (m, 4H), 7.90–7.87 (AA'XX' system, 6H), 7.50–7.46 (m, 8H), 7.17 (s, 2H), 2.94 (s, 2H), 1.44–1.43 (m, 42H); **^{13}C-NMR** (125.7 MHz, THF-d_8): δ (ppm) = The low solubility of this product prevented the registration of a clear ^{13}C-NMR spectrum; **^{11}B-NMR** (160.4 MHz, THF-d_8): δ (ppm) = −14.22; **HRMS (MALDI-TOF)**: Calculated for $C_{101}H_{83}BN_6OSi_2$: 1463.6292; Found: 1463.6302; **UV/Vis** (toluene): λ_{max} (log ε) = 660 (4.83), 605 (4.57), 564 (5.02), 547 (sh), 524 (4.50), 441 (3.99), 417 (3.73), 373 (4.77), 353 (4.68) nm.

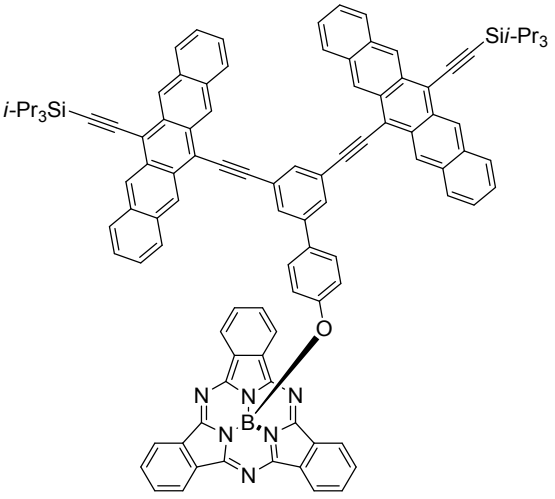

SubPc-Pnc$_2$ 1c. Reaction time: 5 h. SubPc-Pnc$_2$ **1c** was afforded as a purple solid in 16% yield. **^{1}H-NMR** (500 MHz, THF-d_8): δ (ppm) = 9.47 (s, 4H), 9.37 (s, 4H), 8.89–8.86 (AA'XX' system, 6H), 8.45 (s, 1H), 8.22–8.20 (m, 4H), 8.15 (d, J = 1.5 Hz, 2H), 8.01–7.99 (m, 4H), 7.97–7.94 (AA'XX' system, 6H), 7.47–7.43 (m, 8H), 7.41 (d, J = 8.5 Hz, 2H), 5.61 (d, J = 8.5 Hz, 2H), 1.43–1.42 (m, 42H); **^{13}C-NMR** (125.7 MHz,

THF-d_8): The low solubility of this product prevented the registration of a clear ^{13}C-NMR spectrum; **^{11}B-NMR** (160.4 MHz, THF-d_8): δ (ppm) = −14.49; **HRMS (MALDI-TOF)**: Calculated for $C_{106}H_{85}BN_6OSi_2$: 1525.6449; Found: 1525.6489; **UV/Vis** (toluene): λ_{max} (log ε) = 660 (4.77), 604 (4.52), 563 (5.02), 548 (sh), 524 (4.49), 441 (3.98), 417 (3.76), 373 (4.71), 353 (4.66) nm.

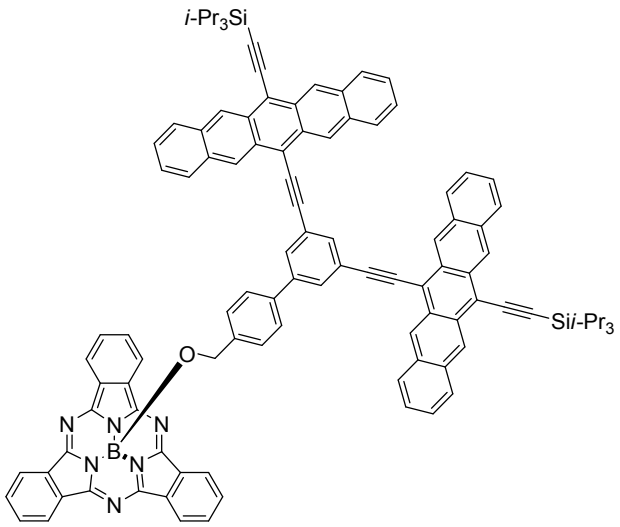

SubPc-Pnc$_2$ 1d. Reaction time: 13 h. H_{12}SubPcOPnc$_2$ **1d** was afforded as a purple solid in 18% yield. **^{1}H-NMR** (300 MHz, $CDCl_3$): δ (ppm) = 9.17 (s, 8H), 8.89–8.84 (AA'XX' system, 6H), 8.27 (s, 1H), 7.96–7.88 (m, 14H), 7.84 (d, *J* = 1.5 Hz, 2H), 7.42–7.30 (m, 10H), 6.67 (d, *J* = 8.1 Hz, 2H), 2.83 (s, 1H), 1.39–1.38 (m, 42H); **^{13}C-NMR** (125.7 MHz, $CDCl_3$): δ (ppm) = 151.54, 142.28, 139.60, 138.19, 133.18, 132.37, 131.17, 130.61, 130.55, 130.33, 129.91, 128.82, 128.78, 126.91, 126.87, 126.60, 126.25, 126.15, 125.90, 124.72, 122.27, 118.80 117.59, 108.11, 107.40, 104.86, 103.78, 89.06, 61.70, 19.19, 11.88; **^{11}B-NMR** (160.4 MHz, $CDCl_3$): δ (ppm) = −14.51; **HRMS (MALDI-TOF**): Calculated for $C_{107}H_{87}BN_6OSi_2$: 1539.6606; Found: 1539.6541; **UV/Vis** (toluene): λ_{max} (log ε) = 660 (4.78), 604 (4.52), 562 (5.02), 546 (sh), 523 (4.48), 441 (3.95), 417 (3.71), 374 (4.73), 353 (4.65) nm.

Figure S35. ^{1}H-NMR spectrum (500 MHz, $CDCl_3$) of SubPc-Pnc$_2$ **1a**. *Inset*: Expansion of the region between 9.43 ppm and 7.33 ppm.

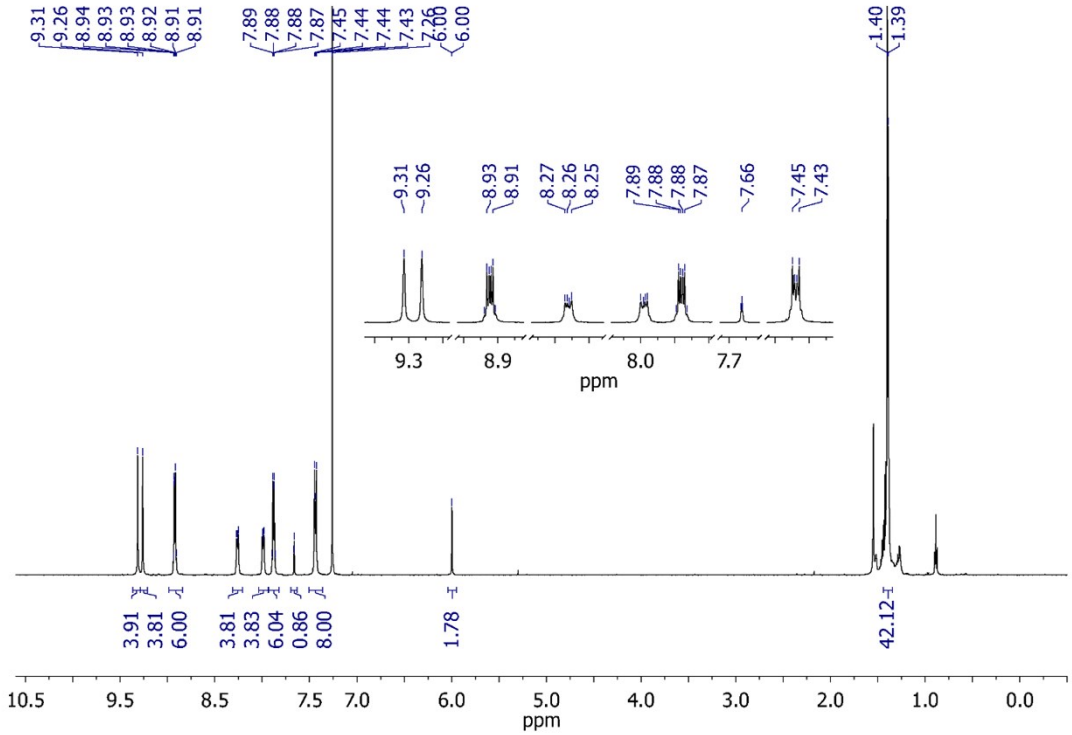

Figure S36. ^{13}C-NMR spectrum (125.7 MHz, $CDCl_3$) of SubPc-Pnc$_2$ **1a**. *Inset*: Expansion of the region between 134 ppm and 116 ppm.

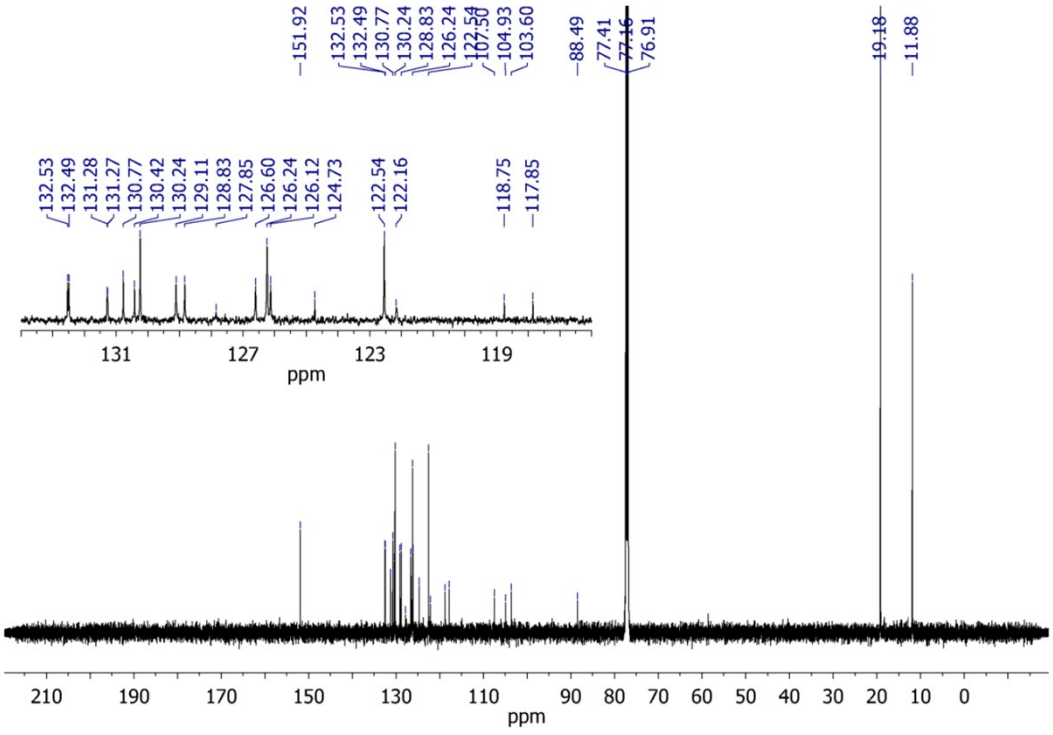

Figure S37. ^{11}B-NMR spectrum (160.4 MHz, $CDCl_3$) of SubPc-Pnc_2 **1a**.

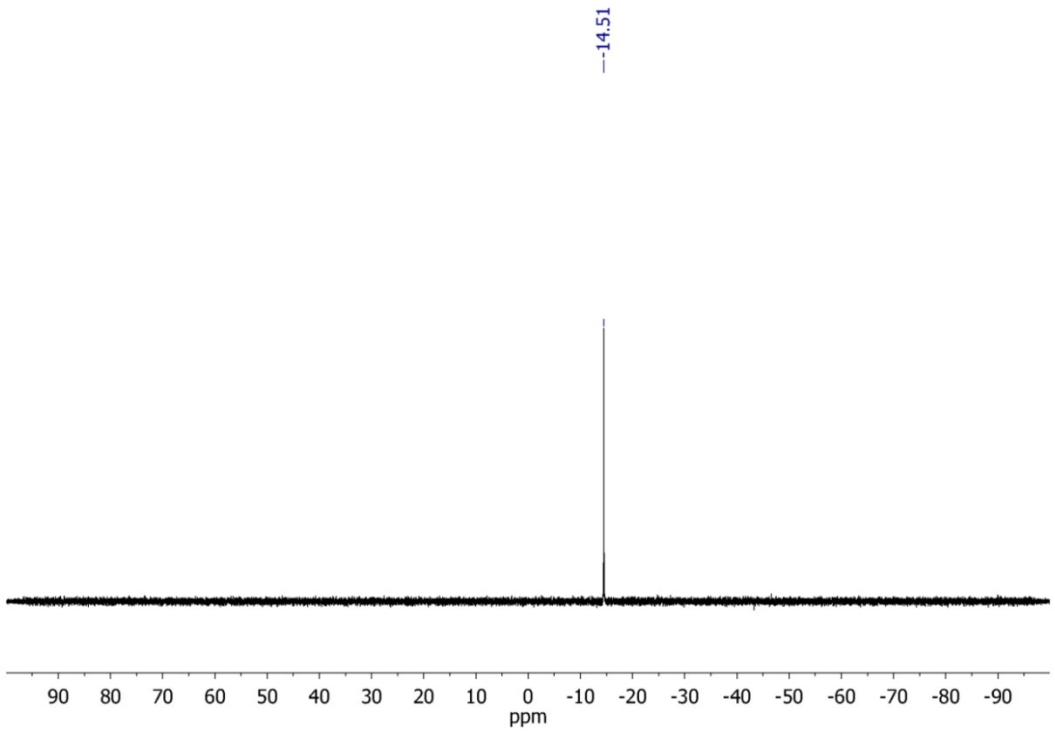

Figure S38. H-H COSY NMR spectrum (500 MHz, $CDCl_3$) of SubPc-Pnc_2 **1a**.

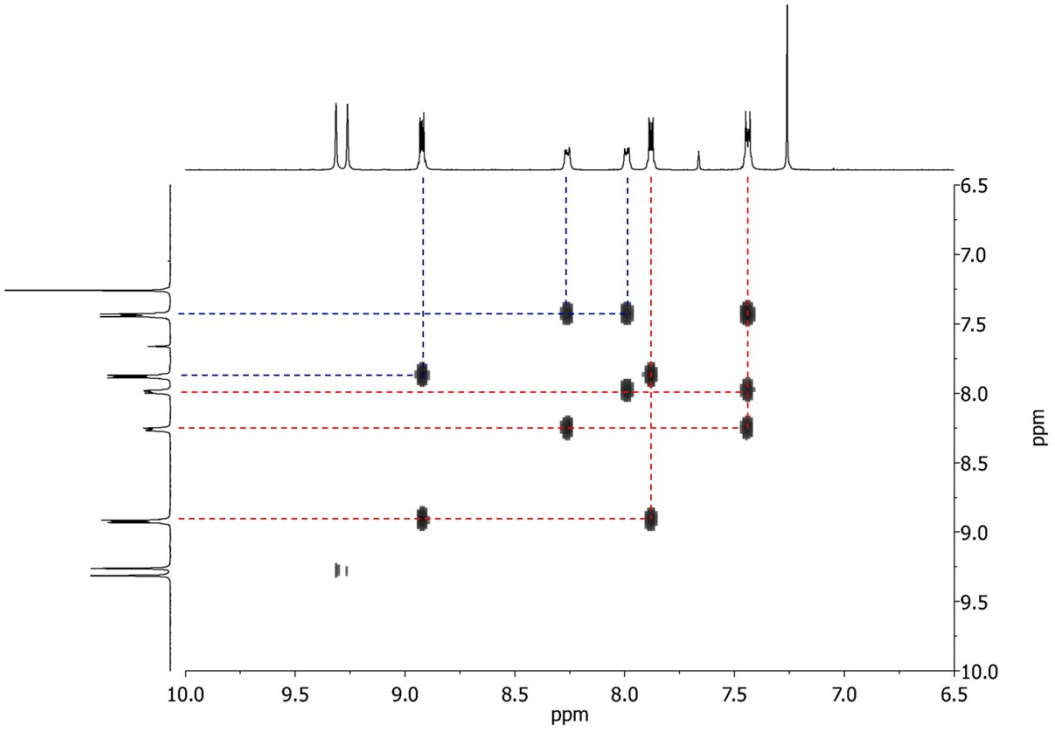

Figure S39. ^{1}H-NMR spectrum (500 MHz, THF-d_8) of SubPc-Pnc$_2$ **1b**. *Inset*: Expansion of the region between 9.55 ppm and 6.52 ppm.

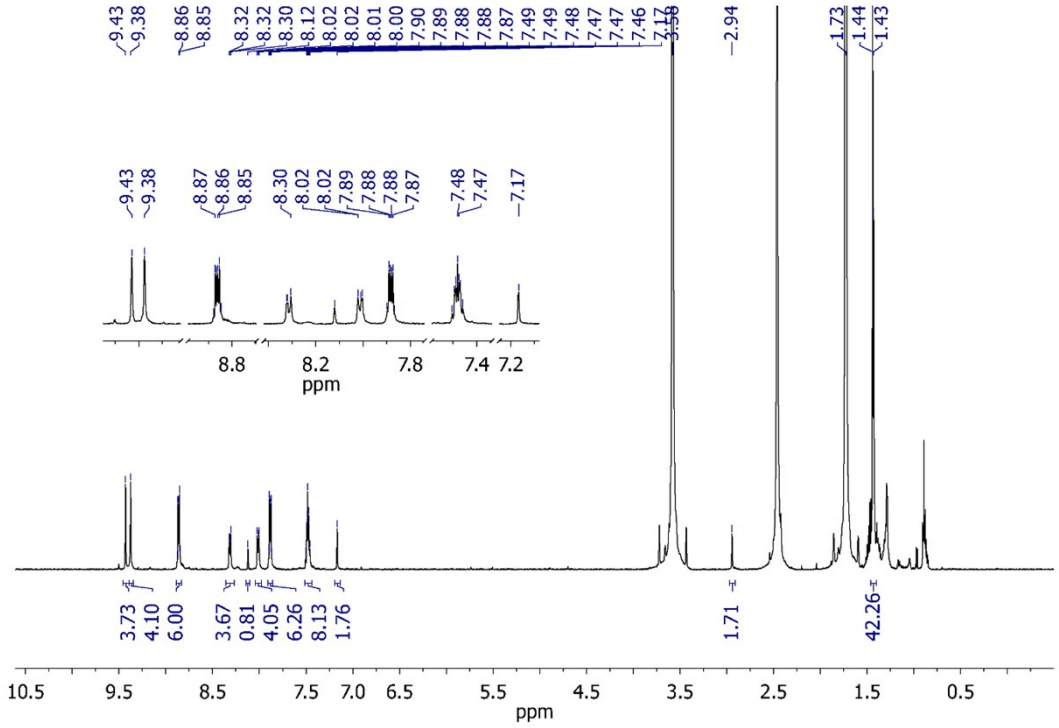

Figure S40. ^{11}B-NMR spectrum (160.4 MHz, THF-d_8) of SubPc-Pnc$_2$ **1b**.

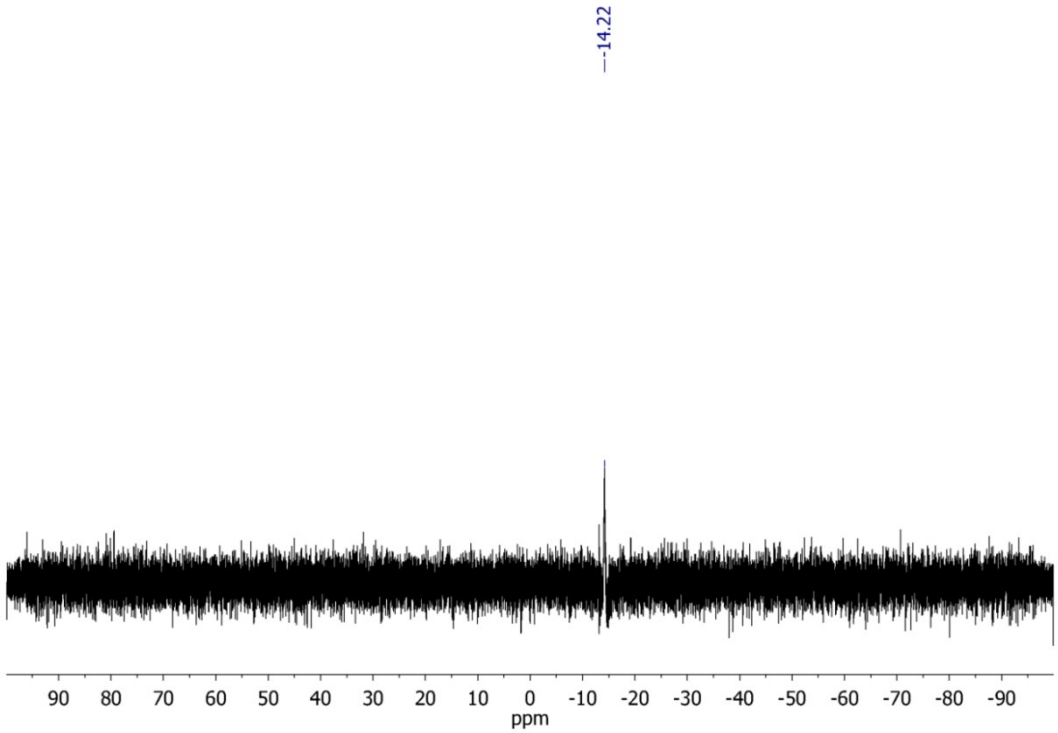

Figure S41. H-H COSY NMR spectrum (500 MHz, THF-d_8) of SubPc-Pnc$_2$ **1b**.

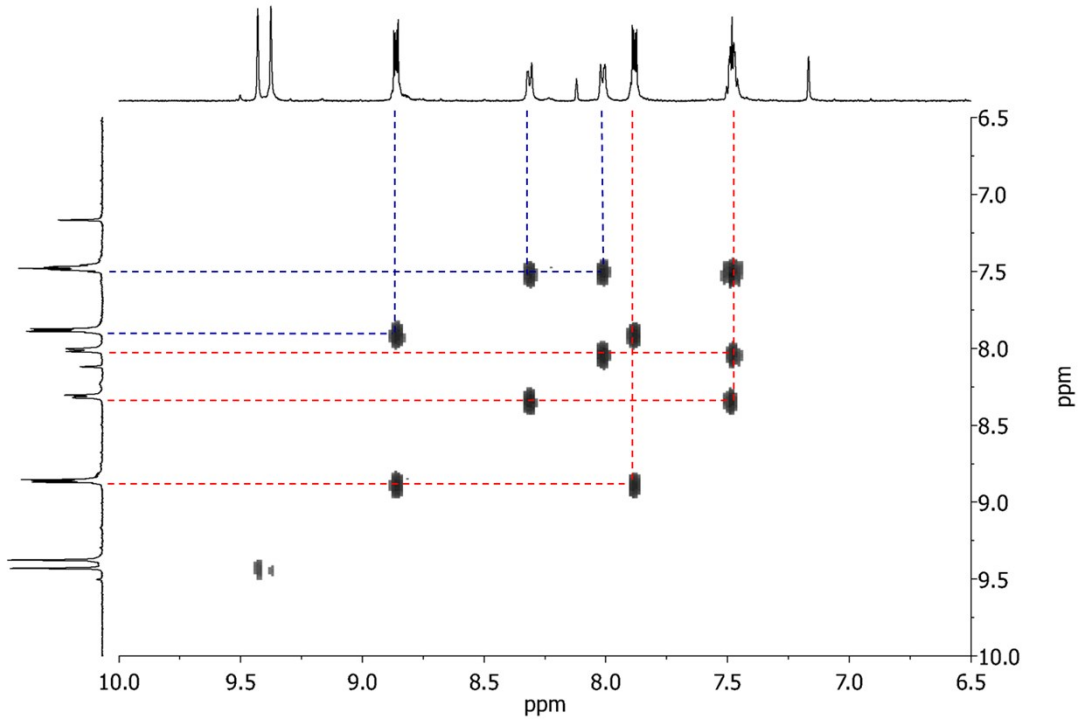

Figure S42. ^{1}H-NMR spectrum (500 MHz, THF-d_8) of SubPc-Pnc$_2$ **1c**. *Inset*: Expansion of the region between 9.58 ppm and 7.28 ppm.

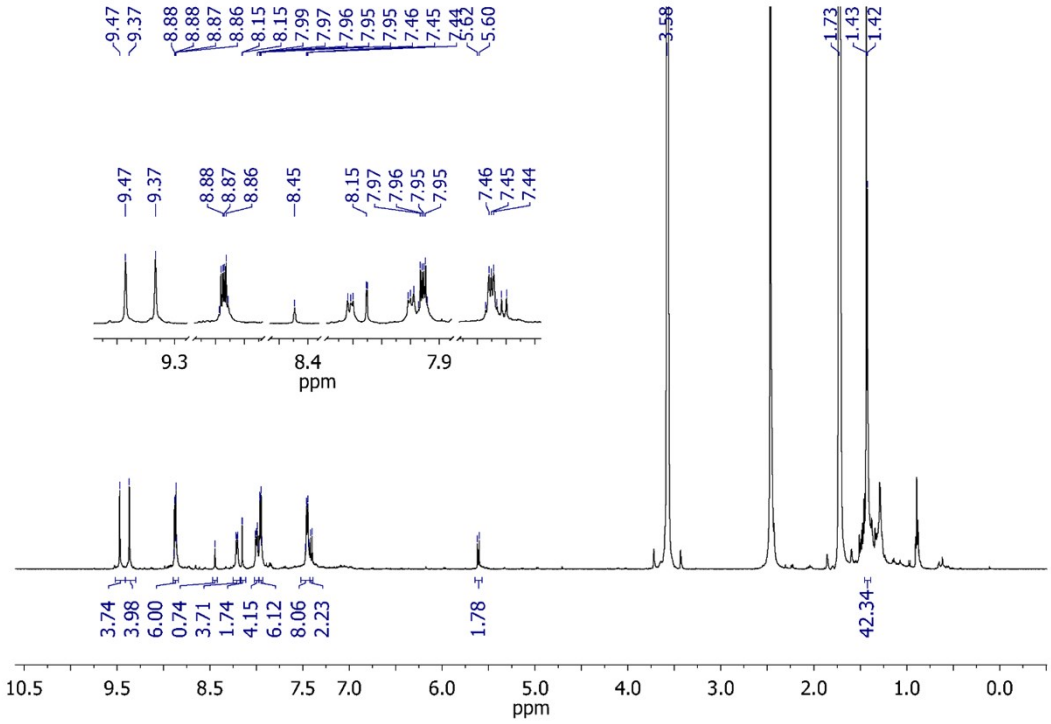

Figure S43. ^{11}B-NMR spectrum (160.4 MHz, THF-d_8) of SubPc-Pnc$_2$ **1c**.

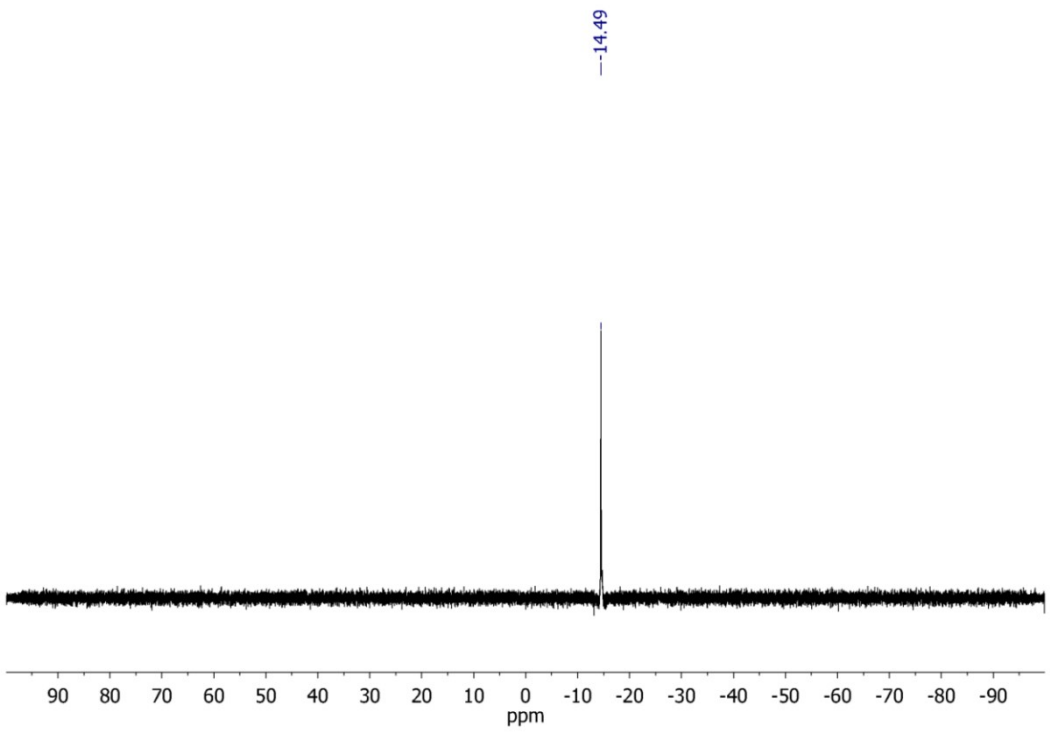

Figure S44. H-H COSY NMR spectrum (500 MHz, THF-d_8) of SubPc-Pnc$_2$ **1c**.

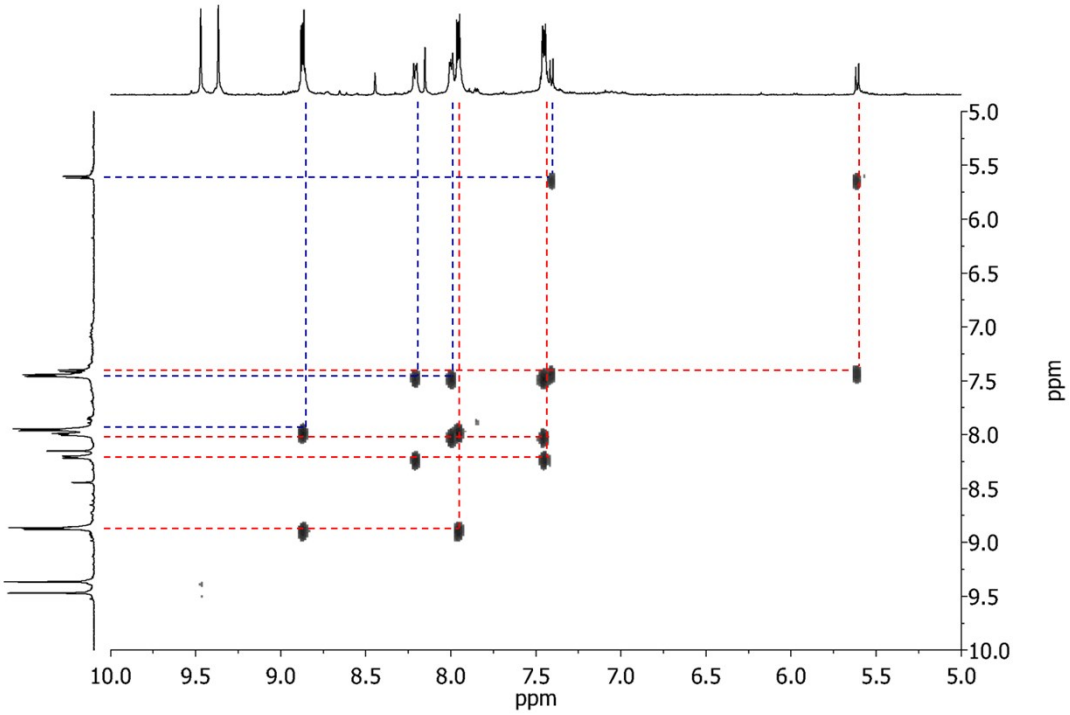

Figure S45. ^{1}H-NMR spectrum (300 MHz, $CDCl_3$) of SubPc-Pnc_2 **1d**. *Inset*: Expansion of the region between 9.31 ppm and 6.52 ppm.

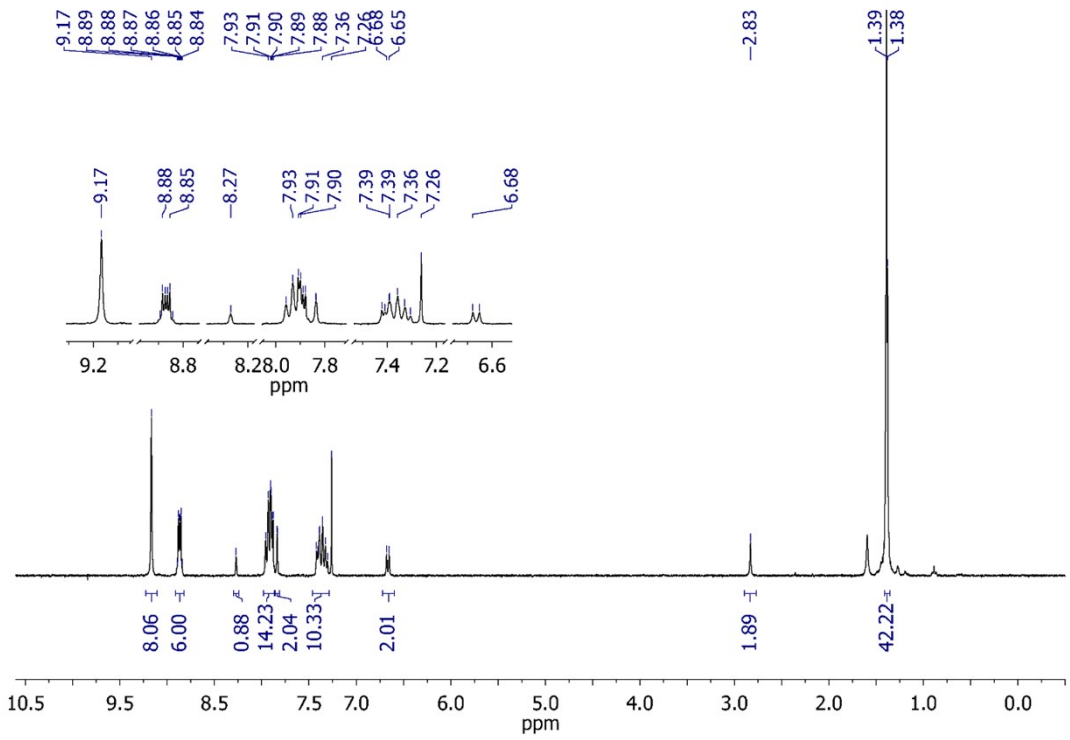

Figure S46. ^{13}C-NMR spectrum (125.7 MHz, $CDCl_3$) of SubPc-Pnc$_2$ **1d**. *Inset*: Expansion of the region between 144 ppm and 115 ppm.

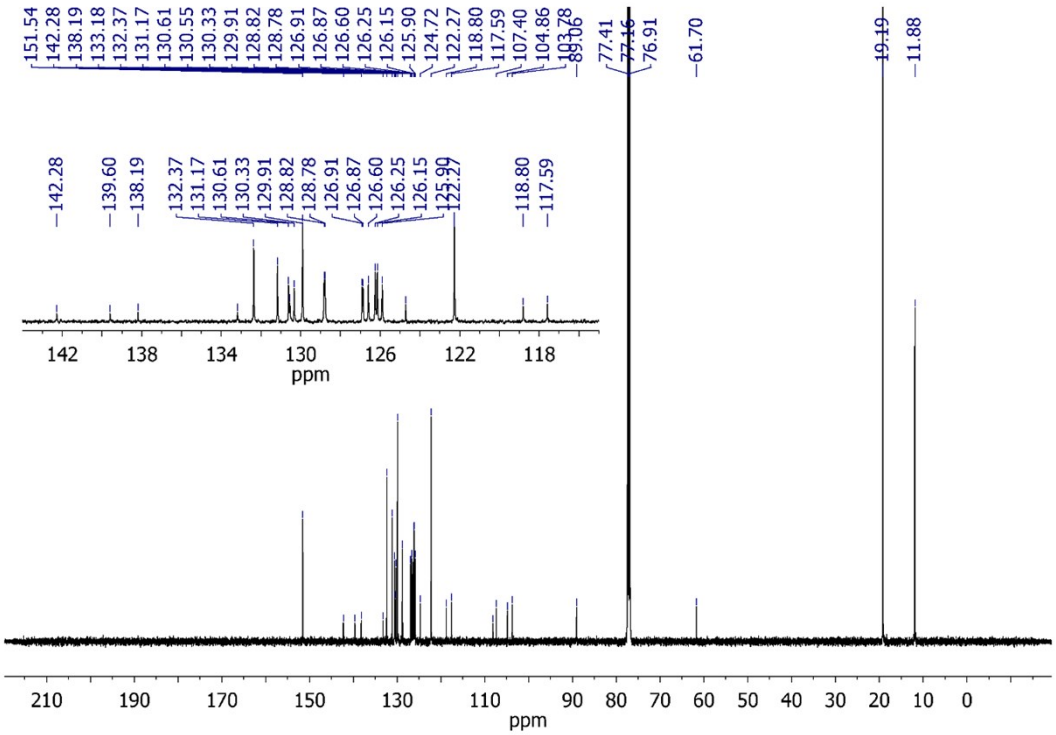

Figure S47. ^{11}B-NMR spectrum (160.4 MHz, $CDCl_3$) of SubPc-Pnc_2 **1d**.

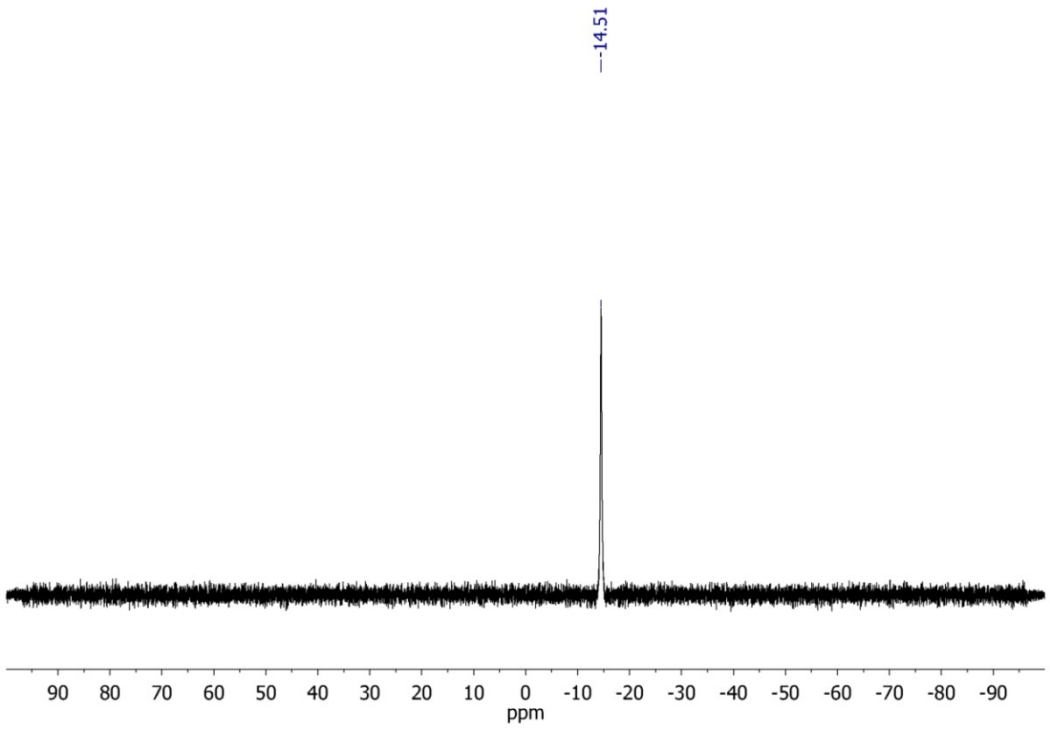

Figure S48. H-H COSY NMR spectrum (500 MHz, $CDCl_3$) of SubPc-Pnc_2 **1d**.

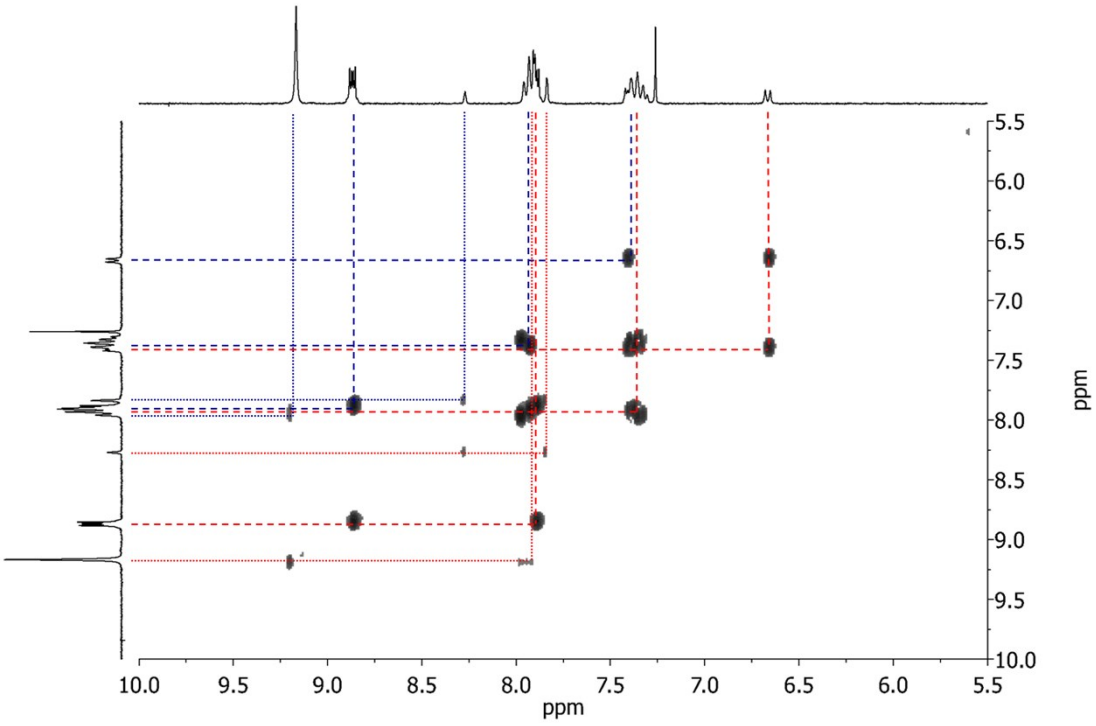

Figure S49. MALDI-TOF mass spectrum (in DCTB matrix) of SubPc-Pnc$_2$ **1a**.

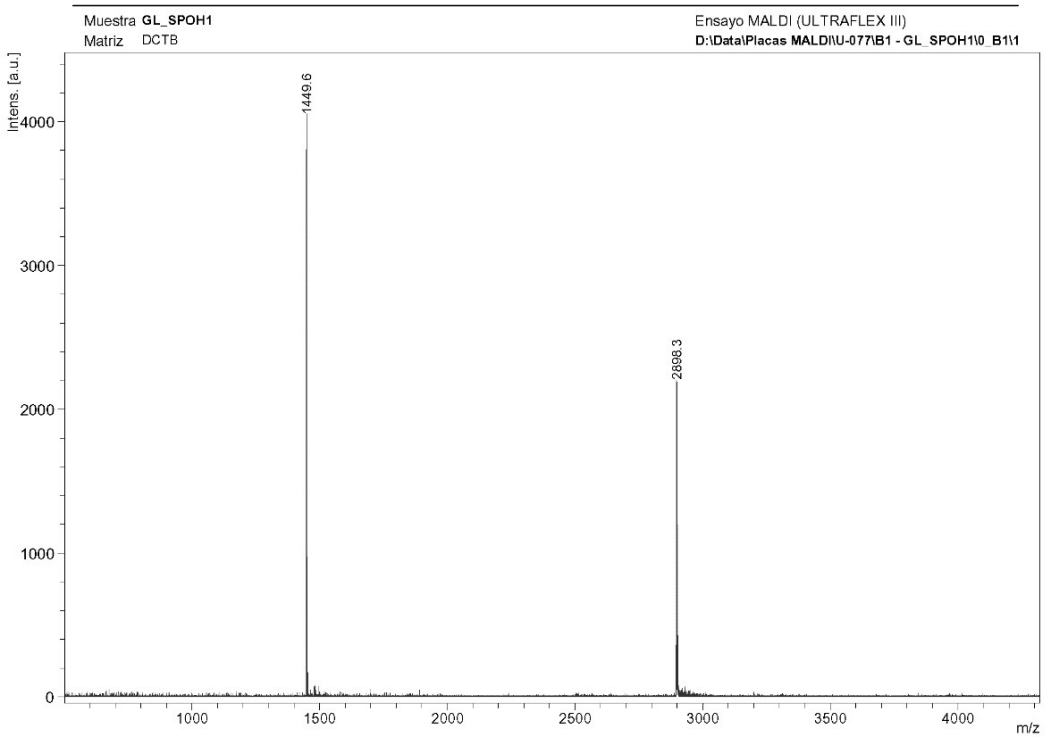

Figure S50. *Upper part* – HRMS (MALDI-TOF) spectrum (in DCTB + PPG1000 + 2000 matrix) of SubPc-Pnc_2 **1a**. *Lower part* – Calculated isotopic pattern of SubPc-Pnc_2 **1a**.

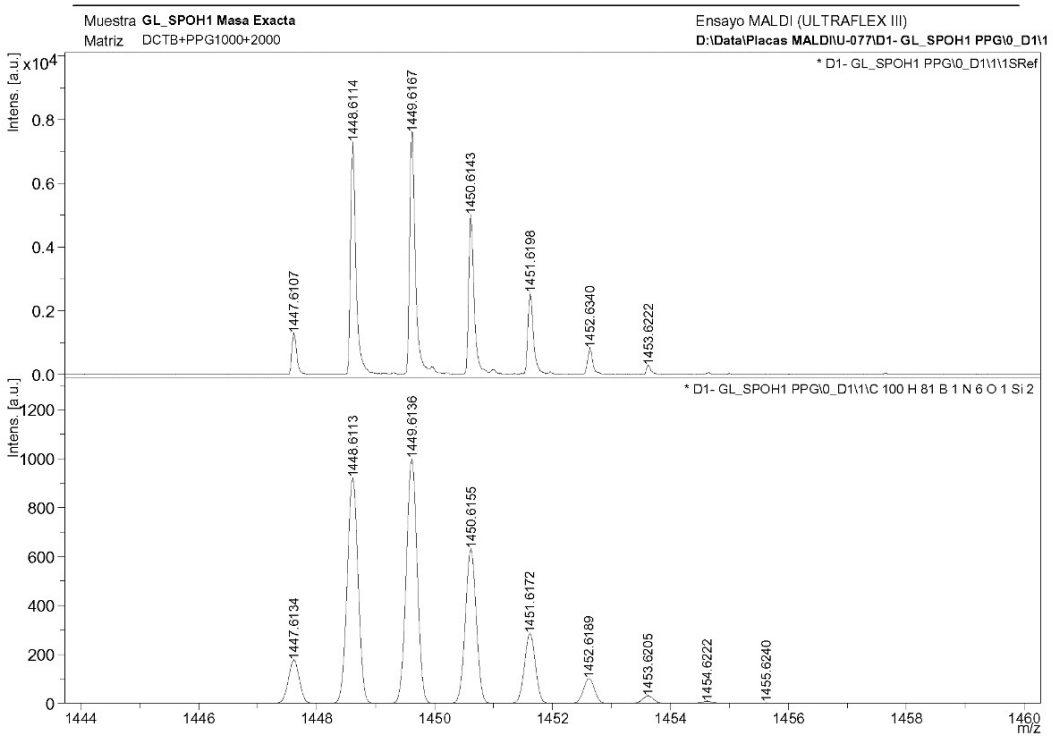

Figure S51. MALDI-TOF mass spectrum (in DCTB matrix) of SubPc-Pnc$_2$ **1b**.

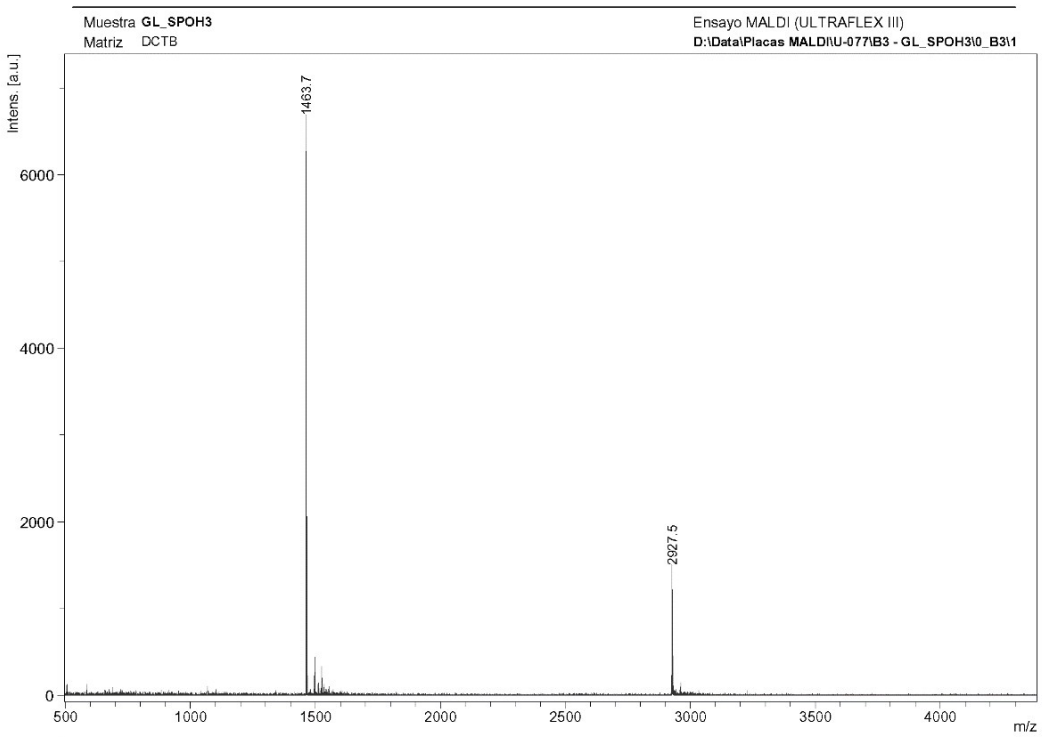

Figure S52. *Upper part* – HRMS (MALDI-TOF) spectrum (in DCTB + PPG1000 + 2000 matrix) of SubPc-Pnc_2 **1b**. *Lower part* – Calculated isotopic pattern of SubPc-Pnc_2 **1b**.

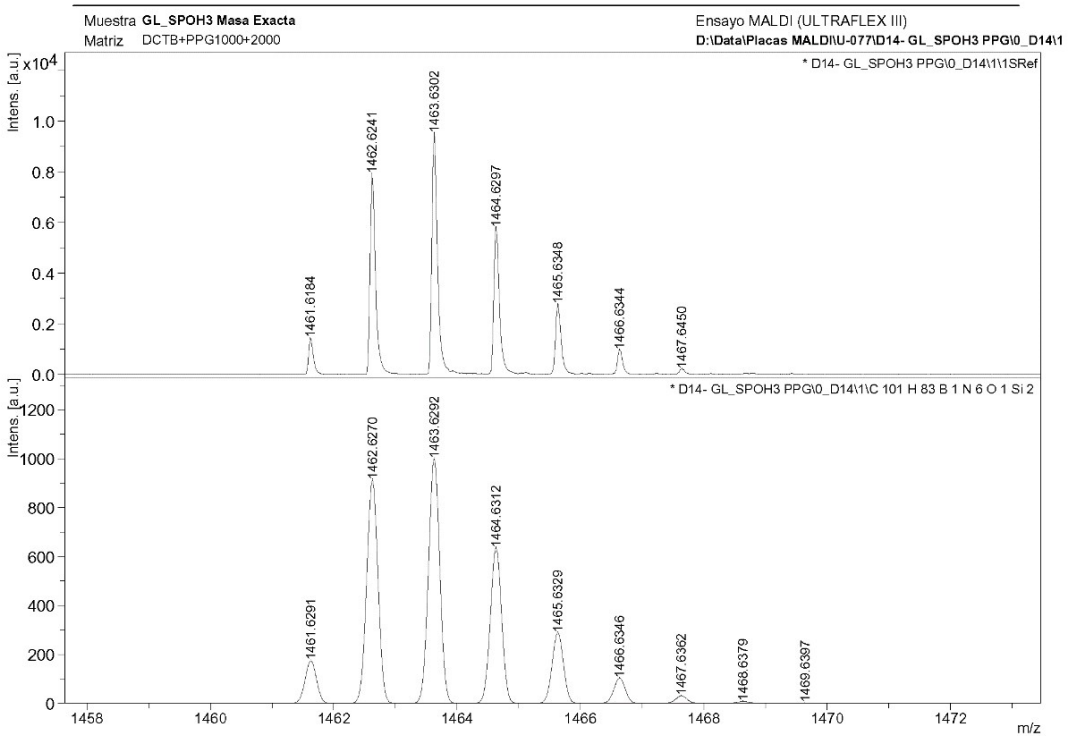

Figure S53. MALDI-TOF mass spectrum (in DCTB matrix) of SubPc-Pnc$_2$ **1c**.

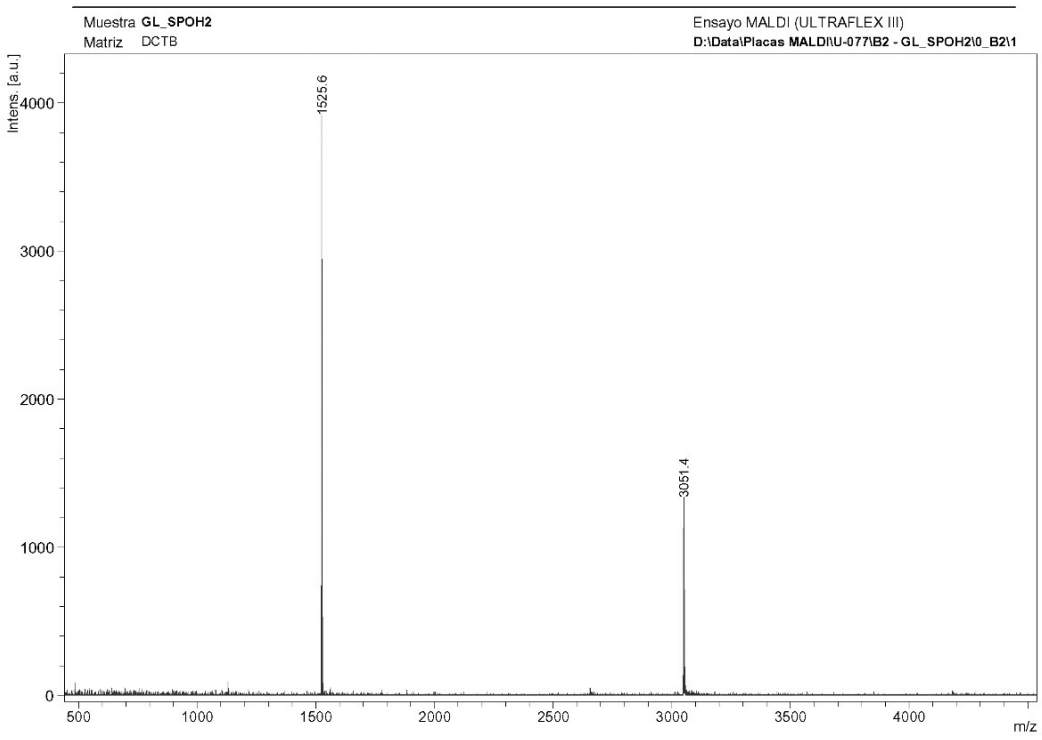

Figure S54. *Upper part* – HRMS (MALDI-TOF) spectrum (in DCTB + PPG1000 + 2000 matrix) of SubPc-Pnc_2 **1c**. *Lower part* – Calculated isotopic pattern of SubPc-Pnc_2 **1c**.

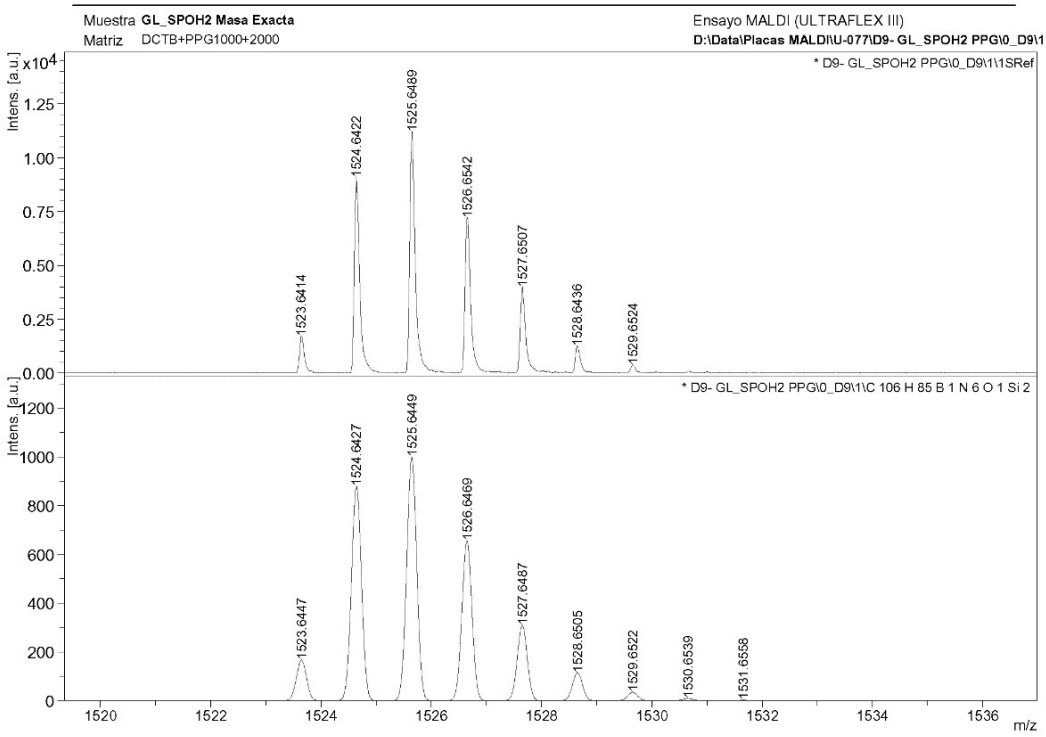

Figure S55. MALDI-TOF mass spectrum (in DCTB matrix) of SubPc-Pnc$_2$ **1d**.

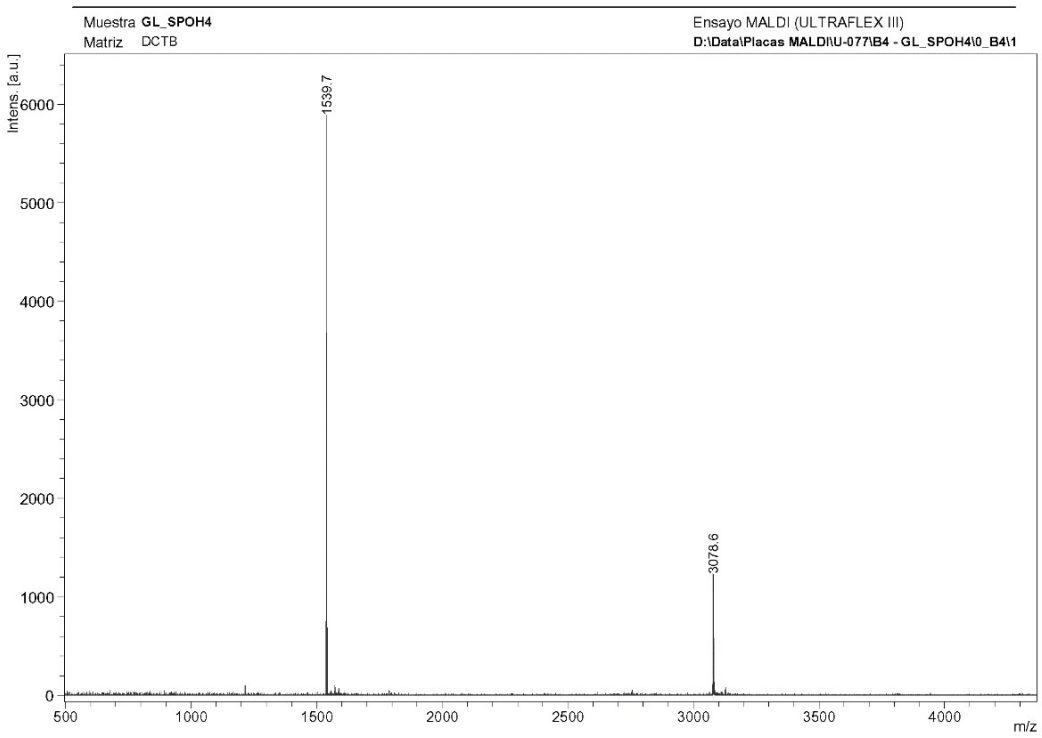

Figure S56. *Upper part* – HRMS (MALDI-TOF) spectrum (in DCTB + PPG1000 + 2000 matrix) of SubPc-Pnc_2 **1d**. *Lower part* – Calculated isotopic pattern of SubPc-Pnc_2 **1d**.

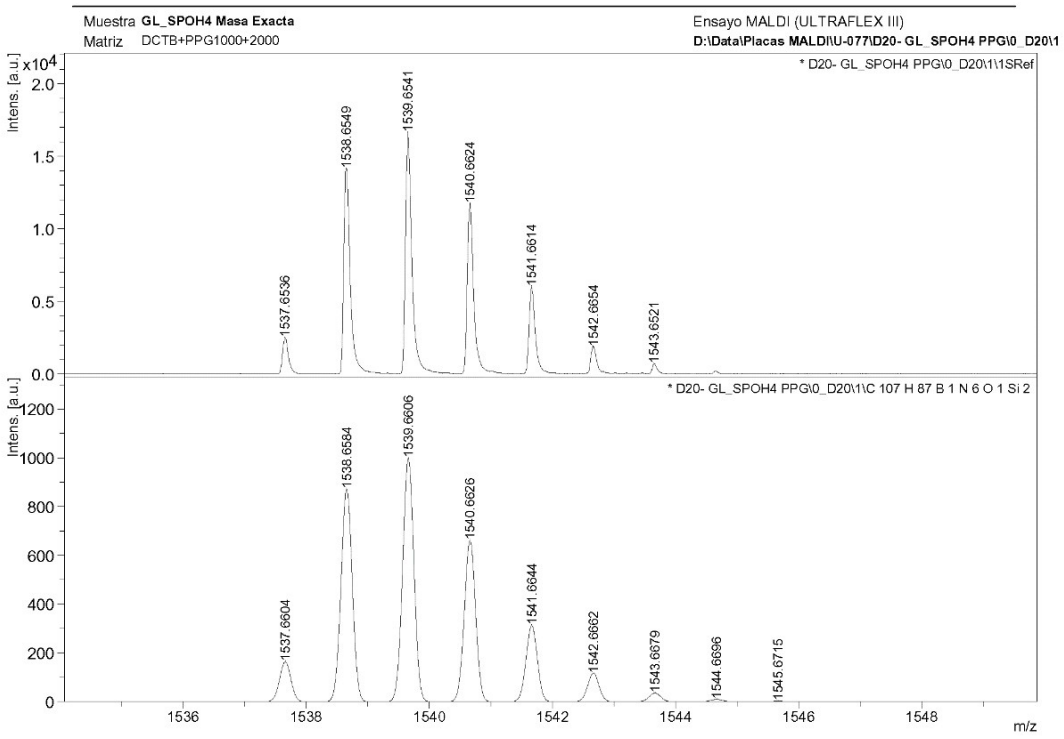

Photophysics

Figure S57. Steady-state absorption spectra of SubPcCl **9**, Pnc_2 **2a**, and SubPc-Pnc_2 **1a** in toluene (rt) – see figure legends for details.

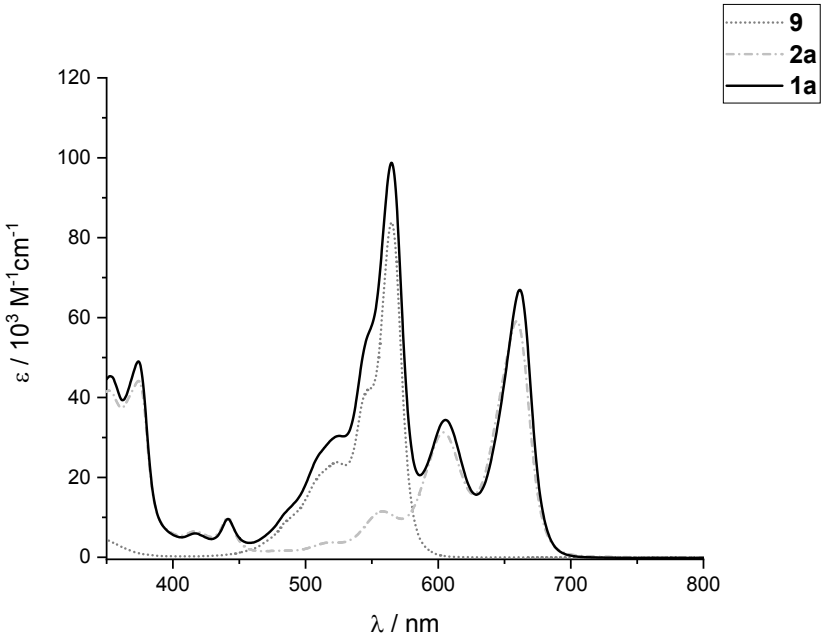

Figure S58. Steady-state absorption spectra of SubPcCl **9**, Pnc_2 **2b**, and SubPc-Pnc_2 **1b** in toluene (rt) – see figure legends for details.

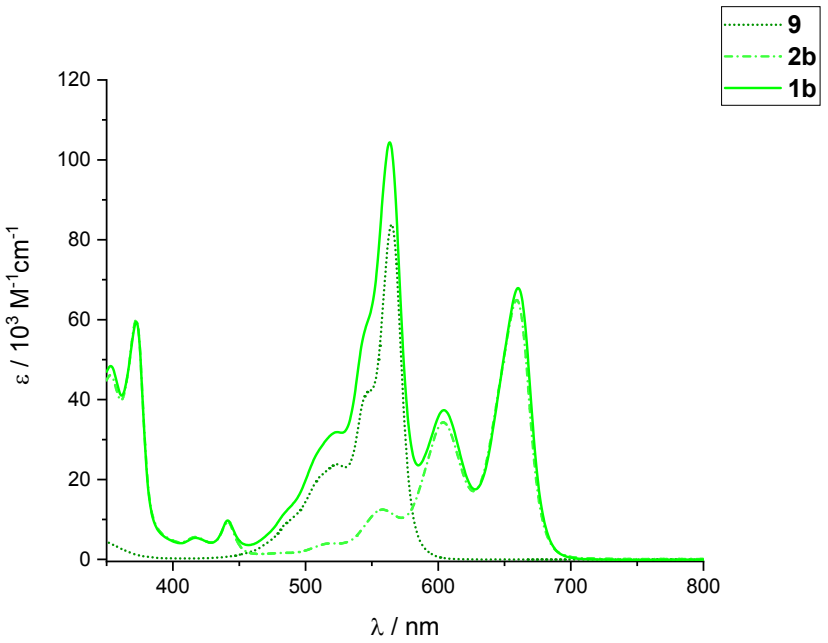

Figure S59. Steady-state absorption spectra of SubPcCl **9**, Pnc_2 **2d**, and SubPc-Pnc_2 **1d** in toluene (rt) – see figure legends for details.

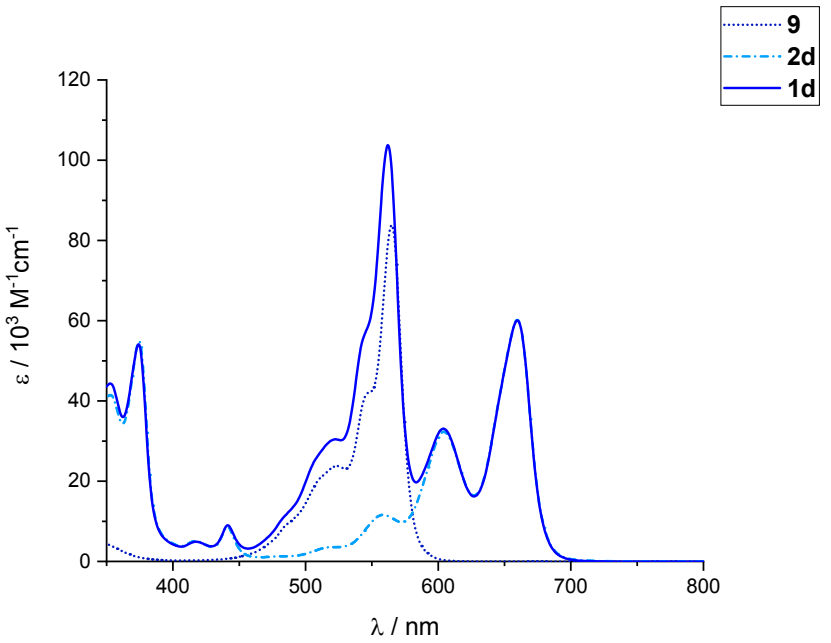

Figure S60. Steady-state fluorescence spectra obtained upon 500 nm photoexcitation of SubPcCl **9**, Pnc_2 **2a**, and SubPc-Pnc_2 **1a** in toluene (rt) – see figure legends for details.

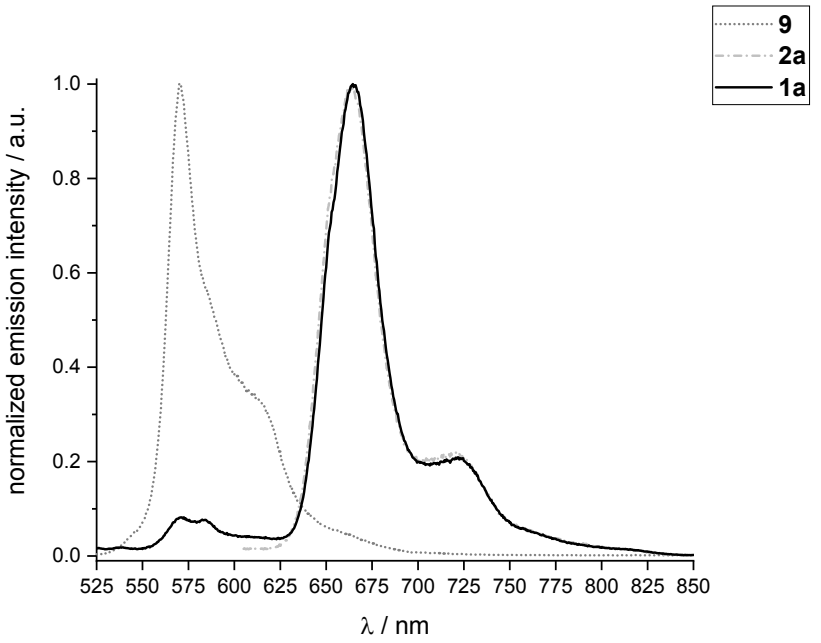

Figure S61. Steady-state fluorescence spectra obtained upon 500 nm photoexcitation of SubPcCl **9**, Pnc_2 **2b**, and SubPc-Pnc_2 **1b** in toluene (rt) – see figure legends for detail.

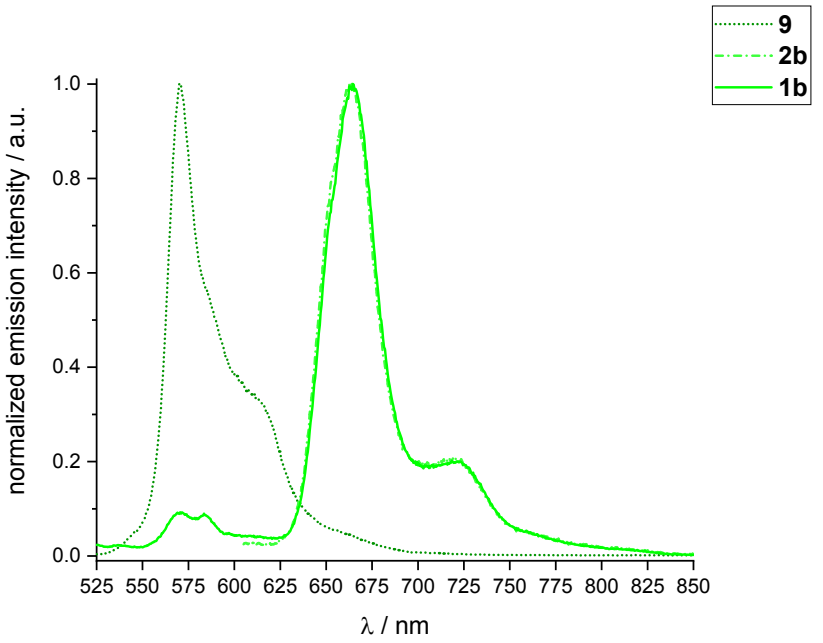

Figure S62. Steady-state fluorescence spectra obtained upon 500 nm photoexcitation of SubPcCl **9**, Pnc_2 **2d**, and SubPc-Pnc_2 **1d** in toluene (rt) – see figure legends for details.

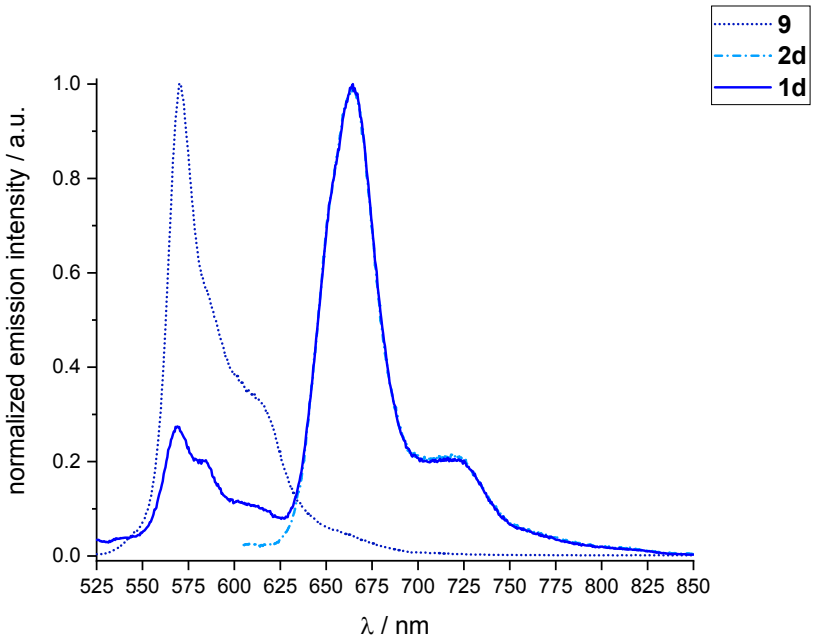

Table S2. Summary of photophysical properties of Pnc_2s **2a**-**d**, SubPc-Pnc_2 conjugates **1a**-**d**, and SubPc **9** in toluene.

	λ_{abs} / nm		λ_{em} / nm		Φ_F / %	τ_F
	SubPc	**Pnc_2**	**SubPc**	**Pnc_2**	**SubPc / Pnc_2**	**SubPc[a, d]**
1a	565	662	571	665	0.05 / 1.06	<50 ps[b]
2a	−	659	−	664	− / 1.47	<100 ps[b, c]
1b	564	660	571	665	0.03 / 0.90	<50 ps[b]
2b	−	659	−	664	− / 0.75	<100 ps[b, c]
1c	563	660	570	664	0.12 / 1.19	<50 ps[b]
2c	−	660	−	664	− / 1.03	<100 ps[b, c]
1d	562	660	569	665	0.09 / 0.66	<50 ps[b]
2d	−	660	−	665	− / 0.80	<100 ps[c]
9	565	−	570	−	28.81 / −	3.35 ns

[a] values refer to the SubPc centered fluorescence if not stated otherwise. [b] lifetime is below the resolution limit of our time-correlated single photon counting (TCSPC) setup. [c] value refers to the Pnc_2 centered fluorescence. [d] An additional, long-lived component with lifetimes similar to those of the corresponding reference compounds points to minor contributions from free, highly fluorescent SubPcs and Pnc monomer.

Figure S63. (A) Differential absorption spectra (visible) obtained upon fsTA experiments (632 nm) of Pnc_2 **2b** in toluene with several time delays between 0 and 5500 ps at room temperature. Single wavelength kinetics at 450 (black), 505 (red), 601 (blue), and 663 nm (green) monitoring the singlet excited state ($^1(S_1S_0)$: 17.13 ps), intermediate state ($^{CT}(S_1S_0)$: 88.83 ps), and triplet excited state ($^1(T_1T_1)$: 2.50 ns) dynamics as well as fits to the data (red lines) are shown in the *inset*. **(B)** Evolution associated spectra of the transient absorption data of Pnc_2 **2b** shown in **(A)**. The red spectrum illustrates the initially formed Pnc_2 $^1(S_1S_0)$ state, while the blue and green spectra are those of the intermediate Pnc_2 $^{CT}(S_1S_0)$ state and the multiexcitonic Pnc_2 $^1(T_1T_1)$ state, respectively. The *inset* depicts the relative populations of $^1(S_1S_0)$, $^{CT}(S_1S_0)$, and $^1(T_1T_1)$.

(A)

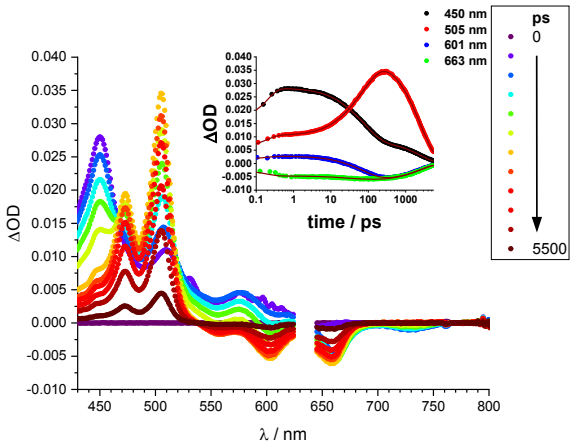

(B)

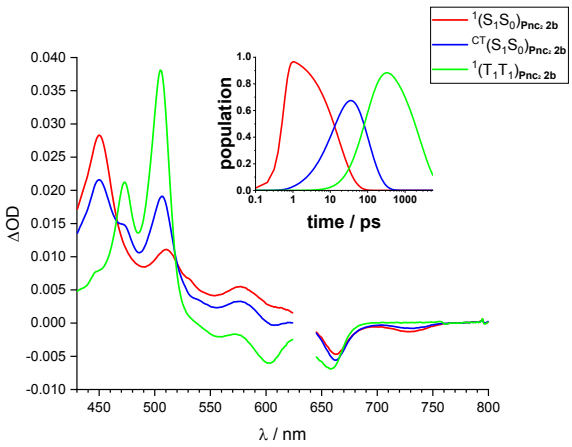

Figure S64. (A) Differential absorption spectra (visible) obtained upon fsTA experiments (632 nm) of Pnc_2 **2d** in toluene with several time delays between 0 and 5500 ps at room temperature. Single wavelength kinetics at 450 (black), 505 (red), 603 (blue), and 663 nm (green) monitoring the singlet excited state ($^1(S_1S_0)$: 16.62 ps), intermediate state ($^{CT}(S_1S_0)$: 104.92 ps), and triplet excited state ($^1(T_1T_1)$: 2.68 ns) dynamics as well as fits to the data (red lines) are shown in the *inset*. **(B)** Evolution associated spectra of the transient absorption data of Pnc_2 **2d** shown in **(A)**. The red spectrum illustrates the initially formed Pnc_2 $^1(S_1S_0)$ state, while the blue and green spectra are those of the intermediate Pnc_2 $^{CT}(S_1S_0)$ state and the multiexcitonic Pnc_2 $^1(T_1T_1)$ state, respectively. The *inset* depicts the relative populations of $^1(S_1S_0)$, $^{CT}(S_1S_0)$, and $^1(T_1T_1)$.

(A)

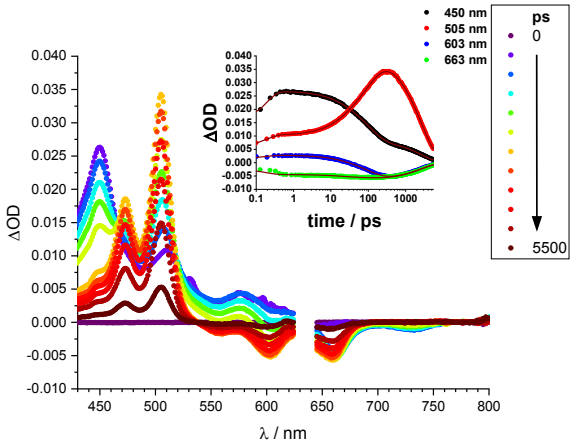

(B)

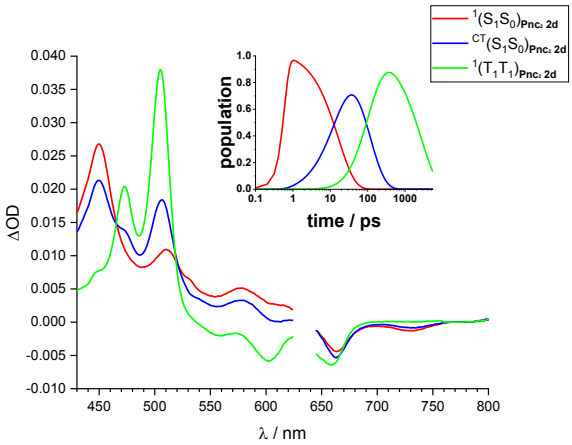

Figure S65. (A) Differential absorption spectra (visible) obtained upon fsTA experiments (530 nm) of SubPc-Pnc_2 **1b** in toluene with several time delays between 0 and 5500 ps at room temperature. Single wavelength kinetics at 450 (black), 506 (red), 564 (blue), and 663 nm (green) monitoring the singlet excited state ($^1(S_1)$: 0.70 ps), singlet excited state ($^1(S_1S_0)$: 7.28 ps), intermediate state ($^{CT}(S_1S_0)$: 77.38 ps), and triplet excited state ($^1(T_1T_1)$: 2.51 ns) dynamics as well as fits to the data (red lines) are shown in the *inset*. **(B)** Evolution associated spectra of the transient absorption data of **1b** shown in **(A)**. The black spectrum illustrates the initially formed SubPc $^1(S_1)$ state, while the red, blue, and green spectra are those of the Pnc_2 $^1(S_1S_0)$ state, the intermediate Pnc_2 $^{CT}(S_1S_0)$ state, and the multiexcitonic Pnc_2 $^1(T_1T_1)$ state, respectively. The *inset* depicts the relative populations of $^1(S_1)$, $^1(S_1S_0)$, $^{CT}(S_1S0)$, and $^1(T_1T_1)$.

(A)

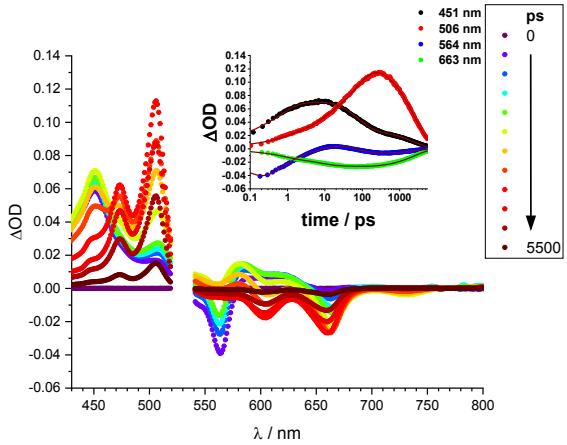

(B)

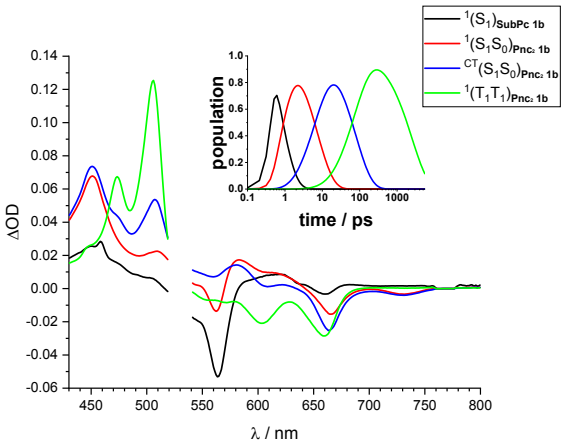

Figure S66. (A) Differential absorption spectra (visible) obtained upon fsTA experiments (530 nm) of SubPc-Pnc_2 **1d** in toluene with several time delays between 0 and 5500 ps at room temperature. Single wavelength kinetics at 450 (black), 505 (red), 562 (blue), and 663 nm (green) monitoring the singlet excited state ($^1(S_1)$: 1.28 ps), singlet excited state ($^1(S_1S_0)$: 14.74 ps), intermediate state ($^{CT}(S_1S_0)$: 104.09 ps), and triplet excited state ($^1(T_1T_1)$: 2.88 ns) dynamics as well as fits to the data (red lines) are shown in the *inset*. **(B)** Evolution associated spectra of the transient absorption data of **1d** shown in **(A)**. The black spectrum illustrates the initially formed SubPc $^1(S_1)$ state, while the red, blue, and green spectra are those of the Pnc_2 $^1(S_1S_0)$ state, the intermediate Pnc_2 $^{CT}(S_1S_0)$ state, and the multiexcitonic Pnc_2 $^1(T_1T_1)$ state, respectively. The *inset* depicts the relative populations of $^1(S_1)$, $^1(S_1S_0)$, $^{CT}(S_1S0)$, and $^1(T_1T_1)$.

(A)

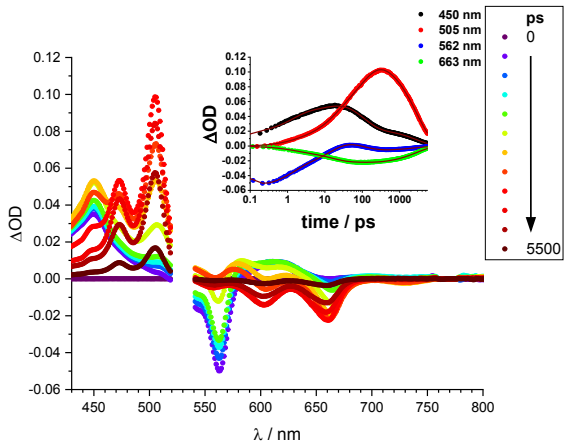

(B)

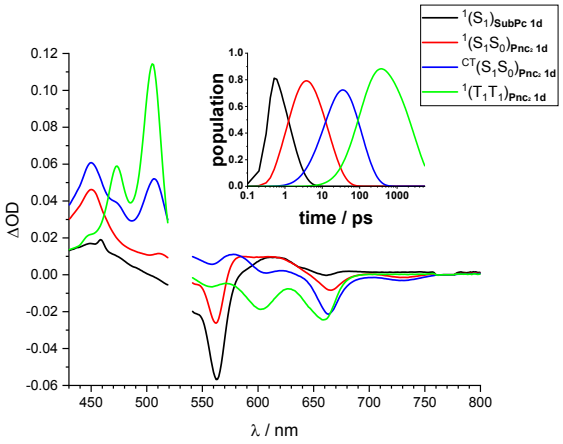

Figure S67. (A) Differential absorption spectra (visible) obtained upon nsTA experiments (530 nm) of SubPcCl **9** in toluene with several time delays between 0 and 400 µs at room temperature. Single wavelength kinetics at 451 (black), 519 (red), 569 (blue), and 611 nm (green) monitoring the singlet excited state ($^1(S_1)$: 3.55 ns) and triplet excited state ($^1(T_1T_1)$: 51.64 µs) dynamics as well as fits to the data (red lines) are shown in the *inset*. **(B)** Evolution associated spectra of the transient absorption data of **9** shown in **(A)**. The black spectrum illustrates the initially formed SubPc $^1(S_1)$ state, while the orange spectrum is that of the SubPc $^3(T_1)$ state. The *inset* depicts the relative populations of $^1(S_1)$ and $^3(T_1)$.

(A)

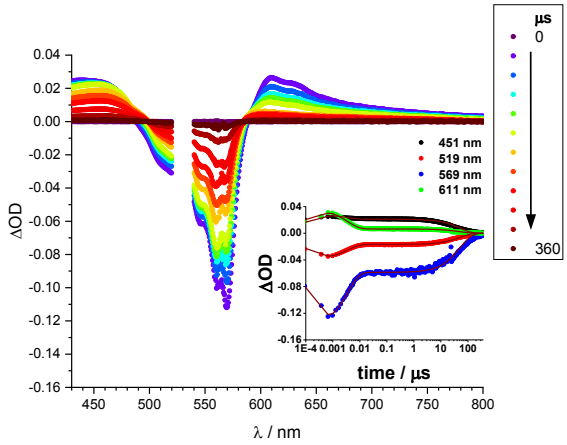

(B)

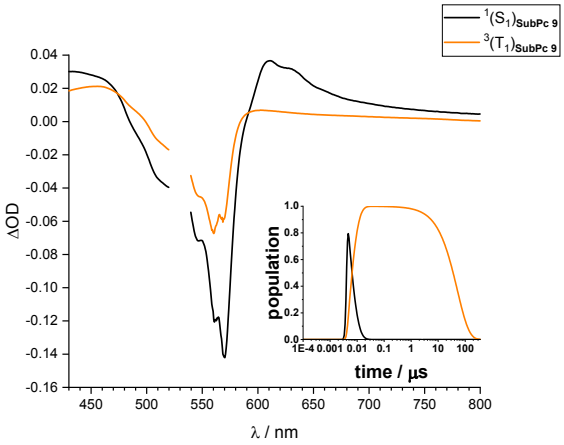

Computational Details

Geometries were optimized at the B3LYP[16]/6-31G(d)[17] level of density-functional theory with Grimme's D3 dispersion correction.[18] Two alternative conformations were investigated for **1a**-**c** and three for **1d**. Additional geometry optimizations using a polarizable continuum model for solvation in toluene[19] gave little change compared to the gas-phase calculations. The first two conformations differ in the orientation of the pentacenes to each other and the third conformation for **1d** used a stretched conformation for the linker.

Absorption spectra were calculated using the AM1 semiempirical Hamiltonian[20] using a singles-only configuration interaction (CIS) with 32 occupied and 32 virtual orbitals in the active space. Initial tests with larger active spaces and an SCRF continuum solvent treatment[21] for toluene showed no significant changes in the calculated spectra. FRET orientation factors κ^2 were calculated according to Loura[22] using the AM1-CIS transition dipoles for the relevant excited singlets from the ground state.

Figure S68. Optimized geometries of **1a** with the respective energies in kcal mol^{-1} in the gas phase and toluene (in parentheses).

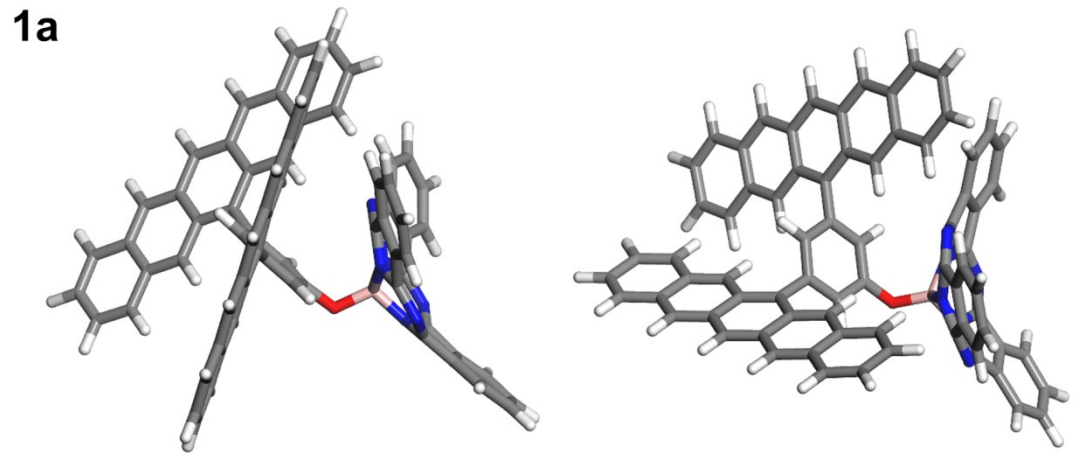

Figure S69. Optimized geometries of **1b** with the respective energies in kcal mol^{-1} in the gas phase and toluene (in parentheses).

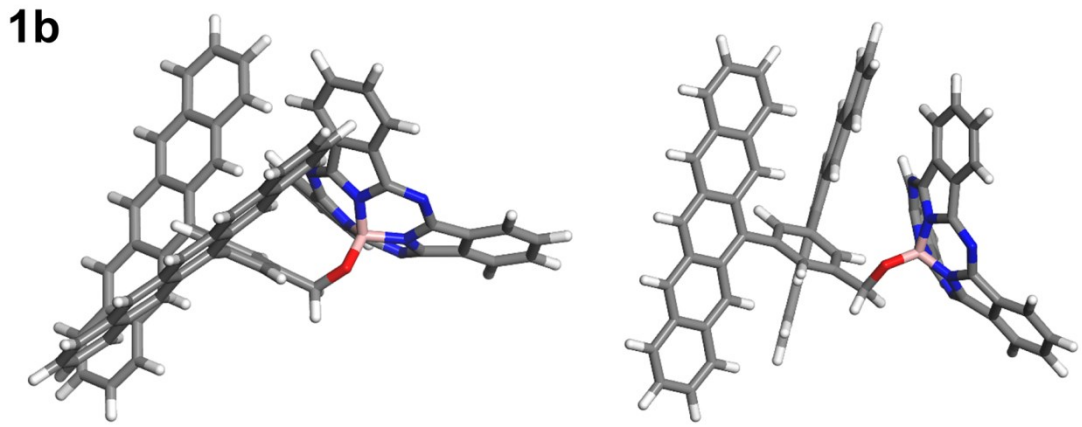

Figure S70. Optimized geometries of **1c** with the respective energies in kcal mol^{-1} in the gas phase and toluene (in parentheses).

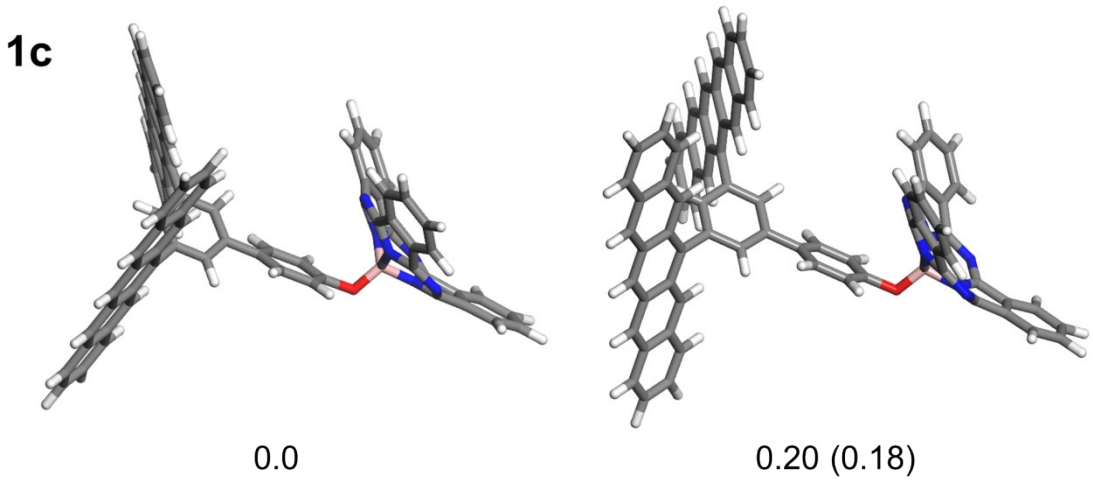

Figure S71. Optimized geometries of **1d** with the respective energies in kcal mol^{-1} in the gas phase and toluene (in parentheses).

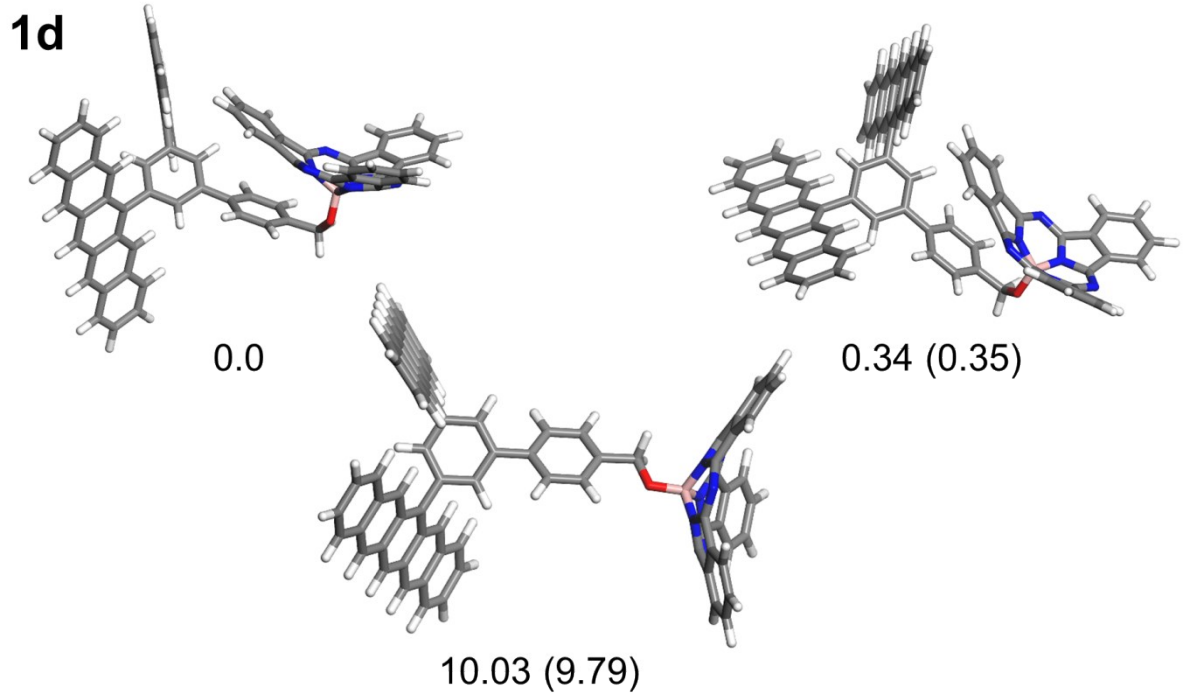

Table S3. Calculated vertical absorption energies, inter-chromophore distances and angles between transition dipoles for compound **1a**-**d**. The results are shown for the most stable conformation in every case except **1d**, for which the extended conformation is also shown.

Compound	Excitation energy (eV)			R^a (Å)	Angle[b] (°)	κ^2/R^6
	SubPc	Pentacene	Δ			
1A	2.080 2.093	2.378	0.285	2.776	35	0.001268
1B	2.087 2.102	2.369	0.267	2.661	62	0.002277
1C	2.099 2.102	2.393	0.291	6.492	62	1.08E-05
1D extended	2.108 2.109	2.395	0.286	12.635	8	2.36E-07
1D	2.091 2.107	2.393	0.286	2.725	82	0.002937

Figure S72. Correlation between the experimental FRET quenching and calculated κ^2/R^6 for **1a**-**d**.

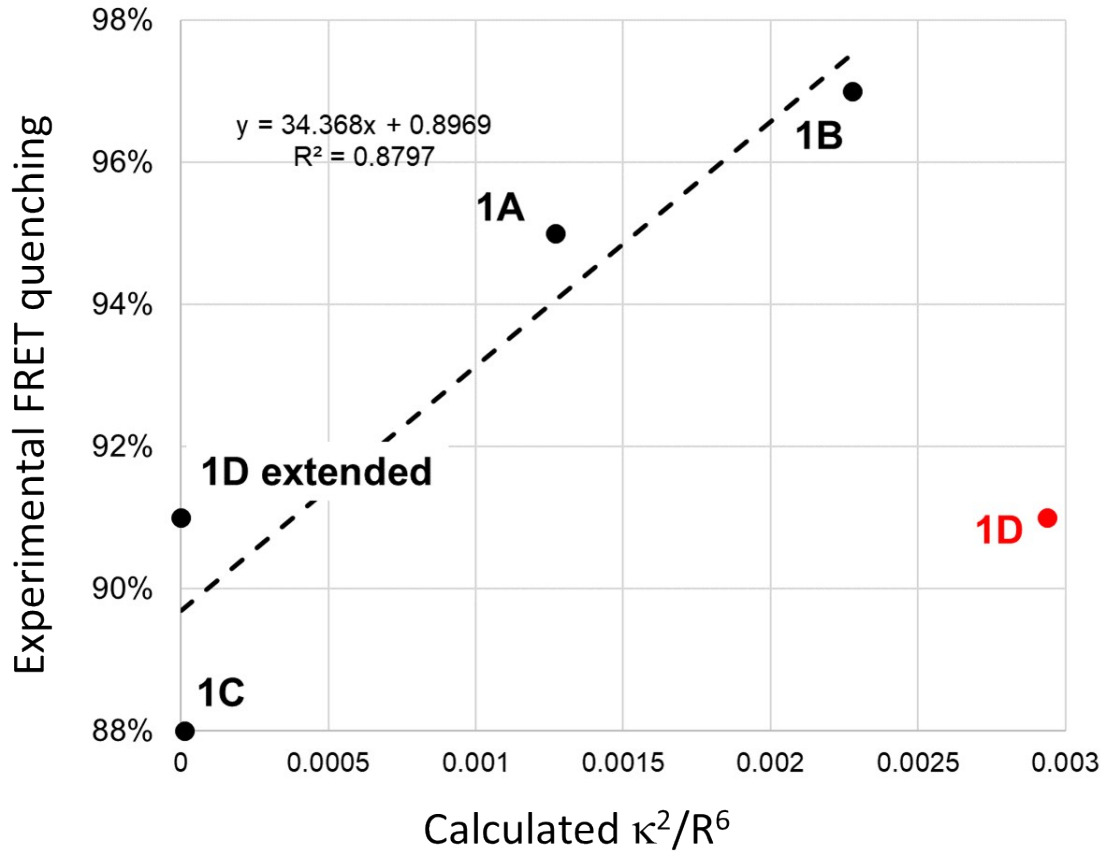

Author Contributions

R.R.T., T.T., and D.M.G. designed the research. J.Z. performed the photophysical studies. G.L. performed the synthesis of **1a**-**d** and **9**, while H.G. and L.C. synthesized **2a**-**d** and the corresponding precursors. J.Z., I.P. and D.M.G. analyzed the photophysical data. T.C. performed the computational studies. All authors contributed to the writing and editing of the paper.

Supplementary References

1 C. G. Claessens, D. González-Rodríguez, B. del Rey, T. Torres, G. Mark, H. P. Schuchmann, C. von Sonntag, J. G. MacDonald and R. S. Nohr, *Eur. J. Org. Chem.*, 2003, **14**, 2547.

2 L. Feng, M. Rudolf, O. Trukhina, Z. Slanina, F. Uhlik, X. Lu, T. Torres, D. M. Guldi and T. Akasaka, *Chem. Commun.*, 2015, **51**, 330.

3 R. F. Kubin and A. N. Fletcher, *J. Lumin.*, 1982, **27**, 455.

4 S. L. Murov, I. Carmichael and G. L. Hug, *Handbook of Photochemistry*, Marcel Dekker, Inc., New York, USA, 1993.

5 J. J. Snellenburg, S. Laptenok, R. Seger, K. M. Mullen and I. H. M. van Stokkum, *J. Stat. Softw.*, 2012, **49**, 1.

6 I. H. M. van Stokkum, D. S. Larsen and R. van Grondelle, *Biochim. Biophys. Acta*, 2004, **1657**, 82.

7 K. M. Mullen and I. H. M. van Stokkum, *J. Stat. Softw.*, 2007, **18**, 1.

8 M. A. Hink, N. V. Visser, J. W. Borst, A. van Hoek and A. J. W. G. Visser, *J. Fluoresc.,* 2003, **13**, 185.

9 C. Wohlfarth, *Refractive Indices of Pure Liquids and Binary Liquid Mixtures (Supplement to III/38)*, Springer-Verlag, Heidelberg, Berlin, 2008.

10 B. Wardle, *Principles and Applications of Photochemistry*, John Wiley & Sons, Chichester, 2009.

11 We thank M. A. Hink and N. V. Visser for incorporating their published procedure to calculate the critical energy donor-acceptor distance R_0 into a Microsoft Excel spreadsheet.

12 D. Lehnherr, A. H. Murray, R. McDonald and R. R. Tykwinski, *Angew. Chem. Int. Ed.*, 2010, **49**, 6190.

13 G. J. Capitosti, C. D. Guerrero, D. E. Binkley, Jr., C. S. Rajesh and D. A. Modarelli, *J. Org. Chem.*, 2003, **68**, 247.

14 M. E. Bakkari and J.-M. Vincent. *Org. Lett.*, 2004, **6**, 2765.

15 H.-B. Yang, A. M. Hawkridge, S. D. Huang, N. Das, S. D. Bunge, D. C. Muddiman and P. J. Stang, *J. Am. Chem. Soc.*, 2007, **129**, 2120.

16 A. D. Becke, *J. Chem. Phys.*, 1993, **98**, 5648.

17 R. Ditchfield, W. J. Hehre and J. A. Pople, *J. Chem. Phys.*, 1971, **54**, 724.

18 S. Grimme, J. Antony, S. Ehrlich and H. Krieg, *J. Chem. Phys.*, 2010, **132**, 154104.

19 J. Tomasi, B. Mennucci and R. Cammi, *Chem. Rev.*, 2005, **105**, 2999.

20 M. J. S. Dewar, E. G. Zoebisch, E. F. Healy and J. J. P. Stewart, *J. Am. Chem. Soc.*, 1985, **107**, 3902.

21 G. Rauhut, T. Clark and T. Steinke, *J. Am. Chem. Soc.*, 1993, **115**, 9174.

22 L. M. S. Loura, *Int. J. Mol. Sci.*, 2012, **13**, 15252.